

## Supporting Information

### **Catalyst-free diboration and silaboration of alkenes and alkynes using bis(9-heterofluorenyls)**

Jannik Gilmer, Timo Trageser, Luis Čaić, Alexander Virovets, Michael Bolte, Hans-Wolfram Lerner, Felipe Fantuzzi,\* and Matthias Wagner\*

## Table of contents

1. Experimental details and characterization data .....	3
1.1 Diboration reactions with M[ <b>3</b> ] .....	4
1.2 Silaboration reactions with <b>2</b> (thf) and <b>9</b> (thf) .....	10
1.3 Synthesis of <b>14</b> .....	14
1.4 Synthesis of <b>18</b> (thf) and treatment with ethylene or 3,3-dimethyl-but-1-yne.....	16
2. Plots of the NMR spectra .....	20
3. X-ray crystal structure determinations .....	57
3.1 Single-crystal X-ray analysis of [K(thf) <sub>2</sub> ][ <b>5</b> ] .....	64
3.2 Single-crystal X-ray analysis of [K(thf) <sub>2</sub> ][K(thf) <sub>3</sub> ][FluB( $\mu$ -CH <sub>2</sub> CH <sub>2</sub> )( $\mu$ -OH)BFlu] <sub>2</sub> .....	65
3.3 Single-crystal X-ray analysis of [K(thf) <sub>2</sub> ][ <b>11</b> ] <sub>0.73</sub> [ <b>12</b> ] <sub>0.27</sub> .....	66
3.4 Single-crystal X-ray analysis of [Li(thf) <sub>4</sub> ][ <b>12</b> ] .....	68
3.5 Single-crystal X-ray analysis of [K(thf) <sub>2</sub> ][ <b>16</b> ] .....	69
3.6 Single-crystal X-ray analysis of <b>6</b> (thf).....	70
3.7 Single-crystal X-ray analysis of <b>10</b> (thf).....	71
3.8 Single-crystal X-ray analysis of <b>13</b> .....	72
3.9 Single-crystal X-ray analysis of <b>14</b> .....	73
3.10 Single-crystal X-ray analysis of <b>17</b> .....	74
3.11 Single-crystal X-ray analysis of <b>20</b> .....	75
4. Computational details.....	76
4.1 <sup>13</sup> C NMR-shift calculations of [ <b>5</b> ] <sup>-</sup> and [ <b>S4</b> ] <sup>-</sup> .....	80
4.2 Rearrangement mechanism of the anion [ <b>3</b> <sup>C</sup> ] <sup>-</sup> .....	82
4.3 Diboration mechanisms of ethylene with [ <b>3</b> <sup>C</sup> ] <sup>-</sup> .....	84
4.4 Silaboration mechanisms of ethylene with <b>2</b> (thf) .....	87
4.5 Computed F <sup>-</sup> -ion affinities .....	89
4.6 Intrinsic bond orbital calculations .....	90
4.7 Natural bond orbital calculations.....	92
4.8 Corrected free energy values of computed compounds .....	93
5. References .....	104

## 1. Experimental details and characterization data

**General considerations:** All reactions, manipulations, and analyses were carried out under an atmosphere of dry argon in a glovebox or by applying standard Schlenk techniques. THF, Et<sub>2</sub>O, and C<sub>6</sub>H<sub>6</sub> were dried over Na/benzophenone; *n*-hexane was dried over Na without benzophenone. THF-*d*<sub>8</sub> and C<sub>6</sub>D<sub>6</sub> were dried over Na-K alloy without benzophenone (2–3 d). Prior to use, the solvents were distilled from the drying agent, degassed by applying three freeze-pump-thaw cycles, and stored over activated molecular sieves (3 Å). 3,3-Dimethyl-but-1-ene and 3,3-dimethyl-but-1-yne were degassed by applying three freeze-pump-thaw cycles and stored over activated molecular sieves (3 Å) prior to use. Before the ethylene was condensed onto the sample, it was passed through a U-shaped tube cooled to –78 °C to remove traces of water. Cl(H)Ph<sub>2</sub> was dried over CaH<sub>2</sub>, distilled, and degassed by applying three freeze-pump-thaw cycles prior to use. The compounds M[**3**] (M = Li or K),<sup>S1</sup> Na[**4**],<sup>S2</sup> **9**(thf),<sup>S2</sup> FluB–CH<sub>2</sub>–CH<sub>2</sub>–BFlu (**S1**),<sup>S3</sup> Cl(H)SiFlu (**15**),<sup>S2</sup> and (HBFlu)<sub>2</sub><sup>S4</sup> were synthesized according to literature procedures (EFlu = 2,7-di-*tert*-butyl-9-heterofluorene; E = B, Si).

Unless stated otherwise, the NMR spectra were recorded at 298 K using Bruker Avance II 300, or Avance III 500 HD spectrometers; NMR samples were investigated in flame-sealed NMR tubes. Chemical shift values are referenced to (residual) solvent signals (<sup>1</sup>H/<sup>13</sup>C{<sup>1</sup>H}); THF-*d*<sub>8</sub>: δ = 3.58/67.21 ppm or external BF<sub>3</sub>·Et<sub>2</sub>O (<sup>11</sup>B/<sup>1</sup>B{<sup>1</sup>H}) and SiMe<sub>4</sub> (<sup>29</sup>Si).<sup>S5</sup> Abbreviations: s = singlet, d = doublet, dd = doublet of doublets, t = triplet, vt = virtual triplet, m = multiplet, br = broad, br d = broad doublet, n.r. = multiplet expected in the NMR spectrum but not resolved. NMR signals of hydrogen atoms bonded to boron atoms (i.e. B(μ-H)B) were in some cases broadened beyond detection due to the quadrupolar relaxation of boron. However, in the single-crystal X-ray structure analysis of the respective compounds, these hydrogen atoms could be unequivocally located in the difference Fourier maps and freely refined. Resonances of carbon or silicon atoms attached to boron atoms were typically broadened and could sometimes be localized only via <sup>1</sup>H-<sup>13</sup>C- and <sup>1</sup>H-<sup>29</sup>Si-HMBC NMR experiments, respectively, due to the quadrupolar relaxation of boron. Whenever the two phenylene rings within the same bora- or silafluorene unit have different chemical shift values due to lack of symmetry, the corresponding hydrogen/carbon atoms were labeled “ X ” and “ X' ”. However, it was not possible to determine, which of the two phenylene rings is the one with or without the index, so this assignment is interchangeable.

The salts M[**3**], M[**5**] (M = Li or K), and Na[**4**] are formed as THF solvates, which were typically dried in a dynamic vacuum (oil pump; approximately 10<sup>-3</sup> torr, room temperature, 10 to 20 min). After this drying process, the number of remaining THF molecules typically varies between individual samples and with respect to the THF content of corresponding single-crystalline material (cf. the X-ray crystal structure analyses). It is therefore advisable to determine the individual THF content of each sample by means of <sup>1</sup>H NMR spectroscopy. Whenever a molecule (e.g. THF) serves as a ligand, its acronym is written in lower case letters (e.g. thf).

## 1.1 Diboration reactions with M[3]

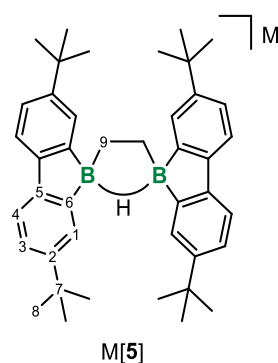
### Reaction of M[3] with ethylene to give M[5]:

*General procedure:* In an NMR tube, M[3] was dissolved in THF-*d*<sub>8</sub> (0.55 mL). The NMR tube was cooled with N<sub>2</sub>(liq) to -196 °C and an excess of dried ethylene was condensed onto the frozen solution. After removal of the cooling bath, the NMR tube was slowly allowed to reach room temperature. The NMR tube was gently shaken to promote absorption of ethylene by the solution. At this point, the previously yellow solution decolorized. Subsequently, the NMR tube was cooled again to -196 °C, evacuated, and flame-sealed. <sup>1</sup>H and <sup>11</sup>B NMR spectra recorded after 15 min at room temperature revealed that M[3] had vanished and one new compound, M[5], had selectively formed. The sample was evaporated to dryness under reduced pressure.

*Note:* It is essential to use carefully dried ethylene (cf. the general considerations), because otherwise M[5] may be contaminated with the corresponding B(μ-OH)B hydrolysis product (see Figure S8 and Figure S66).

[Li(thf)<sub>3</sub>][5]: [Li(thf)<sub>3</sub>][3] (40 mg, 52 μmol); yield: 41 mg (51 μmol, 99 %; colorless oil).

[K(thf)<sub>2</sub>][5]: [K(thf)<sub>2</sub>][3] (40 mg, 54 μmol); yield: 42 mg (54 μmol, 99 %; colorless solid). Colorless single crystals of [K(thf)<sub>2</sub>][5] suitable for X-ray diffraction were grown through gas-phase diffusion of *n*-hexane into a concentrated THF solution of K[5] at ambient temperature while maintaining inert conditions.



#### NMR shift values of Li[5]:

<sup>1</sup>H NMR (300.0 MHz, THF-*d*<sub>8</sub>): δ = 8.13 (dd, <sup>4</sup>J<sub>H,H</sub> = 2.1 Hz, <sup>5</sup>J<sub>H,H</sub> = 0.6 Hz, 4H; H-1), 7.25 (dd, <sup>3</sup>J<sub>H,H</sub> = 7.9 Hz, <sup>5</sup>J<sub>H,H</sub> = 0.6 Hz, 4H; H-4), 7.01 (dd, <sup>3</sup>J<sub>H,H</sub> = 7.9 Hz, <sup>4</sup>J<sub>H,H</sub> = 2.1 Hz, 4H; H-3), 1.44 (br, 4H; H-9), 1.38 (s, 36H; H-8). A signal assignable to the B(μ-H)B atom was not observed.

<sup>11</sup>B NMR (160.5 MHz, THF-*d*<sub>8</sub>): δ = 8.5 (*h*<sub>1/2</sub> ≈ 420 Hz).

<sup>13</sup>C{<sup>1</sup>H} NMR (125.8 MHz, THF-*d*<sub>8</sub>): δ = 158.4 (br; C-6), 146.9 (C-5), 146.9 (C-2), 128.5 (C-1), 122.7 (C-3), 117.4 (C-4), 35.1 (C-7), 32.5 (C-8), 15.3 (br; C-9).

NMR shift values of K[5]:

**<sup>1</sup>H NMR (300.0 MHz, THF-*d*<sub>8</sub>):**  $\delta$  = 8.13 (d, <sup>4</sup>*J*<sub>H,H</sub> = 1.9 Hz, 4H; H-1), 7.29 (d, <sup>3</sup>*J*<sub>H,H</sub> = 7.9 Hz, 4H; H-4), 7.04 (dd, <sup>3</sup>*J*<sub>H,H</sub> = 7.9 Hz, <sup>4</sup>*J*<sub>H,H</sub> = 1.9 Hz, 4H; H-3), 1.47 (br, 4H; H-9), 1.38 (s, 36H; H-8). A signal assignable to the B( $\mu$ -H)B atom was not observed.

**<sup>11</sup>B NMR (160.5 MHz, THF-*d*<sub>8</sub>):**  $\delta$  = 9.3 (*h*<sub>1/2</sub>  $\approx$  480 Hz).

**<sup>13</sup>C{<sup>1</sup>H} NMR (125.8 MHz, THF-*d*<sub>8</sub>):**  $\delta$  = 157.8 (br; C-6), 147.2 (C-5), 146.8 (C-2), 128.5 (C-1), 123.1 (C-3), 117.7 (C-4), 35.1 (C-7), 32.4 (C-8), 15.2 (br; C-9).

**Control reaction of FluB–CH<sub>2</sub>–CH<sub>2</sub>–BFlu (S1) with Li[Et<sub>3</sub>BH] to give Li[5]:**

In an NMR tube, S1(thf) (21 mg, 32  $\mu$ mol) was dissolved in THF (0.55 mL). Li[Et<sub>3</sub>BH] (1 M in THF, 29.1  $\mu$ L, 29.1  $\mu$ mol) was added at room temperature, whereupon the previously yellow solution almost decolorized. All volatiles were removed under reduced pressure and the pale yellow solid was redissolved in THF-*d*<sub>8</sub> (0.55 mL). <sup>1</sup>H and <sup>11</sup>B NMR spectroscopy revealed that S1(thf) had vanished and one new main product, Li[5] ( $\approx$  80 % selectivity), had formed (see Figure S4).

### Reaction of M[3] with 3,3-dimethyl-but-1-ene to give M[11] and M[12]:

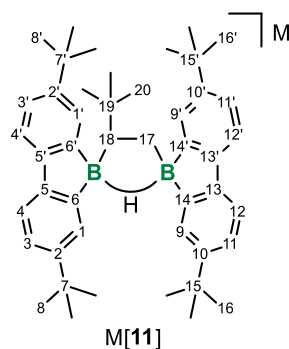
*General procedure:* In an NMR tube, M[3] was dissolved in THF-*d*<sub>8</sub> (0.55 mL). 3,3-Dimethyl-but-1-ene was added at room temperature, whereupon the previously yellow solution almost decolorized. <sup>1</sup>H and <sup>11</sup>B NMR spectra recorded after 15 min revealed that 90 % of M[3] had vanished and two new compounds, M[11] and M[12] (stoichiometry 10:1), had formed. A complete conversion to these two products was observed after *n* d (Li<sup>+</sup> salt: *n* = 3; K<sup>+</sup> salt: *n* = 1); the product ratio remained unchanged. Upon heating the flame-sealed NMR tube to 50 °C for *n* d (Li<sup>+</sup> salt: *n* = 3; K<sup>+</sup> salt: *n* = 5), a rearrangement of the major product M[11] (which vanishes completely) to the previously minor product M[12] takes places with ≈ *m* % selectivity (Li<sup>+</sup> salt: *m* = 80; K<sup>+</sup> salt: *m* = 95; <sup>1</sup>H and <sup>11</sup>B NMR spectroscopy).

Li[11]/Li[12]: [Li(thf)<sub>3</sub>][3] (12 mg, 15 μmol), 3,3-dimethyl-but-1-ene (2.0 μL, 15 μmol).

K[11]/K[12]: [K(thf)<sub>2</sub>][3] (14 mg, 19 μmol), 3,3-dimethyl-but-1-ene (2.5 μL, 19 μmol). Colorless single crystals of [K(thf)<sub>2</sub>]{[11]<sub>0.73</sub>[12]<sub>0.27</sub>} suitable for X-ray diffraction were grown at ambient temperature through gas-phase diffusion of *n*-hexane into the reaction mixture (inert conditions); note that at no time this sample was exposed to temperatures higher than room temperature.

*Alternative procedure for the synthesis of Li[12]:* In an NMR tube, [Li(thf)<sub>3</sub>][3] (11 mg, 14 μmol) was dissolved in C<sub>6</sub>D<sub>6</sub> (0.55 mL). 3,3-Dimethyl-but-1-ene (1.8 μL, 14 μmol) was added at room temperature; the solution maintained its yellow color. <sup>1</sup>H and <sup>11</sup>B NMR spectra revealed that Li[3] had vanished and one new main product, Li[12] (≈ 70 % selectivity), had formed. After the addition of *n*-hexane (0.5 mL), the reaction solution was cooled to −30 °C, resulting in the precipitation of Li[12] as a yellow microcrystalline solid after 1 d. The mother liquor was removed via syringe and the solid residue dried under reduced pressure.

Yellow single crystals of [Li(thf)<sub>4</sub>][12] suitable for X-ray diffraction were grown through gas-phase diffusion of *n*-hexane into a concentrated THF solution of Li[12] at ambient temperature while maintaining inert conditions.



NMR shift values of Li[11]:

**$^1\text{H}$  NMR (500.2 MHz, THF- $d_8$ ):**  $\delta$  = 8.55 (d,  $^4J_{\text{H,H}} = 2.0$  Hz, 1H; H-9), 8.50 (d,  $^4J_{\text{H,H}} = 2.0$  Hz, 1H; H-1'), 7.86 (d,  $^4J_{\text{H,H}} = 2.0$  Hz, 1H; H-9'), 7.82 (d,  $^4J_{\text{H,H}} = 2.0$  Hz, 1H; H-1), 7.32–7.29 (m, 2H; H-4' and H-12), 7.22–7.19 (m, 2H; H-4 and H-12'), 7.11–7.08 (m, 2H; H-3' and H-11), 6.92–6.88 (m, 2H; H-3 and H-11'), 2.49 (dd,  $^3J_{\text{H,H}} = 14.5$  Hz,  $^3J_{\text{H,H}} = 5.9$  Hz, 1H; H-18), 1.84 (dd,  $^2J_{\text{H,H}} = 10.8$  Hz,  $^3J_{\text{H,H}} = 14.5$  Hz, 1H; H-17a), 1.50 / 1.49 / 1.27 / 1.27 (4  $\times$  s, 4  $\times$  9H; H-8, H-8', H-16, and H-16'), 0.98–0.93 (m, 1H; H-17b), 0.71 (s, 9H; H-20). A signal assignable to the B( $\mu$ -H)B atom was not observed.

**$^{11}\text{B}$  NMR (160.5 MHz, THF- $d_8$ ):**  $\delta$  = 8.9, 6.1.

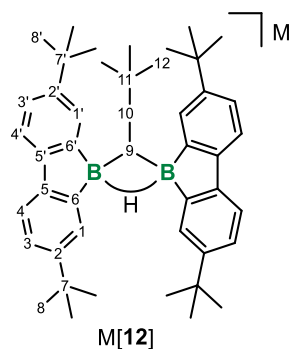
**$^{13}\text{C}\{^1\text{H}\}$  NMR (125.8 MHz, THF- $d_8$ ):**  $\delta$  = 159.2 (br; C-14), 158.5 (br; C-6), 157.5 (br; C-14'), 156.3 (br; C-6'), 147.8 (C-5'), 147.3 (C-13), 147.0 (C-2 or C-2' or C-10 or C-10'), 147.0 (C-13'), 146.6 (C-2 or C-2' or C-10 or C-10'), 146.6 (C-5), 146.2 (C-2 or C-2' or C-10 or C-10'), 145.8 (C-2 or C-2' or C-10 or C-10'), 131.7 (C-1'), 129.1 (C-9'), 129.0 (C-1), 128.2 (C-9), 123.1 (C-11), 123.0 (C-3'), 122.1 (C-11'), 121.9 (C-3), 117.8 (C-4'), 117.7 (C-12), 117.0 (C-4), 116.9 (C-12'), 41.1 (br; C-18), 35.3 (C-19), 35.1 / 35.1 / 35.0 / 35.0 (C-7, C-7', C-15, and C-15'), 32.5 / 32.5 / 32.4 (C-8, C-8', C-16, and C-16'), 31.2 (C-20), 17.0 (br; C-17).

NMR shift values of K[11]:

**$^1\text{H}$  NMR (500.2 MHz, THF- $d_8$ ):**  $\delta$  = 8.55 (n.r., 1H; H-9), 8.50 (d,  $^4J_{\text{H,H}} = 2.0$  Hz, 1H; H-1'), 7.87 (n.r., 1H; H-9'), 7.84 (d,  $^4J_{\text{H,H}} = 2.0$  Hz, 1H; H-1), 7.37–7.33 (m, 2H; H-4' and H-12), 7.29–7.24 (m, 2H; H-4 and H-12'), 7.16–7.11 (m, 2H; H-3' and H-11), 7.00–6.94 (m, 2H; H-3 and H-11'), 2.53 (dd,  $^3J_{\text{H,H}} = 14.6$  Hz,  $^3J_{\text{H,H}} = 5.9$  Hz, 1H; H-18), 1.89 (dd,  $^2J_{\text{H,H}} = 10.9$  Hz,  $^3J_{\text{H,H}} = 14.6$  Hz, 1H; H-17a), 1.50 / 1.49 / 1.27 / 1.27 (4  $\times$  s, 4  $\times$  9H; H-8, H-8', H-16, and H-16'), 1.04–0.98 (m, 1H; H-17b), 0.75 (s, 9H; H-20). A signal assignable to the B( $\mu$ -H)B atom was not observed.

**$^{11}\text{B}$  NMR (160.5 MHz, THF- $d_8$ ):**  $\delta$  = 9.8, 6.1.

**$^{13}\text{C}\{^1\text{H}\}$  NMR (125.8 MHz, THF- $d_8$ ):**  $\delta$  = 158.2 (br; C-14), 157.7 (br; C-6), 156.7 (br; C-14'), 155.5 (br; C-6'), 147.6 (C-5'), 147.5 (C-10 or C-10'), 147.3 (C-10 or C-10'), 147.3 (C-2 or C-2'), 147.0 (C-13'), 146.9 (C-13), 146.4 (C-2 or C-2'), 146.0 (C-5), 131.6 (C-1'), 128.9 (C-9'), 128.8 (C-1), 128.2 (C-9), 123.6 (C-11), 123.5 (C-3'), 122.8 (C-11'), 122.5 (C-3), 118.2 (C-4'), 118.1 (C-12), 117.5 (C-12'), 117.4 (C-4), 41.1 (br; C-18), 35.3 (C-19), 35.2 / 35.1 / 35.1 / 35.0 (C-7, C-7', C-15, and C-15'), 32.4 / 32.4 / 32.3 (C-8, C-8', C-16, and C-16'), 31.1 (C-20), 16.6 (br; C-17).



NMR shift values of Li[12]:

**$^1\text{H}$  NMR (500.2 MHz, THF- $d_8$ ):**  $\delta$  = 8.16 (d,  $^4J_{\text{H,H}} = 1.5$  Hz, 2H; H-1), 8.05 (d,  $^4J_{\text{H,H}} = 1.6$  Hz, 2H; H-1'), 7.44 (d,  $^3J_{\text{H,H}} = 7.9$  Hz, 2H; H-4), 7.42 (d,  $^3J_{\text{H,H}} = 7.9$  Hz, 2H; H-4'), 7.08–7.06 (m, 4H; H-3 and H-3'), 2.01 (br, 1H; BHB), 2.01 (d,  $^3J_{\text{H,H}} = 7.1$  Hz, 2H; H-10), 1.45 (s, 18H; H-8), 1.44 (s, 18H; H-8'), 0.97 (t,  $^3J_{\text{H,H}} = 7.1$  Hz, 1H; H-9), 0.53 (s, 9H; H-12).

**$^{11}\text{B}$  NMR (160.5 MHz, THF- $d_8$ ):**  $\delta$  = -13.4 ( $h_{1/2} \approx 360$  Hz).

**$^{13}\text{C}\{^1\text{H}\}$  NMR (125.8 MHz, THF- $d_8$ ):**  $\delta$  = 159.6 (br; C-6'), 157.2 (br; C-6), 148.1 (C-5), 147.5 (C-5'), 146.4 (C-2'), 145.9 (C-2), 130.5 (C-1), 127.9 (C-1'), 121.6 (C-3'), 121.4 (C-3), 117.7 (C-4), 117.6 (C-4'), 44.7 (C-10), 35.2 (C-7 or C-7'), 35.2 (C-7 or C-7'), 32.8 (C-11), 32.7 (C-8 or C-8'), 32.6 (C-8 or C-8'), 30.1 (C-12), 15.0 (br; C-9).

NMR shift values of K[12]:

**$^1\text{H}$  NMR (500.2 MHz, THF- $d_8$ ):**  $\delta$  = 8.18 (d,  $^4J_{\text{H,H}} = 2.0$  Hz, 2H; H-1), 8.07 (d,  $^4J_{\text{H,H}} = 2.0$  Hz, 2H; H-1'), 7.50 (d,  $^3J_{\text{H,H}} = 7.9$  Hz, 2H; H-4), 7.48 (d,  $^3J_{\text{H,H}} = 7.9$  Hz, 2H; H-4'), 7.13–7.11 (m, 4H; H-3 and H-3'), 2.01 (br, 1H; BHB), 2.00 (d,  $^3J_{\text{H,H}} = 7.1$  Hz, 2H; H-10), 1.45 (s, 18H; H-8), 1.44 (s, 18H; H-8'), 1.06 (t,  $^3J_{\text{H,H}} = 7.1$  Hz, 1H; H-9), 0.54 (s, 9H; H-12).

**$^{11}\text{B}$  NMR (160.5 MHz, THF- $d_8$ ):**  $\delta$  = -12.4 ( $h_{1/2} \approx 550$  Hz).

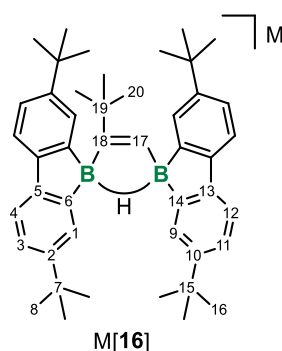
**$^{13}\text{C}\{^1\text{H}\}$  NMR (125.8 MHz, THF- $d_8$ ):**  $\delta$  = 159.0 (br; C-6'), 156.7 (br; C-6), 148.0 (C-5), 147.3 (C-5'), 147.0 (C-2'), 146.4 (C-2), 130.5 (C-1), 127.9 (C-1'), 122.1 (C-3'), 121.9 (C-3), 118.0 (C-4), 117.9 (C-4'), 44.8 (C-10), 35.3 (C-7 or C-7'), 35.2 (C-7 or C-7'), 32.7 (C-11), 32.6 (C-8 or C-8'), 32.6 (C-8 or C-8'), 30.1 (C-12), 15.7 (br; C-9).

### Reaction of M[BHB] with 3,3-dimethyl-but-1-yne to give M[16]:

*General procedure:* An NMR tube was charged with M[3]. 3,3-Dimethyl-but-1-yne was separately diluted with THF-*d*<sub>8</sub> (0.55 mL) and then transferred to the NMR tube, whereupon the reaction mixture turned orange. <sup>1</sup>H and <sup>11</sup>B NMR spectra recorded after 15 min revealed that M[3] had vanished and one new product, M[16], had selectively formed.

Li[16]: [Li(thf)<sub>3</sub>][3] (13 mg, 17 μmol), 3,3-dimethyl-but-1-yne (2.1 μL, 17 μmol).

K[16]: [K(thf)<sub>2</sub>][3] (40 mg, 54 μmol), 3,3-dimethyl-but-1-yne (6.7 μL, 54 μmol). Orange single crystals of [K(thf)<sub>2</sub>][16] suitable for X-ray diffraction were grown through gas-phase diffusion of *n*-hexane into a concentrated THF solution of K[16] at ambient temperature while maintaining inert conditions.



#### NMR shift values of Li[16]:

<sup>1</sup>H NMR (500.2 MHz, THF-*d*<sub>8</sub>):  $\delta$  = 7.99 (d, <sup>4</sup>J<sub>H,H</sub> = 2.0 Hz, 2H; H-9), 7.92 (d, <sup>4</sup>J<sub>H,H</sub> = 2.0 Hz, 2H; H-1), 7.27–7.23 (m, 4H; H-4 and H-12), 7.02–7.00 (m, 4H; H-3 and H-11), 6.05 (d, <sup>3</sup>J<sub>H,H</sub> = 8.2 Hz, 1H; H-17), 2.23 (br d, <sup>3</sup>J<sub>H,H</sub> = 8.2 Hz, 1H; BHB), 1.38 (s, 36H; H-8 and H-16), 0.86 (s, 9H; H-20).

<sup>11</sup>B NMR (160.5 MHz, THF-*d*<sub>8</sub>):  $\delta$  = 8.4 (*h*<sub>1/2</sub> ≈ 880 Hz).

<sup>13</sup>C{<sup>1</sup>H} NMR (125.8 MHz, THF-*d*<sub>8</sub>):  $\delta$  = 167.5 (br, C-18), 158.1 (br, C-6), 157.8 (br, C-14), 147.5 (C-5), 147.1 (C-13), 146.7 (C-2 or C-10), 146.6 (C-2 or C-10), 132.9 (br, C-17), 130.2 (C-9), 129.1 (C-1), 123.1 (C-3 or C-11), 122.7 (C-3 or C-11), 117.4 (C-4 or C-12), 117.4 (C-4 or C-12), 37.2 (C-19), 35.1 (C-7 and C-15), 32.5 (C-8 and C-16), 32.1 (C-20).

#### NMR shift values of K[16]:

<sup>1</sup>H NMR (500.2 MHz, THF-*d*<sub>8</sub>):  $\delta$  = 8.01 (d, <sup>4</sup>J<sub>H,H</sub> = 2.0 Hz, 2H; H-9), 7.94 (d, <sup>4</sup>J<sub>H,H</sub> = 2.0 Hz, 2H; H-1), 7.35–7.32 (m, 4H; H-4 and H-12), 7.10–7.08 (m, 4H; H-3 and H-11), 6.10 (d, <sup>3</sup>J<sub>H,H</sub> = 8.1 Hz, 1H; H-17), 2.18 (br d, <sup>3</sup>J<sub>H,H</sub> = 8.1 Hz, 1H; BHB), 1.40 (s, 36H; H-8 and H-16), 0.91 (s, 9H; H-20).

<sup>11</sup>B NMR (160.5 MHz, THF-*d*<sub>8</sub>):  $\delta$  = 6.8 (*h*<sub>1/2</sub> ≈ 730 Hz).

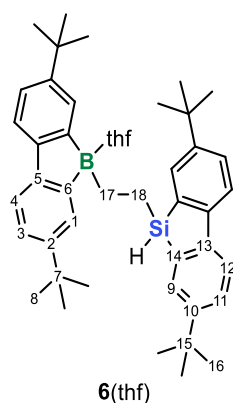
<sup>13</sup>C{<sup>1</sup>H} NMR (125.8 MHz, THF-*d*<sub>8</sub>):  $\delta$  = 167.6 (br, C-18), 157.0 (br, C-6), 156.8 (br, C-14), 147.5 (C-2 or C-10), 147.3 (C-2 or C-10), 147.2 (C-5 or C-13), 146.9 (C-5 or C-13), 132.6 (br, C-17), 129.9 (C-9), 129.0 (C-1), 123.8 (C-3 or C-11), 123.4 (C-3 or C-11), 118.0 (C-4 or C-12), 118.0 (C-4 or C-12), 37.3 (C-19), 35.2 (C-7 or C-15), 35.1 (C-7 or C-15), 32.4 (C-8 or C-16), 32.4 (C-8 or C-16), 32.0 (C-20).

## 1.2 Silaboration reactions with 2(thf) and 9(thf)

### Reaction of 2(thf) (generated in situ from Na[4]/Me<sub>3</sub>SiBr) with ethylene to give 6(thf):

In a flask fitted with a J. Young PTFE valve and an additional port capped with a rubber septum, [Na(thf)<sub>0.25</sub>][4] (120 mg, 196 μmol) was dissolved in THF (4 mL). The flask was cooled with N<sub>2</sub>(liq) to -196 °C and an excess of dried ethylene was condensed onto the frozen solution. The solution was then warmed to -78 °C and Me<sub>3</sub>SiBr (0.25 mL, 1.9 mmol) was added via a syringe through the septum. The slightly turbid colorless solution was stirred at -78 °C for 10 min and at room temperature for 20 min before all volatiles were removed under reduced pressure. <sup>1</sup>H and <sup>11</sup>B NMR spectroscopy revealed that Na[4] had vanished and one new main product, 6(thf) (90 % selectivity), had formed. The solid residue was again suspended in THF (4 mL) and insoluble salts were removed by using a syringe filter. Slow evaporation of the filtrate to dryness at ambient pressure and temperature while maintaining inert conditions gave 6(thf) as a colorless crystalline solid, which was washed with *n*-hexane (2 × 0.5 mL) and THF (0.2 mL) and subsequently dried in a dynamic vacuum. Yield: 75 mg (110 μmol, 56 %).

Colorless single crystals of 6(thf) · 2 THF suitable for X-ray diffraction were grown from a concentrated solution of 6(thf) in THF/*n*-hexane, which was slowly evaporated at ambient pressure and temperature while maintaining inert conditions.



<sup>1</sup>H NMR (500.2 MHz, THF-*d*<sub>8</sub>): δ = 7.75 (d, <sup>4</sup>J<sub>H,H</sub> = 2.1 Hz, 2H; H-9), 7.71 (d, <sup>3</sup>J<sub>H,H</sub> = 8.2 Hz, 2H; H-12), 7.52 (d, <sup>4</sup>J<sub>H,H</sub> = 2.0 Hz, 2H; H-1), 7.42 (dd, <sup>3</sup>J<sub>H,H</sub> = 8.2 Hz, <sup>4</sup>J<sub>H,H</sub> = 2.1 Hz, 2H; H-11), 7.40 (d, <sup>3</sup>J<sub>H,H</sub> = 7.9 Hz, 2H; H-4), 7.17 (dd, <sup>3</sup>J<sub>H,H</sub> = 7.9 Hz, <sup>4</sup>J<sub>H,H</sub> = 2.0 Hz, 2H; H-3), 4.68 (t, <sup>3</sup>J<sub>H,H</sub> = 3.5 Hz, 1H; SiH), 1.35 (s, 18H; H-16), 1.31 (s, 18H; H-8), 1.21–1.18 (m, 2H; H-17), 0.83–0.78 (m, 2H; H-18).

<sup>11</sup>B NMR (160.5 MHz, THF-*d*<sub>8</sub>): δ = 13.6 (*h*<sub>1/2</sub> ≈ 690 Hz).

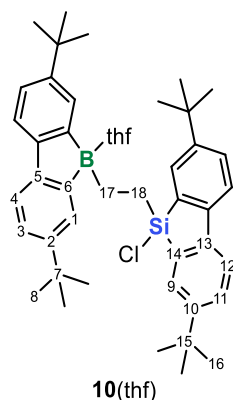
<sup>13</sup>C{<sup>1</sup>H} NMR (125.8 MHz, THF-*d*<sub>8</sub>): δ = 151.5 (br; C-6), 149.8 (C-10), 148.6 (C-2), 147.9 (C-5), 147.0 (C-13), 136.7 (C-14), 131.0 (C-9), 127.6 (C-1 and C-11), 124.6 (C-3), 120.8 (C-12), 118.7 (C-4), 35.0 (C-15), 34.9 (C-7), 31.9 (C-8), 31.6 (C-16), 13.8 (br; C-17), 6.4 (C-18).

<sup>29</sup>Si{<sup>1</sup>H} NMR (99.4 MHz, THF-*d*<sub>8</sub>): δ = -15.3.

### Reaction of **9**(thf) with ethylene to give **10**(thf):

In an NMR tube, **9**(thf) (40 mg, 59  $\mu\text{mol}$ ) was dissolved in THF- $d_8$  (0.55 mL). The NMR-tube was cooled with  $\text{N}_2(\text{liq})$  to  $-196\text{ }^\circ\text{C}$ , and an excess of dried ethylene was condensed onto the frozen solution. After removal of the cooling bath, the NMR tube was slowly allowed to reach room temperature. The NMR tube was gently shaken to promote absorption of ethylene by the solution. Subsequently, the NMR tube was cooled again to  $-196\text{ }^\circ\text{C}$ , evacuated, and flame-sealed.  $^1\text{H}$  and  $^{11}\text{B}$  NMR spectra recorded after 15 min at room temperature revealed that **9**(thf) had vanished and one new compound, **10**(thf), had selectively formed. The sample was evaporated to dryness under reduced pressure, furnishing **10**(thf) as a colorless solid. Yield: 40 mg (57  $\mu\text{mol}$ , 96 %).

Colorless single crystals of **10**(thf)  $\cdot$  1.5  $\text{Et}_2\text{O}$  suitable for X-ray diffraction were grown from a concentrated solution of **10**(thf) in  $\text{Et}_2\text{O}$ , which was slowly evaporated at ambient pressure and temperature while maintaining inert conditions.



$^1\text{H}$  NMR (500.2 MHz, THF- $d_8$ ):  $\delta = 7.72$  (d,  $^4J_{\text{H,H}} = 2.0$  Hz, 2H; H-9), 7.70 (d,  $^3J_{\text{H,H}} = 8.1$  Hz, 2H; H-12), 7.50 (d,  $^4J_{\text{H,H}} = 1.9$  Hz, 2H; H-1), 7.47 (dd,  $^3J_{\text{H,H}} = 8.1$  Hz,  $^4J_{\text{H,H}} = 2.0$  Hz, 2H; H-11), 7.40 (d,  $^3J_{\text{H,H}} = 7.9$  Hz, 2H; H-4), 7.17 (dd,  $^3J_{\text{H,H}} = 7.9$  Hz,  $^4J_{\text{H,H}} = 1.9$  Hz, 2H; H-3), 1.34 (s, 18H; H-16), 1.31 (s, 18H; H-8), 1.23–1.20 (m, 2H; H-17), 1.00–0.96 (m, 2H; H-18).

$^{11}\text{B}$  NMR (160.5 MHz, THF- $d_8$ ):  $\delta = 13.2$  ( $h_{1/2} \approx 640$  Hz).

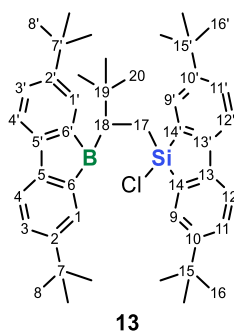
$^{13}\text{C}\{^1\text{H}\}$  NMR (125.8 MHz, THF- $d_8$ ):  $\delta = 151.1$  (br; C-6), 150.8 (C-10), 148.7 (C-2), 147.9 (C-5), 145.5 (C-13), 135.2 (C-14), 130.2 (C-9), 129.0 (C-11), 127.6 (C-1), 124.7 (C-3), 120.9 (C-12), 118.7 (C-4), 35.1 (C-15), 34.9 (C-7), 31.9 (C-8), 31.5 (C-16), 12.0 (br; C-17), 11.5 (C-18).

$^{29}\text{Si}\{^1\text{H}\}$  NMR (99.4 MHz, THF- $d_8$ ):  $\delta = 15.4$ .

### Reaction of 9(thf) with 3,3-dimethyl-but-1-ene to give 13:

An NMR tube was charged with **9**(thf) (15 mg, 22  $\mu\text{mol}$ ). 3,3-Dimethyl-but-1-ene (2.9  $\mu\text{L}$ , 22  $\mu\text{mol}$ ) was separately diluted with THF- $d_8$  (0.55 mL) and then transferred to the NMR tube, whereupon the reaction mixture turned yellow.  $^1\text{H}$  and  $^{11}\text{B}$  NMR spectra recorded after 15 min revealed that **9**(thf) had vanished and one new product, **13**, had selectively formed.

Yellow single crystals of **13** suitable for X-ray diffraction were grown from a concentrated solution of **13** in Et<sub>2</sub>O, which was slowly evaporated at ambient pressure and temperature while maintaining inert conditions.



**$^1\text{H}$  NMR (500.2 MHz, THF- $d_8$ , 243 K):**  $\delta$  = 7.83 (n.r., 1H; H-Ar<sup>BFlu</sup>), 7.81 (d,  $^4J_{\text{H,H}} = 2.1$  Hz, 1H; H-9), 7.72 (d,  $^3J_{\text{H,H}} = 8.2$  Hz, 1H; H-12), 7.57 (dd,  $^3J_{\text{H,H}} = 8.2$  Hz,  $^4J_{\text{H,H}} = 2.1$  Hz, 1H; H-11), 7.47 (d,  $^3J_{\text{H,H}} = 8.2$  Hz, 1H; H-12'), 7.26 (n.r., 1H; H-Ar<sup>BFlu</sup>), 7.21 (d,  $^4J_{\text{H,H}} = 2.1$  Hz, 1H; H-9'), 7.18\* (n.r., 1H; H-Ar<sup>BFlu</sup>), 7.17 (dd,  $^3J_{\text{H,H}} = 8.2$  Hz,  $^4J_{\text{H,H}} = 2.1$  Hz, 1H; H-11'), 7.12 (n.r., 1H; H-Ar<sup>BFlu</sup>), 7.04 (n.r., 1H; H-Ar<sup>BFlu</sup>), 6.76 (n.r., 1H; H-Ar<sup>BFlu</sup>), 2.11 (dd,  $^2J_{\text{H,H}} = 15.0$  Hz,  $^3J_{\text{H,H}} = 11.6$  Hz, 1H; H-17a), 1.94 (dd,  $^2J_{\text{H,H}} = 15.0$  Hz,  $^3J_{\text{H,H}} = 2.2$  Hz, 1H; H-17b), 1.83\*\* (dd,  $^3J_{\text{H,H}} = 11.6$  Hz,  $^3J_{\text{H,H}} = 2.2$  Hz, 1H; H-18), 1.37 (s, 9H; H-16), 1.31 (s, 9H; H-8 or H-8'), 1.21 (s, 9H; H-8 or H-8'), 1.02 (s, 9H; H-16'), 0.87 (s, 9H; H-20). \*) The signal overlaps with the signal assigned to H-11', but the chemical-shift value can be confirmed in the  $^1\text{H}$ - $^{13}\text{C}$ -HSQC NMR experiment; \*\*) The signal partially overlaps with the signal assigned to residual THF- $h_8$ ; BFlu = 2,7-di-*tert*-butyl-9-borafluorene.

**$^{11}\text{B}$  NMR (160.5 MHz, THF- $d_8$ , 243 K):**  $\delta$  = n.o.

**$^{13}\text{C}\{^1\text{H}\}$  NMR (125.8 MHz, THF- $d_8$ , 243 K):**  $\delta$  = 151.6 (br; C-Ar<sup>BFlu</sup>), 151.0 (C-10), 150.2 (C-10'), 150.0\* (br; 2  $\times$  C-Ar<sup>BFlu</sup>), 149.4 (br; C-Ar<sup>BFlu</sup>), 145.9 (C-13 or C-13'), 145.9 (C-13 or C-13'), 144.8 (br; C-6), 143.7 (br; C-6'), 133.2 (br; C-Ar<sup>BFlu</sup>), 133.1 (C-14), 132.3 (C-14'), 130.4 (C-11'), 130.3 (C-9 or C-9'), 130.3 (C-9 or C-9'), 130.0 (br; C-Ar<sup>BFlu</sup>), 129.6\* (br; 2  $\times$  C-Ar<sup>BFlu</sup>), 129.3 (C-11), 121.2 (C-12), 121.0 (C-12'), 119.7 (br; C-Ar<sup>BFlu</sup>), 118.8 (br; C-Ar<sup>BFlu</sup>), 35.9 (br; C-18), 35.3 (C-15), 34.9\* (br; C-7 and C-7'), 34.8 (C-15'), 34.7 (C-19), 31.5 (C-16), 31.4 (C-8 or C-8'), 31.4 (C-8 or C-8'), 31.1 (C-16'), 30.6 (C-20), 15.5 (C-17). \*) The  $^1\text{H}$ - $^{13}\text{C}$ -HSQC and  $^1\text{H}$ - $^{13}\text{C}$ -HMBC NMR experiments indicate that the resonances can each be assigned to two different carbon atoms.

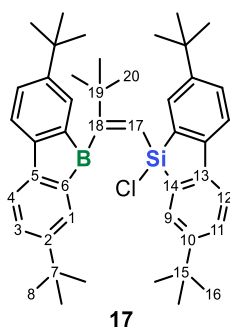
**$^{29}\text{Si}\{^1\text{H}\}$  NMR (99.4 MHz, THF- $d_8$ , 243 K):**  $\delta$  = 15.3.

*Note:* If the  $^1\text{H}$  and  $^{13}\text{C}\{^1\text{H}\}$  NMR spectra are measured at room temperature (298 K), all borafluorene signals are broadened beyond detection. Upon cooling the sample to 243 K, the signals sharpen to such an extent that their chemical shift values (but not their multiplicities) can be determined. A full assignment is, however, not possible. We attribute this phenomenon to an increased rotational barrier of the borafluorene unit (compared to **10**(thf)), which manifests itself in the observed coalescence phenomenon.

### Reaction of 9(thf) with 3,3-dimethyl-but-1-yne to give 17:

An NMR tube was charged with **9**(thf) (15 mg, 22  $\mu\text{mol}$ ). 3,3-Dimethyl-but-1-yne (2.7  $\mu\text{L}$ , 22  $\mu\text{mol}$ ) was separately diluted with THF- $d_8$  (0.55 mL) and then transferred to the NMR tube, whereupon the reaction mixture turned yellow.  $^1\text{H}$  and  $^{11}\text{B}$  NMR spectra recorded after 15 min revealed that **9**(thf) had vanished and one new product, **17**, had selectively formed.

Yellow single crystals of **17** suitable for X-ray diffraction were grown from a concentrated solution of **17** in *n*-hexane, which was slowly evaporated at ambient pressure and temperature while maintaining inert conditions.



$^1\text{H}$  NMR (500.2 MHz, THF- $d_8$ ):  $\delta$  = 7.53 (d,  $^4J_{\text{H,H}} = 2.1$  Hz, 2H; H-9), 7.49 (d,  $^3J_{\text{H,H}} = 8.1$  Hz, 2H; H-12), 7.35 (dd,  $^3J_{\text{H,H}} = 8.1$  Hz,  $^4J_{\text{H,H}} = 2.1$  Hz, 2H; H-11), 7.27 (d,  $^4J_{\text{H,H}} = 1.9$  Hz, 2H; H-1), 7.21 (dd,  $^3J_{\text{H,H}} = 7.8$  Hz,  $^4J_{\text{H,H}} = 1.9$  Hz, 2H; H-3), 7.07 (d,  $^3J_{\text{H,H}} = 7.8$  Hz, 2H; H-4), 6.43 (s, 1H; H-17), 1.21 (s, 18H; H-8 or H-16), 1.20 (s, 18H; H-8 or H-16), 1.14 (s, 9H; H-20).

$^{11}\text{B}$  NMR (160.5 MHz, THF- $d_8$ ):  $\delta$  = n.o.

$^{13}\text{C}\{^1\text{H}\}$  NMR (125.8 MHz, THF- $d_8$ ):  $\delta$  = 179.7 (br; C-18), 151.0 (C-2), 150.8 (C-5 or C-10), 150.8 (C-5 or C-10), 145.5 (C-13), 144.9 (br; C-6), 134.6 (C-14), 132.0 (C-1), 131.3 (C-3), 130.0 (C-9), 129.8 (C-11), 121.1 (C-12), 119.6 (C-4), 119.5 (C-17), 38.7 (C-19), 35.0 (C-15), 34.9 (C-7), 31.4 (C-8 or C-16), 31.4 (C-8 or C-16), 31.0 (C-20).

$^{29}\text{Si}\{^1\text{H}\}$  NMR (99.4 MHz, THF- $d_8$ ):  $\delta$  = 0.9.

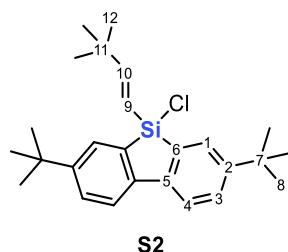
### 1.3 Synthesis of 14

#### Synthesis of S2:

Cl(H)SiFlu\* (**15**; 100 mg, 93 % w/w; 283  $\mu\text{mol}$ ) was placed in a Schlenk flask and dissolved in  $\text{C}_6\text{H}_6$  (2.0 mL). A mixture of 3,3-dimethyl-but-1-yne (60  $\mu\text{L}$ , 490  $\mu\text{mol}$ ) and platinum(0)-1,3-divinyl-1,1,3,3-tetramethyldisiloxane (Karstedt's catalyst; 10.0  $\mu\text{L}$  of a 2 % solution in xylene, 0.91  $\mu\text{mol}$ ; 0.3 mol%) was diluted with  $\text{C}_6\text{H}_6$  (1.0 mL) and then added dropwise with stirring to the silafluorene solution at room temperature *via* syringe. After stirring for 2 h, all volatiles were removed under reduced pressure to give a solid residue. According to integration of characteristic signals in the  $^1\text{H}$  NMR spectrum, the crude product consisted of **S2** and 4,4'-di-*tert*-butyl-biphenyl\* in a ratio of 10:1 (94 % w/w **S2**). Further purification was not performed at this point, as the impurity can be separated in the next step.

\*) In the synthesis of Cl(H)SiFlu (**15**), the non-separable side product 4,4'-di-*tert*-butyl-biphenyl may be formed by traces of adventitious HCl (*cf.* ref. S2). In the available batch, 4,4'-di-*tert*-butyl-biphenyl was present in a ratio of Cl(H)SiFlu : 4,4'-di-*tert*-butyl-biphenyl = 10:1 (93 % w/w Cl(H)SiFlu). According to our observations, this does not affect the hydrosilylation carried out in this study.

*Note:* Due to the comparatively large coupling constant of  $^3J_{\text{H,H}} = 18.8$  Hz between H-9 and H-10, we assume that only the *E* isomer is formed (as would be expected).



$^1\text{H}$  NMR (500.2 MHz,  $\text{C}_6\text{D}_6$ ):  $\delta = 7.94$  (d,  $^4J_{\text{H,H}} = 2.1$  Hz, 2H; H-1), 7.65 (d,  $^3J_{\text{H,H}} = 8.1$  Hz, 2H; H-4), 7.39 (dd,  $^3J_{\text{H,H}} = 8.1$  Hz,  $^4J_{\text{H,H}} = 2.1$  Hz, 2H; H-3), 6.89 (d,  $^3J_{\text{H,H}} = 18.8$  Hz, 1H; H-10), 5.93 (d,  $^3J_{\text{H,H}} = 18.8$  Hz, 1H; H-9), 1.20 (s, 18H; H-8), 0.86 (s, 9H; H-12).

$^{13}\text{C}\{^1\text{H}\}$  NMR (125.8 MHz,  $\text{C}_6\text{D}_6$ ):  $\delta = 165.6$  (C-10), 151.2 (C-2), 145.5 (C-5), 134.1 (C-6), 130.4 (C-1), 129.5 (C-3), 121.1 (C-4), 115.6 (C-9), 35.8 (C-11), 34.8 (C-7), 31.3 (C-8), 28.6 (C-12).

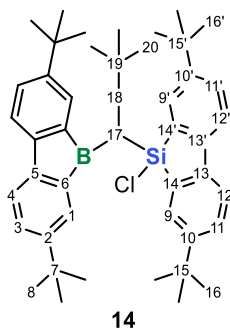
$^{29}\text{Si}\{^1\text{H}\}$  NMR (99.4 MHz,  $\text{C}_6\text{D}_6$ ):  $\delta = 3.2$ .

### Reaction of S2 with (HBFlu)<sub>2</sub> to give 14:

**S2** (60 mg, 94 % w/w, 137  $\mu\text{mol}$ ) was placed in a Schlenk flask and dissolved in  $\text{C}_6\text{H}_6$  (0.75 mL).  $(\text{HBFlu})_2$  (38 mg, 69  $\mu\text{mol}$ ) was dissolved separately in  $\text{C}_6\text{H}_6$  (0.75 mL) and the solution was added dropwise with stirring to the silafluorene solution at room temperature *via* syringe, whereupon the reaction mixture adopted a yellow color. The Schlenk flask was stored at 7  $^\circ\text{C}$ , resulting in the precipitation of **14** as a fine powder after 2 d. The mother liquor was removed *via* syringe and the yellow solid residue was dried under reduced pressure.

Yellow single crystals of **14**  $\cdot$  1.5  $\text{C}_6\text{H}_6$  suitable for X-ray diffraction were grown from a concentrated solution of **14** in  $\text{C}_6\text{H}_6$ , which was slowly evaporated at ambient pressure and temperature while maintaining inert conditions.

*Note:* The reaction in THF gives the same result, but the product **14** does not precipitate even at low temperatures, so that residual 4,4'-di-*tert*-butyl-biphenyl cannot be readily separated.



**<sup>1</sup>H NMR (500.2 MHz, THF-*d*<sub>8</sub>):**  $\delta$  = 7.64 (d,  $^3J_{\text{H,H}} = 7.8$  Hz, 1H; H-12 or H-12'), 7.61–7.59 (m, 2H; (H12 or H-12') and (H-9 or H-9')), 7.47 (n.r., 2H; H-1), 7.42–7.39 (m, 3H; H-11, H-11' and (H-9 or H-9')), 7.23 (dd,  $^3J_{\text{H,H}} = 7.7$  Hz,  $^4J_{\text{H,H}} = 1.9$  Hz, 2H; H-3), 7.18 (d,  $^3J_{\text{H,H}} = 7.7$  Hz, 2H; H-4), 2.72 (vt,  $^2J_{\text{H,H}} = 12.1$  Hz,  $^3J_{\text{H,H}} = 12.1$  Hz, 1H; H-18a), 2.65 (d,  $^3J_{\text{H,H}} = 12.1$  Hz, 1H; H-17), 2.52 (d,  $^2J_{\text{H,H}} = 12.1$  Hz, 1H; H-18b), 1.21 (s, 9H; H-16), 1.19 (s, 18H; H-8), 1.15 (s, 9H; H-16'), 0.84 (s, 9H; H-20).

**<sup>11</sup>B NMR (160.5 MHz, THF-*d*<sub>8</sub>):**  $\delta$  = 68.5 ( $h_{1/2} \approx 1080$  Hz).

**<sup>13</sup>C{<sup>1</sup>H} NMR (125.8 MHz, THF-*d*<sub>8</sub>):**  $\delta$  = 151.2 (br; C-5), 150.9 (C-10 or C-10'), 150.8 (C-10 or C-10'), 150.7 (br; C-2), 145.3 (C-13 or C-13'), 145.0 (C-13 or C-13'), 142.9 (br; C-6), 134.6 (C-14 or C-14'), 133.3 (C-14 or C-14'), 132.8 (br; C-1), 131.3 (C-9 or C-9'), 130.7 (br; C-3), 130.5 (C-9 or C-9'), 129.6 (C-11 or C-11'), 129.5 (C-11 or C-11'), 121.0 (C-12 or C-12'), 121.0 (C-12 or C-12'), 119.2 (C-4), 44.8 (C-18), 35.0 (C-15 or C-15'), 35.0 (C-15 or C-15'), 34.9 (C-7), 33.1 (C-19), 31.4 (C-8 and (C-16 or C-16')), 31.3 (C-16 or C-16'), 29.7 (C-20), 26.6 (br; C-17).

**<sup>29</sup>Si{<sup>1</sup>H} NMR (99.4 MHz, THF-*d*<sub>8</sub>):**  $\delta$  = 7.6.

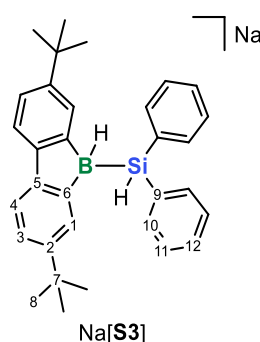
*Note:* If the <sup>1</sup>H NMR spectrum is measured at room temperature (298 K), only one set of signals is observed for both phenylene rings of the borafuorenyl moiety, whereas two sets of signals can be observed for the two phenylene rings of the silafluorenyl substituent. After cooling the sample to 243 K, the signals of the borafuorenyl moiety are broadened beyond detection. When the sample is heated to 331 K, the signal of H-1, in particular, sharpens significantly. We therefore conclude that the borafuorenyl moiety can rotate with a comparatively lower energy barrier than the silafluorenyl moiety. Moreover, at first glance, it is astonishing that H-17 has two such strongly different  $^3J_{\text{H,H}}$  coupling

constants ( $^3J_{\text{H,H}_a} = 12.1 \text{ Hz}$ ,  $^3J_{\text{H,H}_b} \approx 0 \text{ Hz}$ ). However, assuming that the conformation of the molecule in the solid state is due to sterics also maintained in solution, this phenomenon can be explained by the Karplus relation.

#### 1.4 Synthesis of 18(thf) and treatment with ethylene or 3,3-dimethyl-but-1-yne

##### Synthesis of Na[S3]:

(HBFlu)<sub>2</sub> (152 mg, 275 μmol) in THF (2.5 mL) was added to Na metal (399 mg, 17.4 mmol) in THF (2.5 mL) dropwise at  $-78 \text{ }^\circ\text{C}$  over a period of 30 min, whereupon the reaction mixture adopted a dark green color. Stirring was continued at  $-78 \text{ }^\circ\text{C}$  for 2 h and for 2 d at room temperature. The dark green solution of Na<sub>2</sub>[HBFlu] was separated from residual Na metal *via* syringe, placed in a separate Schlenk flask, and stirred (a largely complete transfer was achieved by THF rinses ( $2 \times 0.5 \text{ mL}$ )). In a glovebox, Cl(H)SiPh<sub>2</sub> (100 μL, 511 μmol) was diluted with THF (2.0 mL). The solution was added to the THF solution of Na<sub>2</sub>[HBFlu] dropwise at room temperature by using a syringe, whereupon the reaction mixture adopted a light brown color. All volatiles were removed under reduced pressure to give a solid residue. The residue was suspended in *n*-hexane (5 mL) and collected on a frit. The target product was rinsed from the frit by addition of THF (4 mL), while insoluble salts remained on the disc. All volatiles were removed from the filtrate under reduced pressure to afford [Na(thf)<sub>2</sub>][S3] as a light yellow solid. Yield: 239 mg (381 μmol, 75 %).



**<sup>1</sup>H NMR (500.2 MHz, THF-*d*<sub>8</sub>):**  $\delta = 7.57$  (d,  $^3J_{\text{H,H}} = 7.9 \text{ Hz}$ , 2H; H-4), 7.45–7.40 (m, 4H; H-10), 7.40 (n.r., 2H; H-1), 7.09–7.06 (m, 6H; H-11 and H-12), 7.03 (dd,  $^3J_{\text{H,H}} = 7.9 \text{ Hz}$ ,  $^4J_{\text{H,H}} = 2.1 \text{ Hz}$ , 2H; H-3), 4.16 (s, 1H; SiH), 2.58 (q,  $^1J_{\text{B,H}} = 84 \text{ Hz}$ , 1H; BH), 1.23 (s, 18H; H-8).

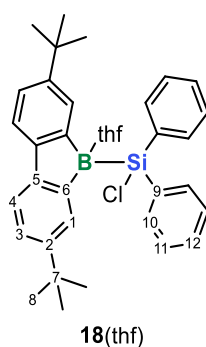
**<sup>11</sup>B NMR (160.5 MHz, THF-*d*<sub>8</sub>):**  $\delta = -22.7$  (d,  $^1J_{\text{B,H}} = 84 \text{ Hz}$ ).

**<sup>13</sup>C{<sup>1</sup>H} NMR (125.8 MHz, THF-*d*<sub>8</sub>):**  $\delta = 161.5$  (q,  $^1J_{\text{C,B}} = 48 \text{ Hz}$ ; C-6), 145.9 (C-5), 145.5 (C-2), 144.7 (C-9), 136.6 (C-10), 128.8 (C-1), 126.9 (C-11), 126.8 (C-12), 120.1 (C-3), 118.4 (C-4), 34.8 (C-7), 32.1 (C-8).

**<sup>29</sup>Si NMR (99.4 MHz, THF-*d*<sub>8</sub>):**  $\delta = -9.2$ .

### Synthesis of **18(thf)**:

In a Schlenk flask,  $[\text{Na}(\text{thf})_2][\mathbf{S3}]$  (301 mg, 480  $\mu\text{mol}$ ) was dissolved in THF (5 mL) and treated with neat  $\text{Me}_3\text{SiCl}$  (0.91 mL, 7.2 mmol) in one portion at room temperature, whereupon the reaction mixture adopted a light yellow color and a colorless solid slowly precipitated. The reaction mixture was stirred for 16 h at room temperature. An  $^1\text{H}$  and  $^{11}\text{B}$  NMR spectroscopic investigation revealed the formation of **18(thf)** with >95 % conversion. All volatiles were removed under reduced pressure to give a solid residue. The residue was suspended in *n*-hexane (4 mL) and collected on a frit. The target product was rinsed from the frit by addition of THF (5 mL), while insoluble salts remained on the disc. All volatiles were removed from the filtrate under reduced pressure to afford **18(thf)** as a light yellow solid. Yield: 175 mg (310  $\mu\text{mol}$ , 65 %).



$^1\text{H}$  NMR (500.2 MHz,  $\text{THF-}d_8$ ):  $\delta$  = 7.68 (dd,  $^4J_{\text{H,H}} = 2.0$  Hz,  $^5J_{\text{H,H}} = 0.7$  Hz, 2H; H-1), 7.41 (dd,  $^3J_{\text{H,H}} = 8.0$  Hz,  $^5J_{\text{H,H}} = 0.7$  Hz, 2H; H-4), 7.27–7.23 (m, 4H; H-10), 7.19 (dd,  $^3J_{\text{H,H}} = 8.0$  Hz,  $^4J_{\text{H,H}} = 2.0$  Hz, 2H; H-3), 7.17–7.13 (m, 2H; H-12), 7.08–7.04 (m, 4H; H-11), 1.29 (s, 18H; H-8).

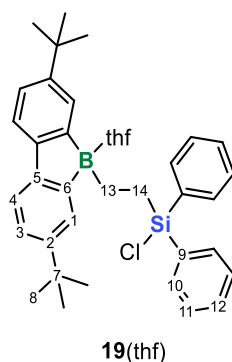
$^{11}\text{B}$  NMR (160.5 MHz,  $\text{THF-}d_8$ ):  $\delta$  = 7.5 ( $h_{1/2} \approx 410$  Hz).

$^{13}\text{C}\{^1\text{H}\}$  NMR (125.8 MHz,  $\text{THF-}d_8$ ):  $\delta$  = 149.2 (br; C-6), 148.5 (C-2), 147.0 (C-5), 139.1 (C-9), 135.3 (C-10), 129.8 (C-1), 129.1 (C-12), 127.6 (C-11), 124.6 (C-3), 119.1 (C-4), 35.0 (C-7), 31.8 (C-8).

$^{29}\text{Si}$  NMR (99.4 MHz,  $\text{THF-}d_8$ ):  $\delta$  = 9.9.

### Reaction of **18**(thf) with ethylene to give **19**(thf):

In an NMR tube, **18**(thf) (11 mg, 19  $\mu\text{mol}$ ) was dissolved in THF- $d_8$  (0.55 mL). The NMR-tube was cooled with  $\text{N}_2(\text{liq})$  to  $-196\text{ }^\circ\text{C}$  and an excess of dried ethylene was condensed onto the frozen solution. After removal of the cooling bath, the NMR tube was slowly allowed to reach room temperature. The NMR tube was gently shaken to promote absorption of ethylene by the solution. Subsequently, the NMR tube was cooled again to  $-196\text{ }^\circ\text{C}$ , evacuated, and flame-sealed.  $^1\text{H}$  and  $^{11}\text{B}$  NMR spectra recorded after 15 min at room temperature revealed that **18**(thf) had vanished and one new compound, **19**(thf), had selectively formed.



$^1\text{H}$  NMR (500.2 MHz, THF- $d_8$ ):  $\delta = 7.55\text{--}7.53$  (m, 4H; H-10), 7.52 (dd,  $^4J_{\text{H,H}} = 2.0$  Hz,  $^5J_{\text{H,H}} = 0.7$  Hz, 2H; H-1), 7.41 (dd,  $^3J_{\text{H,H}} = 7.9$  Hz,  $^5J_{\text{H,H}} = 0.7$  Hz, 2H; H-4), 7.37–7.33 (m, 2H; H-12), 7.32–7.28 (m, 4H; H-11), 7.19 (dd,  $^3J_{\text{H,H}} = 7.9$  Hz,  $^4J_{\text{H,H}} = 2.0$  Hz, 2H; H-3), 1.34 (s, 18H; H-8), 1.14–1.11 (m, 2H; H-13), 1.02–0.99 (m, 2H; H-14).

$^{11}\text{B}$  NMR (160.5 MHz, THF- $d_8$ ):  $\delta = 13.8$  ( $h_{1/2} \approx 690$  Hz).

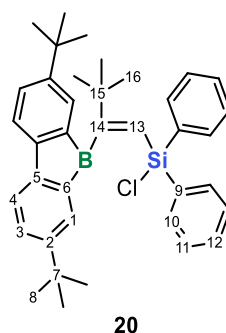
$^{13}\text{C}\{^1\text{H}\}$  NMR (125.8 MHz, THF- $d_8$ ):  $\delta = 151.3$  (br; C-6), 148.7 (C-2), 148.1 (C-5), 135.7 (C-9), 135.0 (C-10), 130.5 (C-12), 128.4 (C-11), 127.6 (C-1), 124.7 (C-3), 118.7 (C-4), 35.0 (C-7), 31.9 (C-8), 11.9 (br; C-13), 11.4 (C-14).

$^{29}\text{Si}$  NMR (99.4 MHz, THF- $d_8$ ):  $\delta = 13.3$ .

### Reaction of **18**(thf) with 3,3-dimethyl-but-1-yne to give **20**:

An NMR tube was charged with **18**(thf) (40 mg, 71  $\mu\text{mol}$ ). 3,3-Dimethyl-but-1-yne (8.8  $\mu\text{L}$ , 71  $\mu\text{mol}$ ) was separately diluted with THF- $d_8$  (0.55 mL) and then transferred to the NMR tube, whereupon the reaction mixture turned yellow.  $^1\text{H}$  and  $^{11}\text{B}$  NMR spectra recorded after 15 min revealed that **18**(thf) had vanished and one new product, **20**, had selectively formed.

Yellow single crystals of **20** suitable for X-ray diffraction were grown from a concentrated solution of **20** in *n*-hexane/THF, which was slowly evaporated at ambient pressure and temperature while maintaining inert conditions.



$^1\text{H}$  NMR (500.2 MHz, THF- $d_8$ ):  $\delta$  = 7.43–7.42 (m, 4H; H-10), 7.31 (d,  $^2J_{\text{H,H}} = 2.0$  Hz, 2H; H-1), 7.19–7.14 (m, 4H; H-3 and H-12), 7.08–7.05 (m, 4H; H-11), 6.99 (d,  $^3J_{\text{H,H}} = 7.8$  Hz, 2H; H-4), 6.55 (s, 1H; H-13), 1.27 (s, 18H; H-8), 1.21 (s, 9H; H-16).

$^{11}\text{B}$  NMR (160.5 MHz, THF- $d_8$ ):  $\delta$  = 68.8 ( $h_{1/2} \approx 1300$  Hz).

$^{13}\text{C}\{^1\text{H}\}$  NMR (125.8 MHz, THF- $d_8$ ):  $\delta$  = 180.5 (br; C-14), 151.0 (C-5), 150.8 (C-2), 144.9 (br, C-6), 136.1 (C-10), 133.9 (C-9), 132.8 (C-1), 131.1 (C-12), 130.7 (C-3), 128.2 (C-11), 121.7 (C-13), 119.3 (C-4), 38.9 (C-15), 35.0 (C-7), 31.4 (C-8), 31.1 (C-16).

$^{29}\text{Si}\{^1\text{H}\}$  NMR (99.4 MHz, THF- $d_8$ ):  $\delta$  = -2.9.

## 2. Plots of the NMR spectra

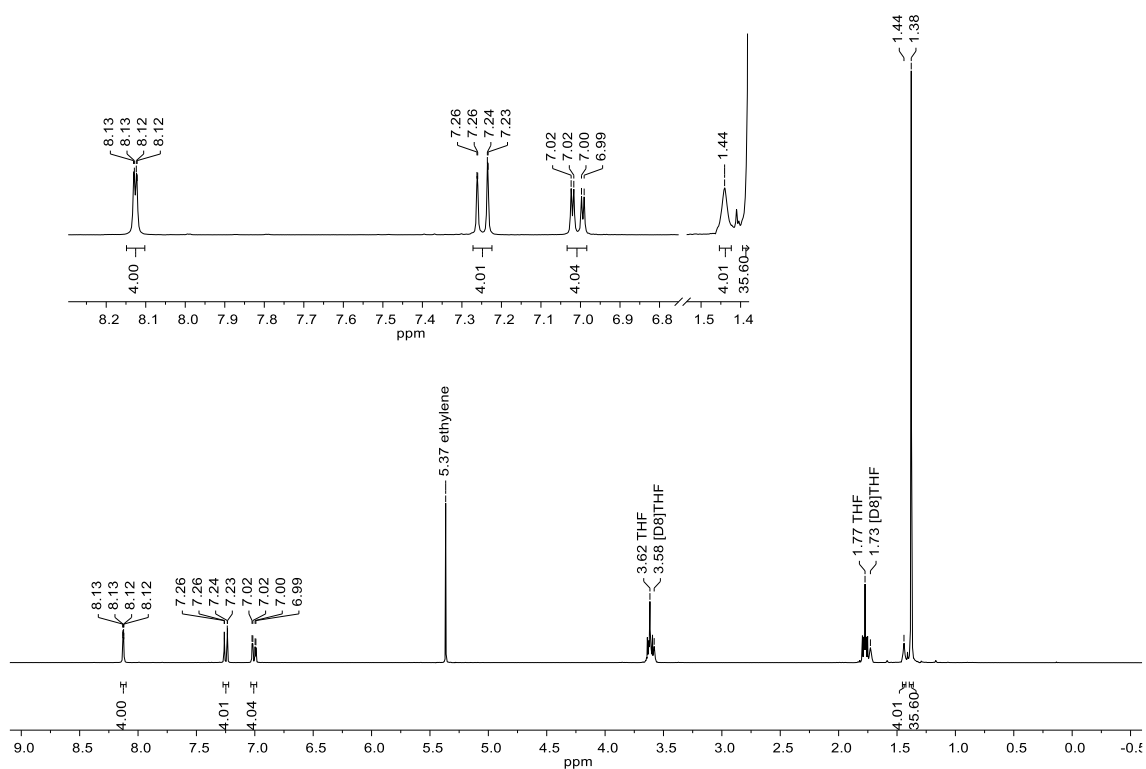


**Figure S1.**  $^1\text{H}$  NMR spectrum (300.0 MHz,  $\text{THF-}d_8$ ) of compound Li[5].

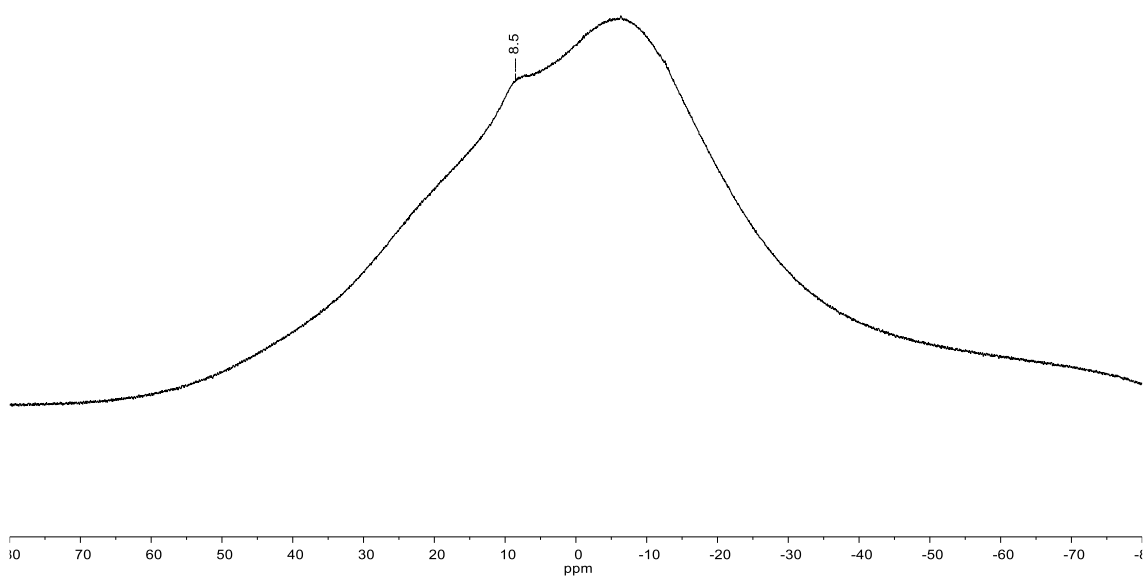


**Figure S2.**  $^{11}\text{B}$  NMR spectrum (160.5 MHz,  $\text{THF-}d_8$ ) of compound Li[5].

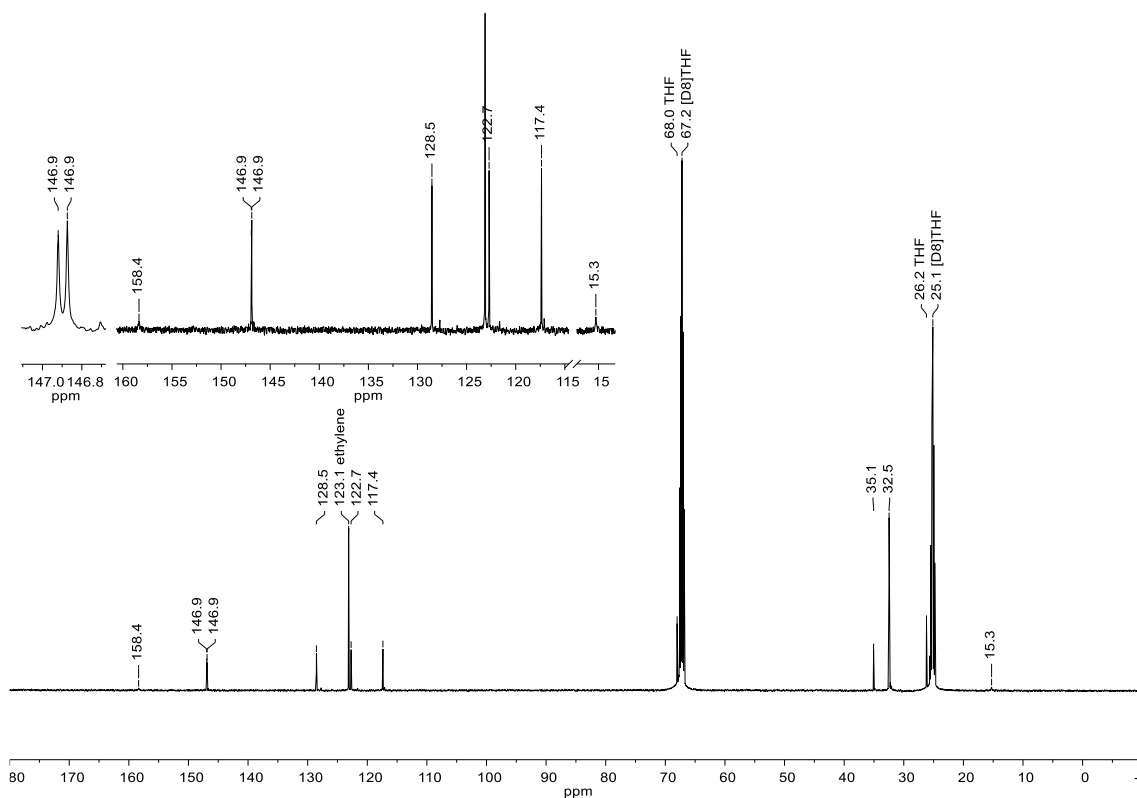


**Figure S3.**  $^{13}\text{C}$  NMR spectrum (125.8 MHz,  $\text{THF-}d_8$ ) of compound **Li[5]**.

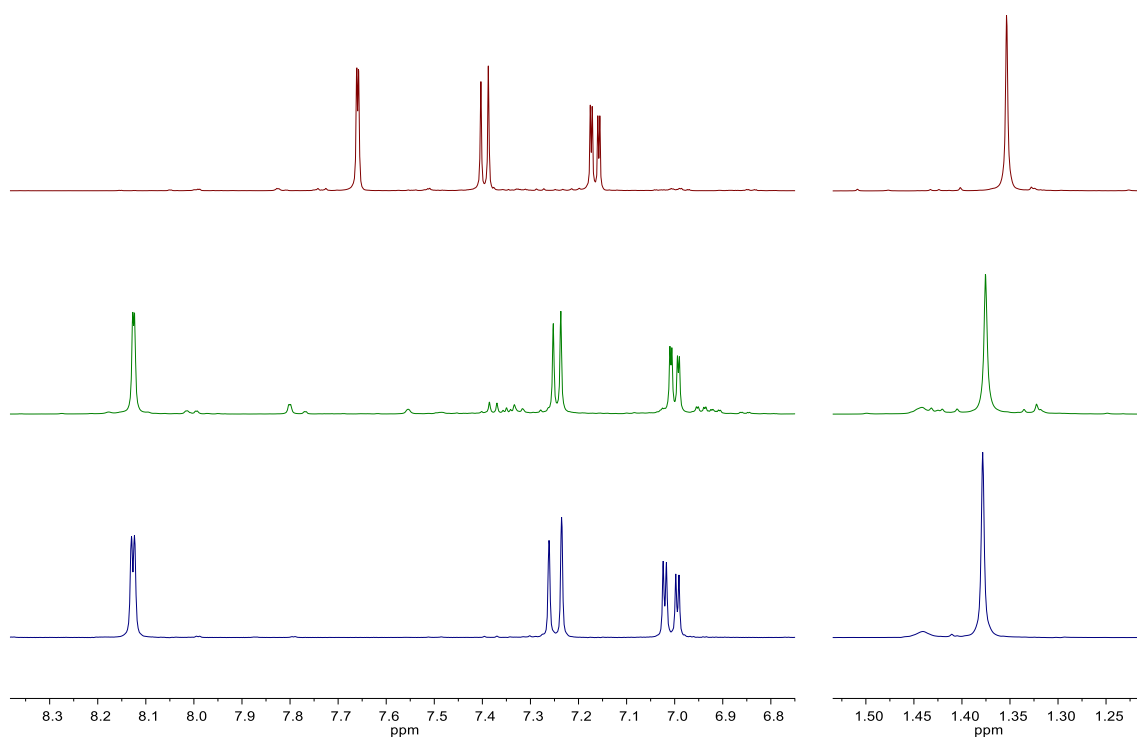


**Figure S4.** Characteristic sections of the  $^1\text{H}$  NMR spectra (top and middle: 500.2 MHz; bottom: 300.0 MHz; all in  $\text{THF-}d_8$ ) of compound **S2** (red, top), **Li[5]** prepared from **S2** and  $\text{Li}[\text{Et}_3\text{BH}]$  (green, middle), and **Li[5]** prepared from **Li[3]** and ethylene (blue, bottom). *Note:* The intensities of the aliphatic vs. aromatic signals are scaled differently.

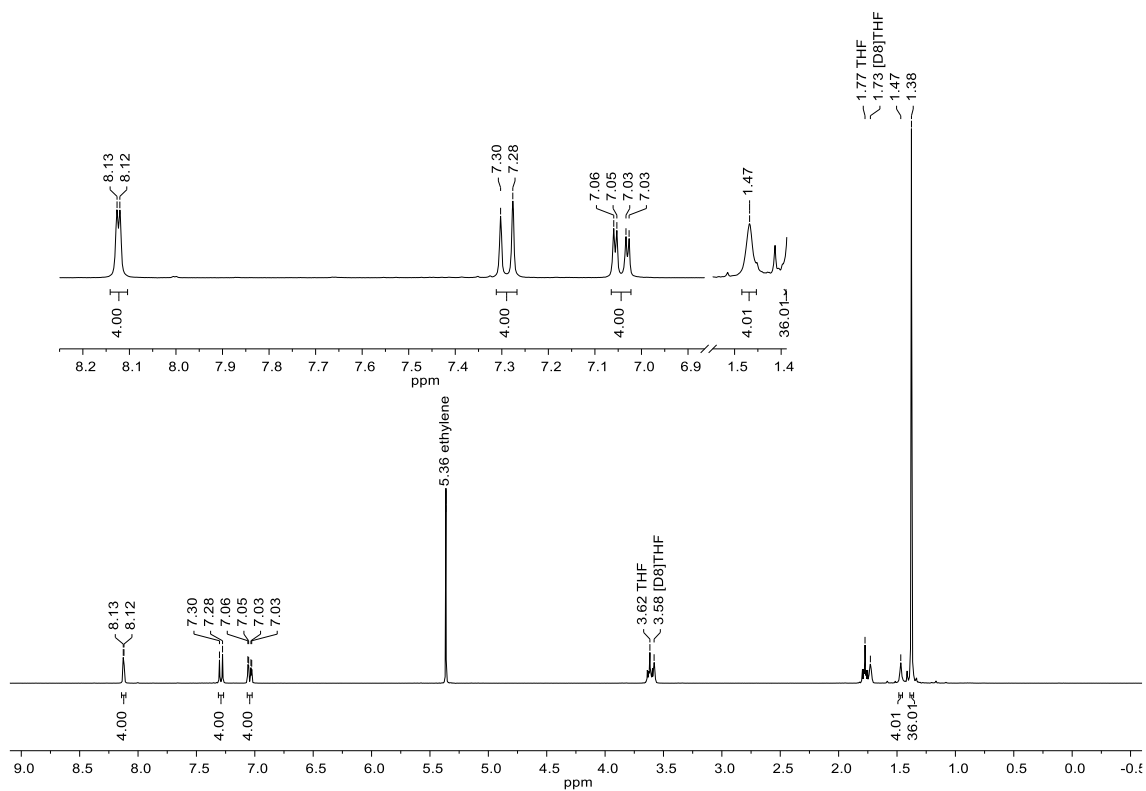


**Figure S5.**  $^1\text{H}$  NMR spectrum (300.0 MHz,  $\text{THF-}d_8$ ) of compound K[5].

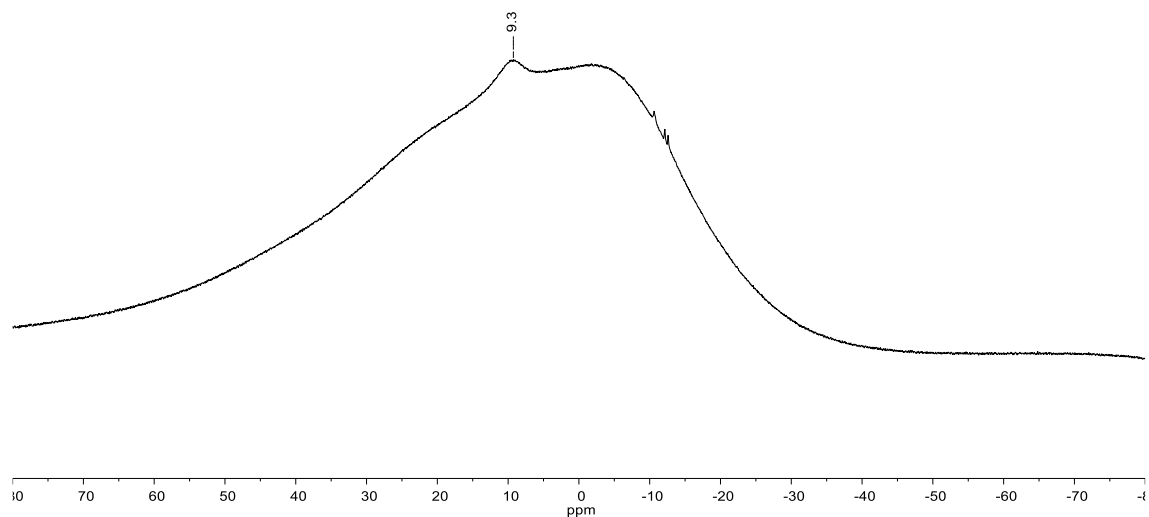


**Figure S6.**  $^{11}\text{B}$  NMR spectrum (160.5 MHz,  $\text{THF-}d_8$ ) of compound K[5].

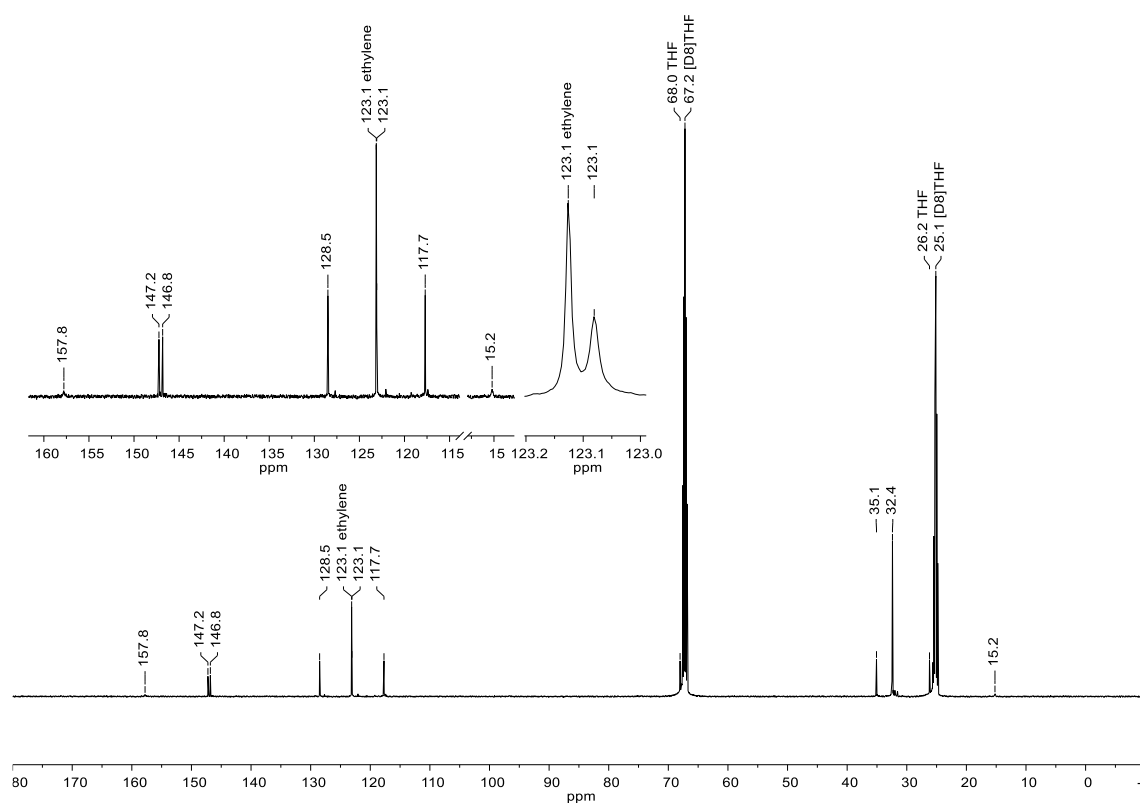


**Figure S7.**  $^{13}\text{C}$  NMR spectrum (125.8 MHz,  $\text{THF-}d_8$ ) of compound K[5].

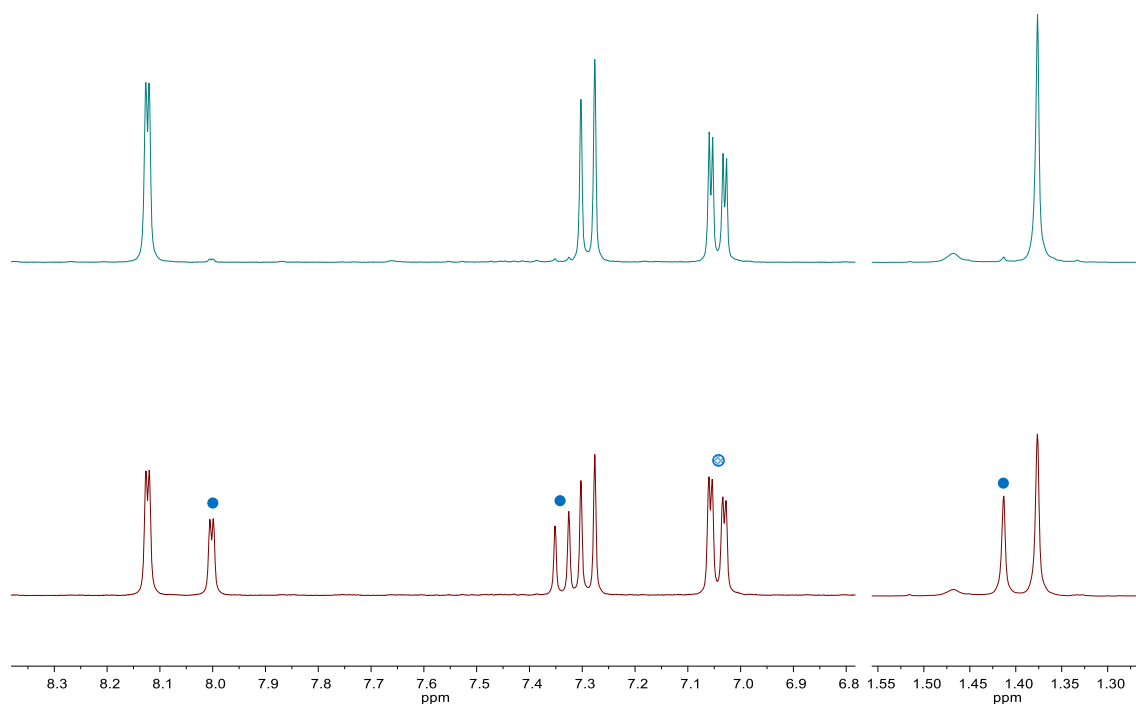


**Figure S8.** Characteristic sections of the  $^1\text{H}$  NMR spectra (300.0 MHz,  $\text{THF-}d_8$ ) from reaction mixtures for which either dried (green, top) or undried (red, bottom) ethylene was used in the course of the reaction. *Note:* The intensities of the aliphatic vs. aromatic signals are scaled differently. Observed side product: likely  $\text{K}[\text{FluB}(\mu\text{-OH})(\text{C}_2\text{H}_4)\text{BFlu}]$  (•; BFlu = 2,7-di-*tert*-butyl-9-borafluorene; see also Scheme S66).

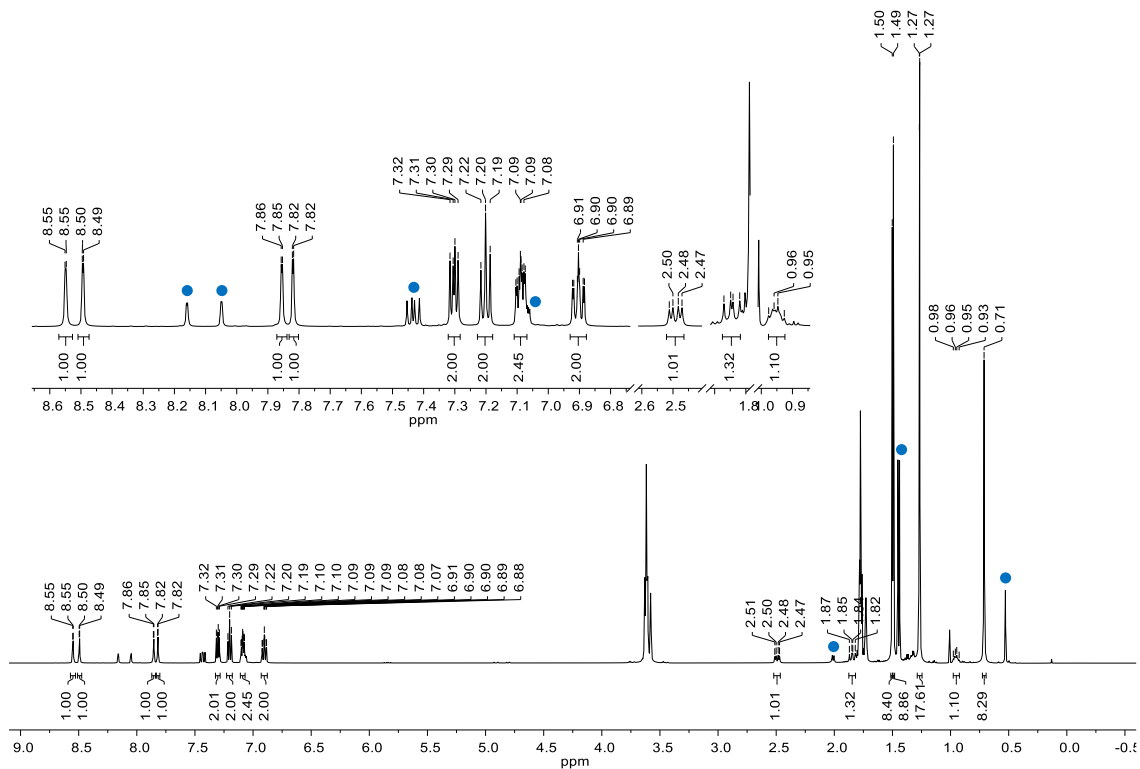


**Figure S9.**  $^1\text{H}$  NMR spectrum (500.2 MHz,  $\text{THF-}d_8$ ) of compound  $\text{Li}[11]$ . Observed minor component:  $\text{Li}[12]$  (●).

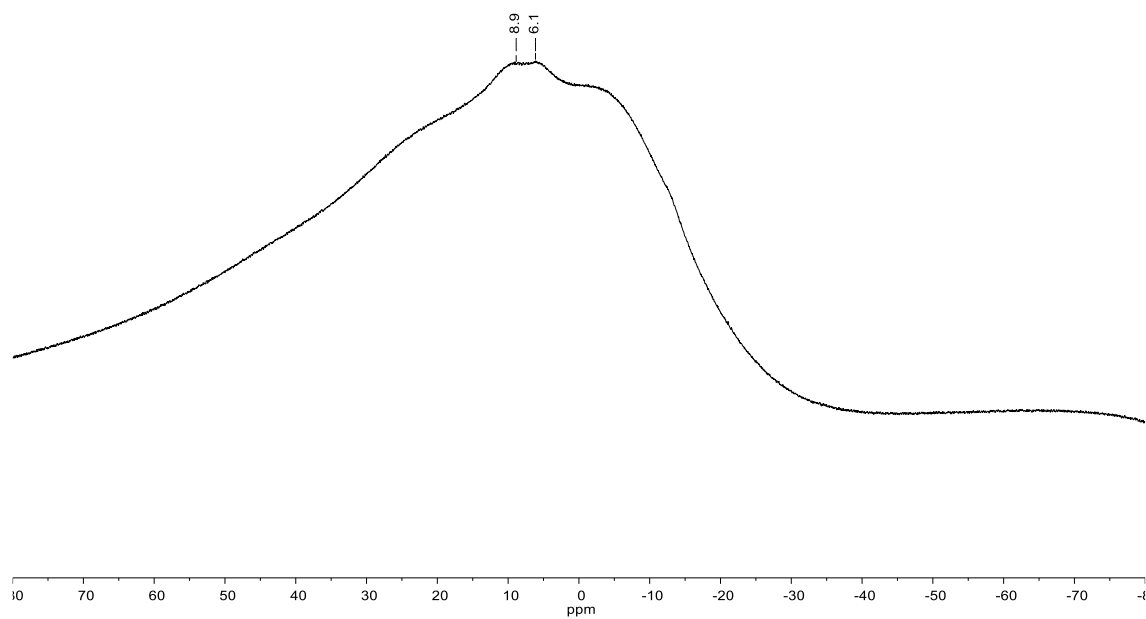


**Figure S10.**  $^{11}\text{B}$  NMR spectrum (160.5 MHz,  $\text{THF-}d_8$ ) of compound  $\text{Li}[11]$ .

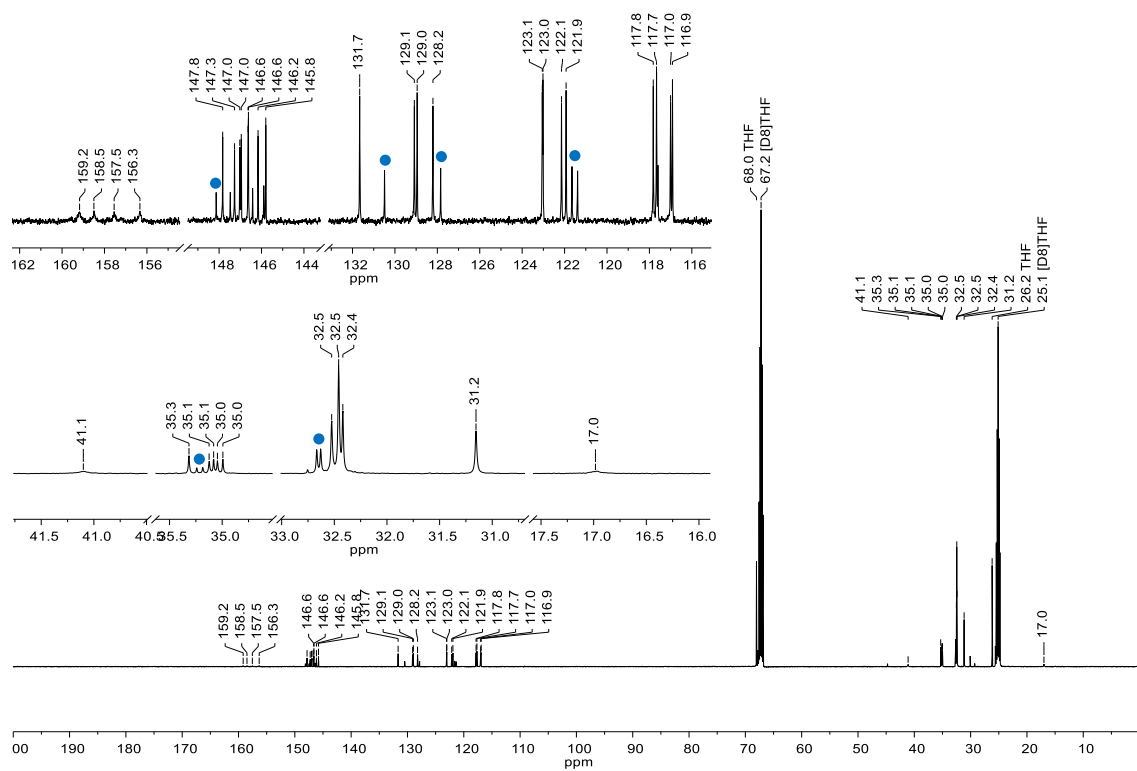


**Figure S11.**  $^{13}\text{C}$  NMR spectrum (125.8 MHz,  $\text{THF-}d_8$ ) of compound Li[11]. Observed minor component: Li[12] (●).

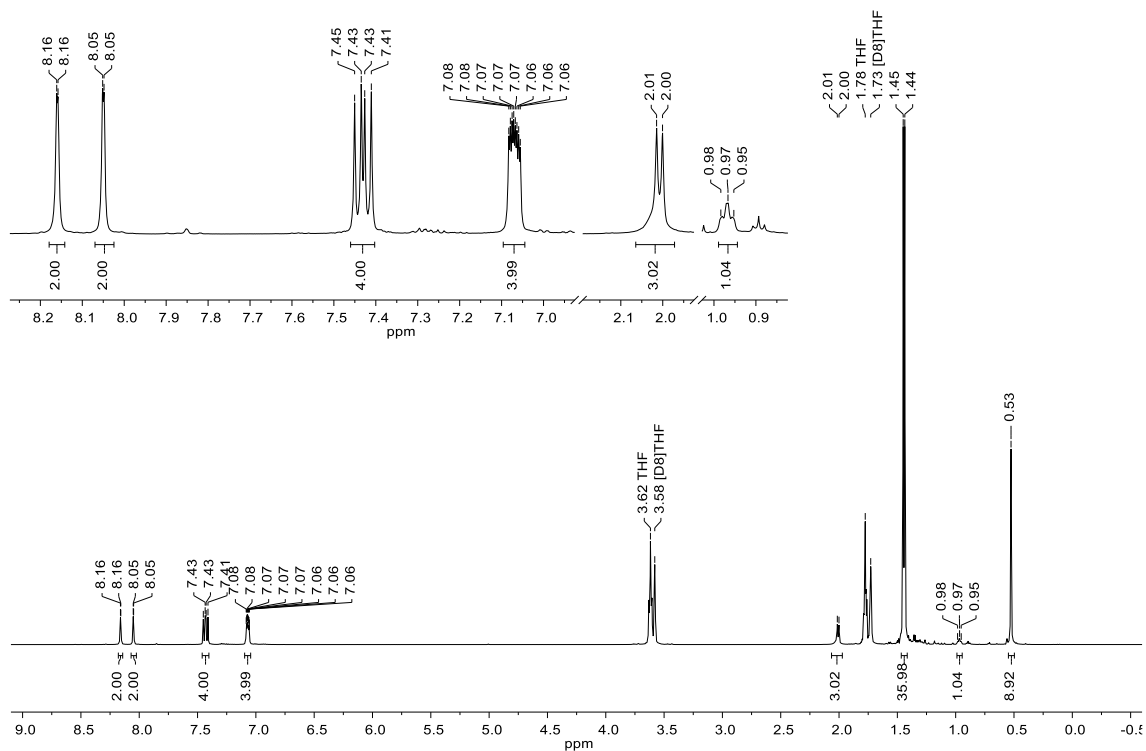


**Figure S12.**  $^1\text{H}$  NMR spectrum (500.2 MHz,  $\text{THF-}d_8$ ) of compound Li[12].

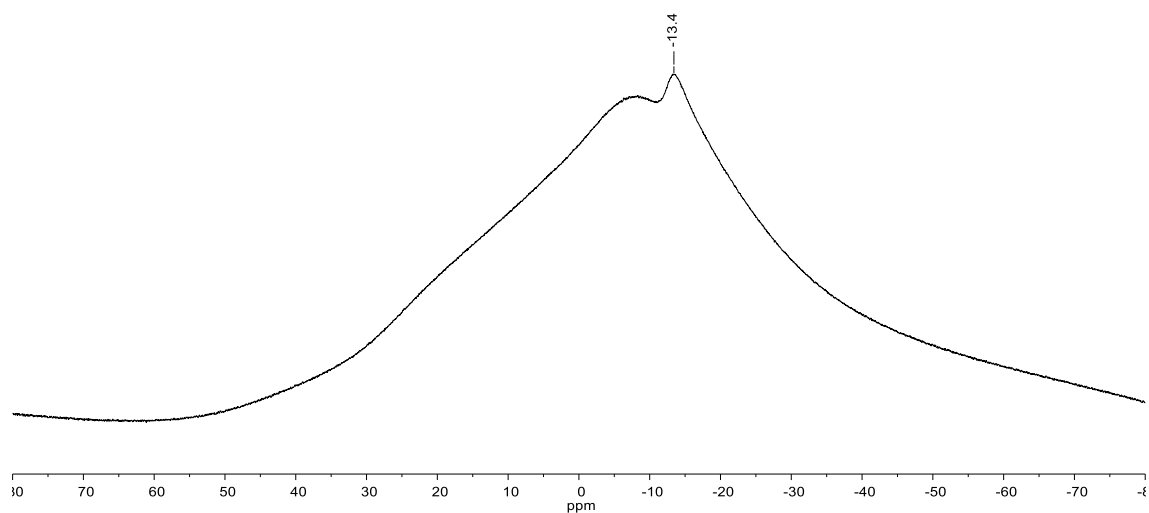


**Figure S13.**  $^{11}\text{B}$  NMR spectrum (160.5 MHz,  $\text{THF-}d_8$ ) of compound Li[12].

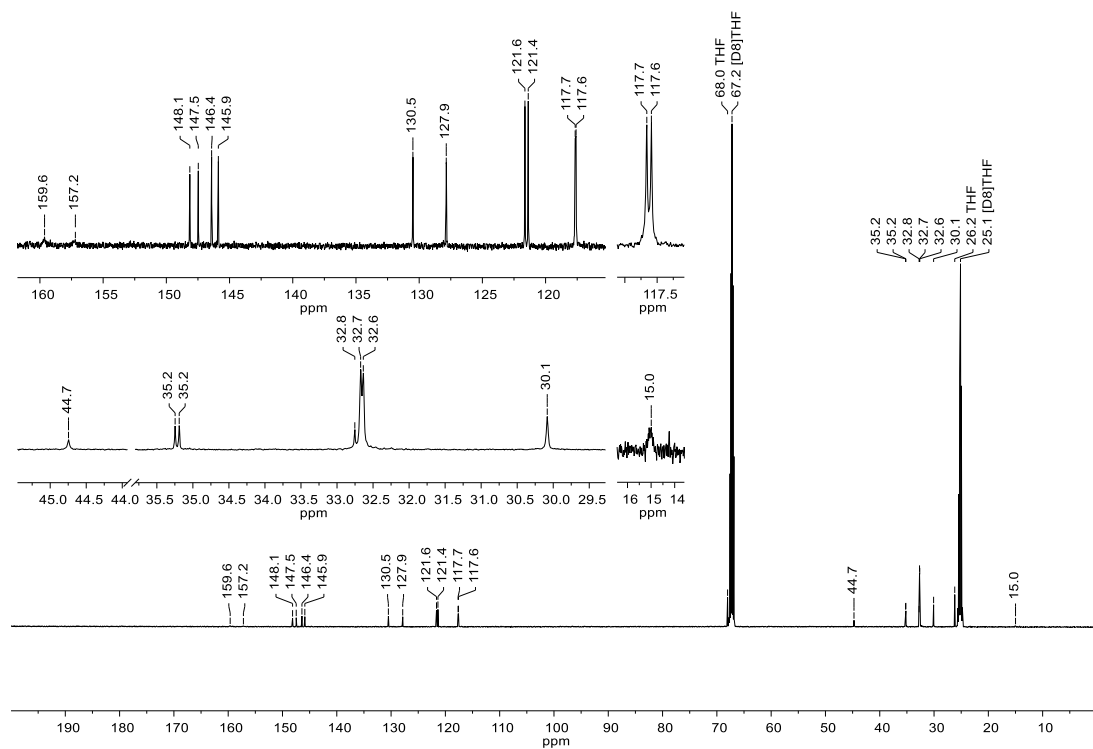


**Figure S14.**  $^{13}\text{C}$  NMR spectrum (125.8 MHz,  $\text{THF-}d_8$ ) of compound Li[12].

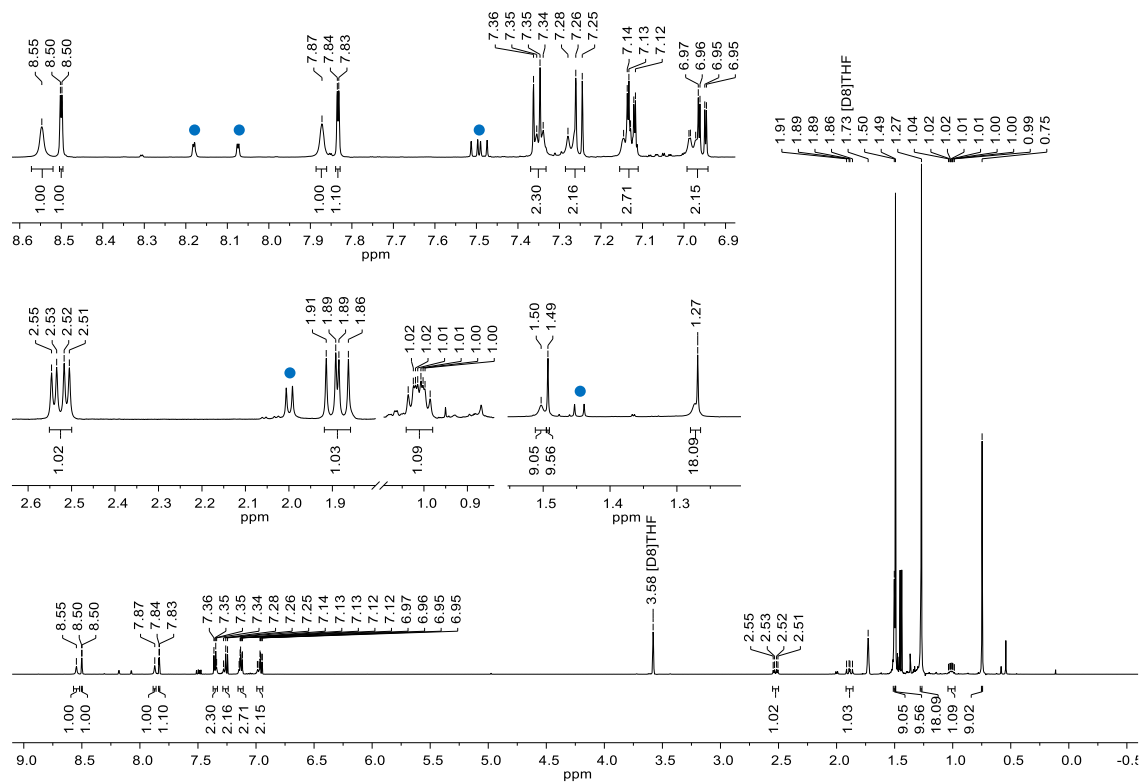


**Figure S15.**  $^1\text{H}$  NMR spectrum (500.2 MHz,  $\text{THF-}d_8$ ) of compound K[11]. Observed minor component: K[12] (●).

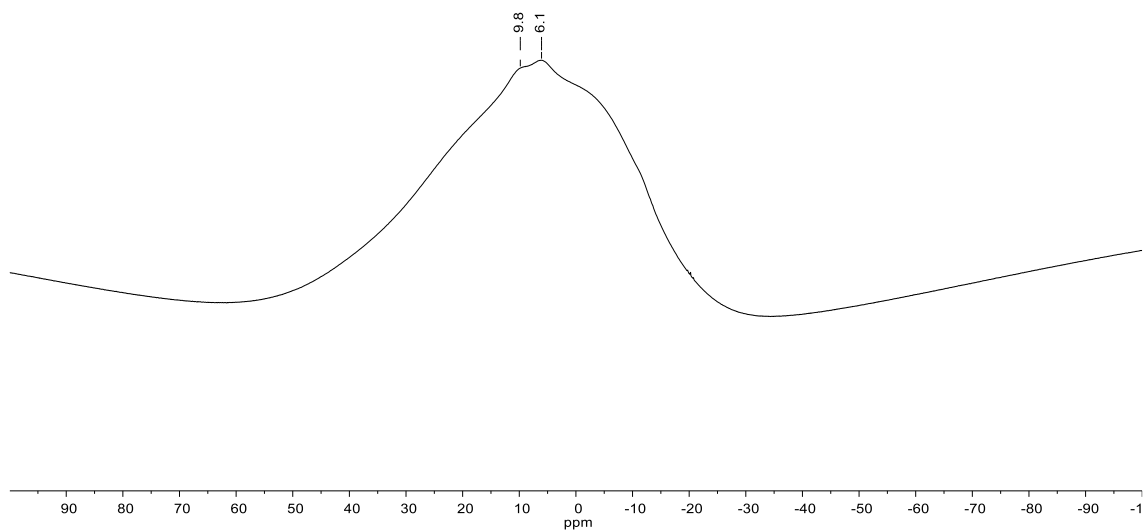


**Figure S16.**  $^{11}\text{B}$  NMR spectrum (160.5 MHz,  $\text{THF-}d_8$ ) of compound K[11].

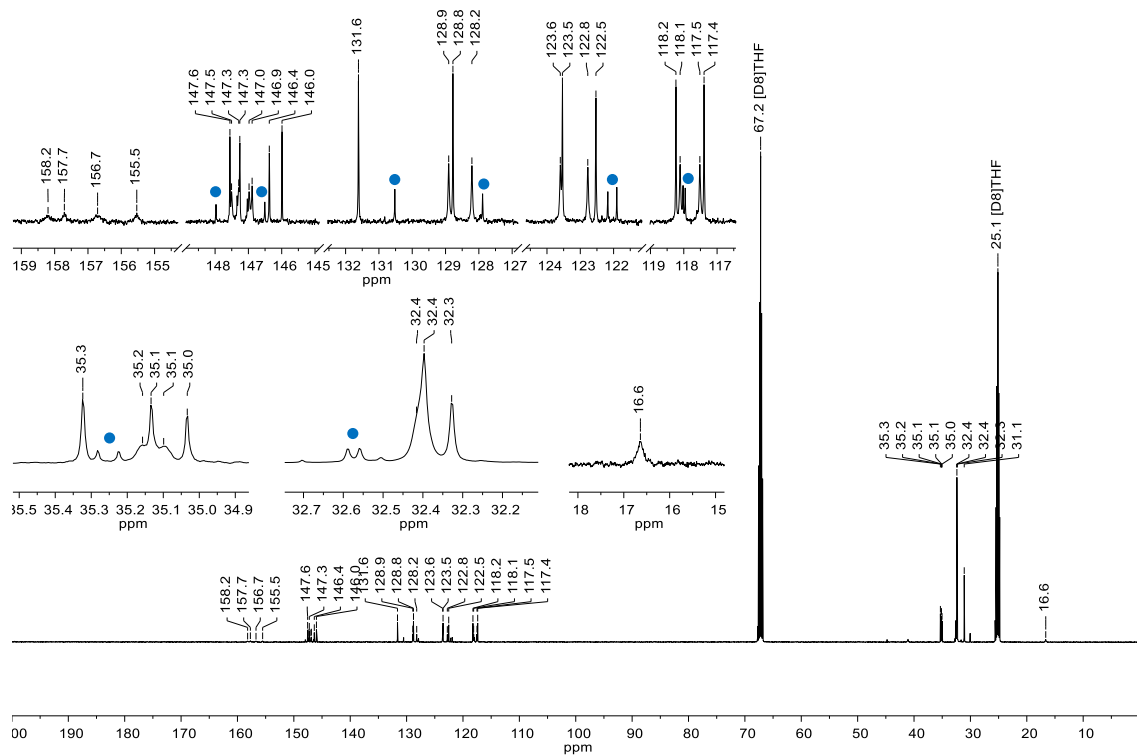


**Figure S17.**  $^{13}\text{C}$  NMR spectrum (125.8 MHz,  $\text{THF-d}_8$ ) of compound K[11]. Observed minor component: K[12] (●).

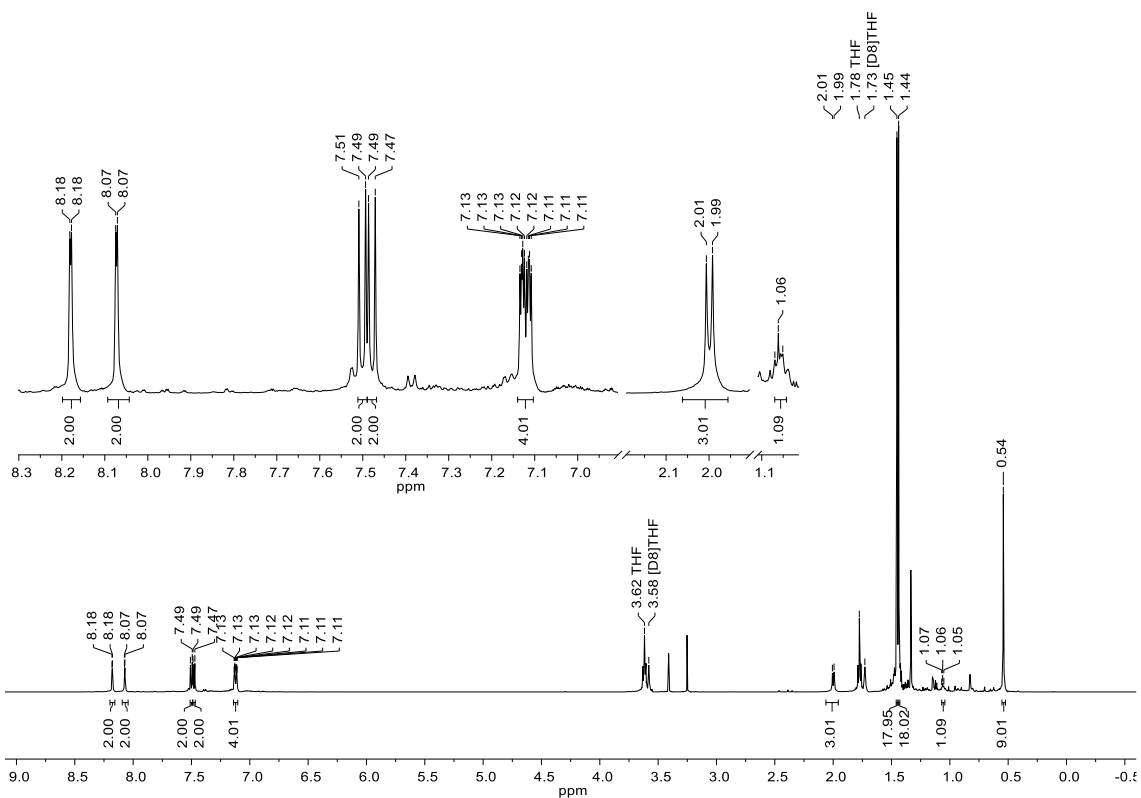


Figure S18.  $^1\text{H}$  NMR spectrum (500.2 MHz,  $\text{THF-}d_8$ ) of compound K[12].

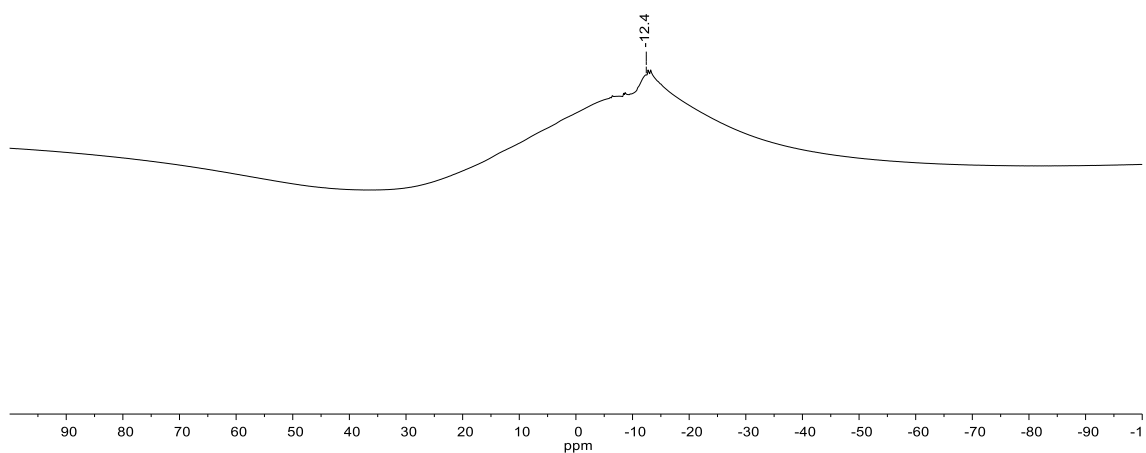
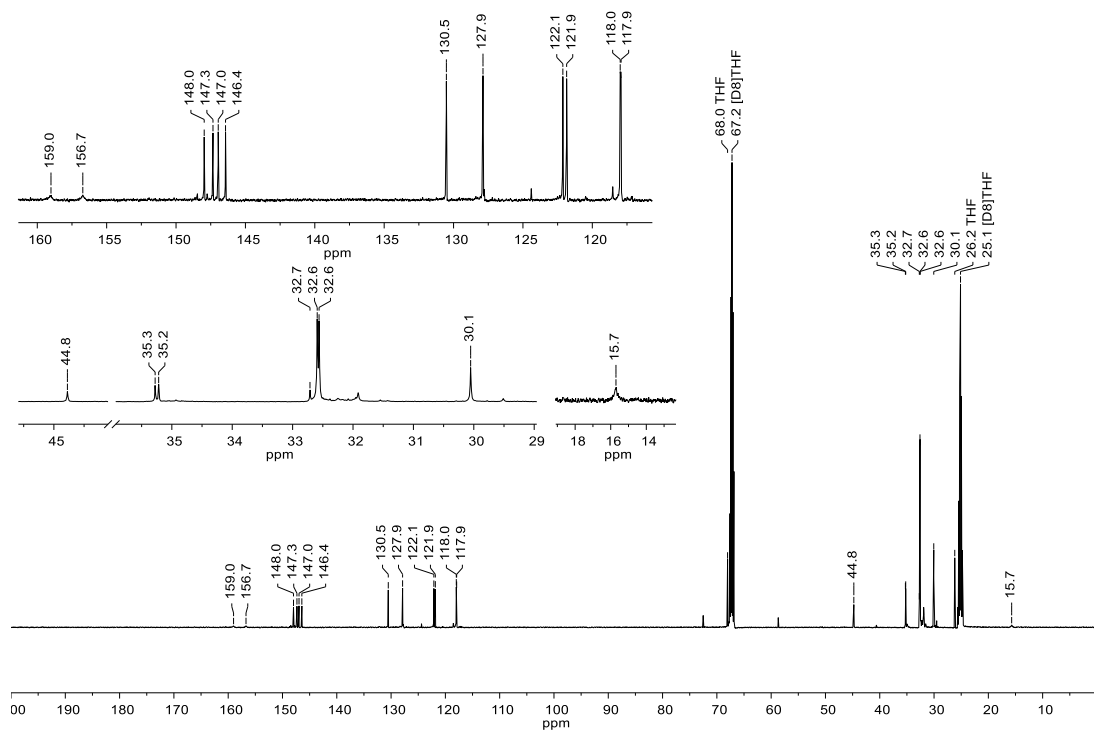
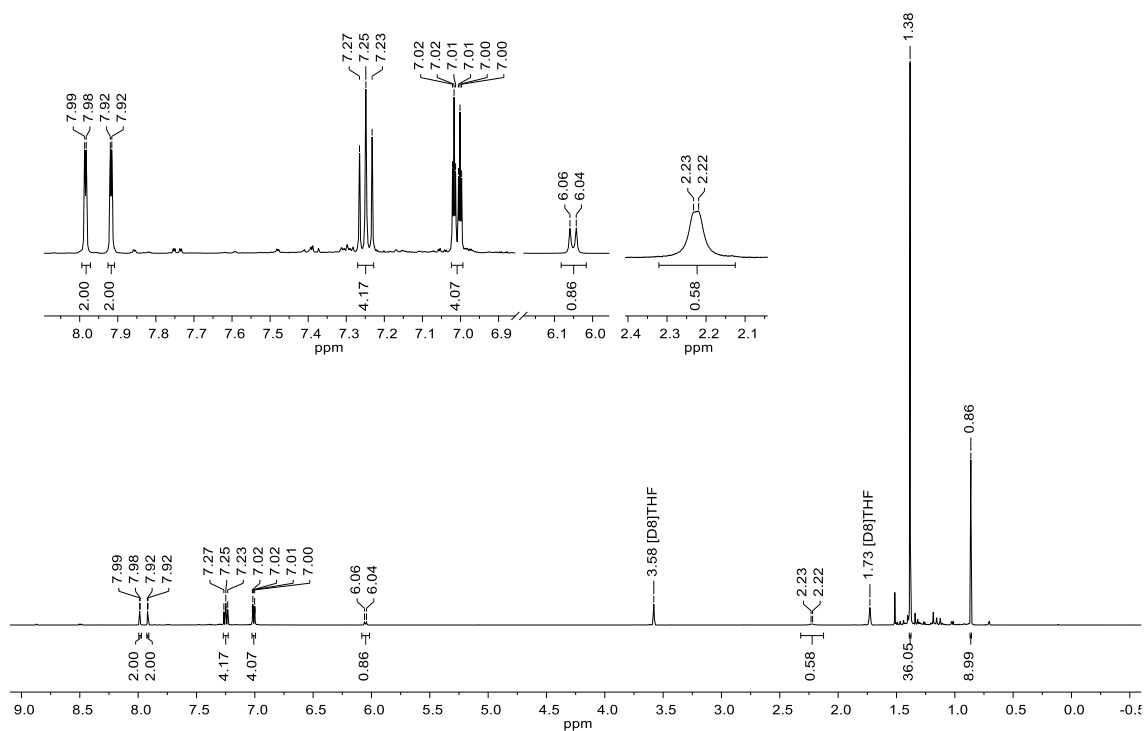


Figure S19.  $^{11}\text{B}$  NMR spectrum (160.5 MHz,  $\text{THF-}d_8$ ) of compound K[12].



**Figure S20.**  $^{13}\text{C}$  NMR spectrum (125.8 MHz,  $\text{THF-}d_8$ ) of compound K[12].



**Figure S21.**  $^1\text{H}$  NMR spectrum (500.2 MHz,  $\text{THF-}d_8$ ) of compound Li[16].

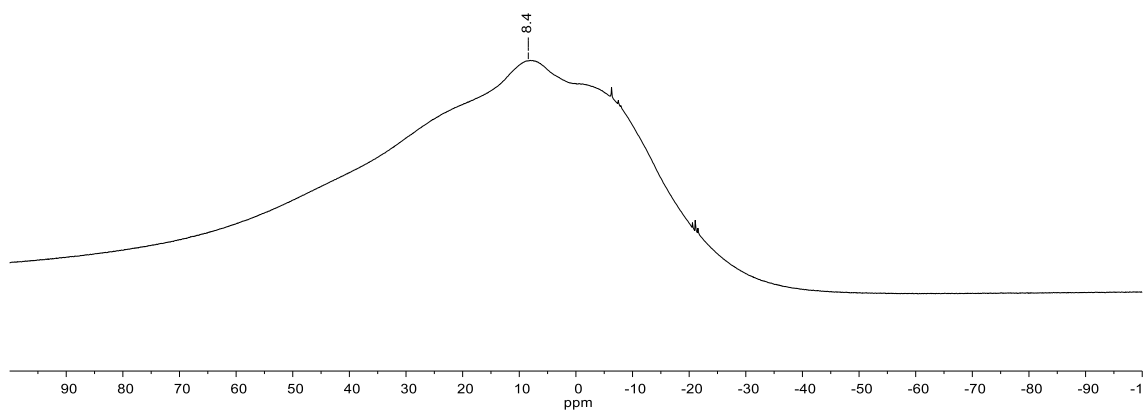


**Figure S22.**  $^{11}\text{B}$  NMR spectrum (160.5 MHz,  $\text{THF-}d_8$ ) of compound Li[16].

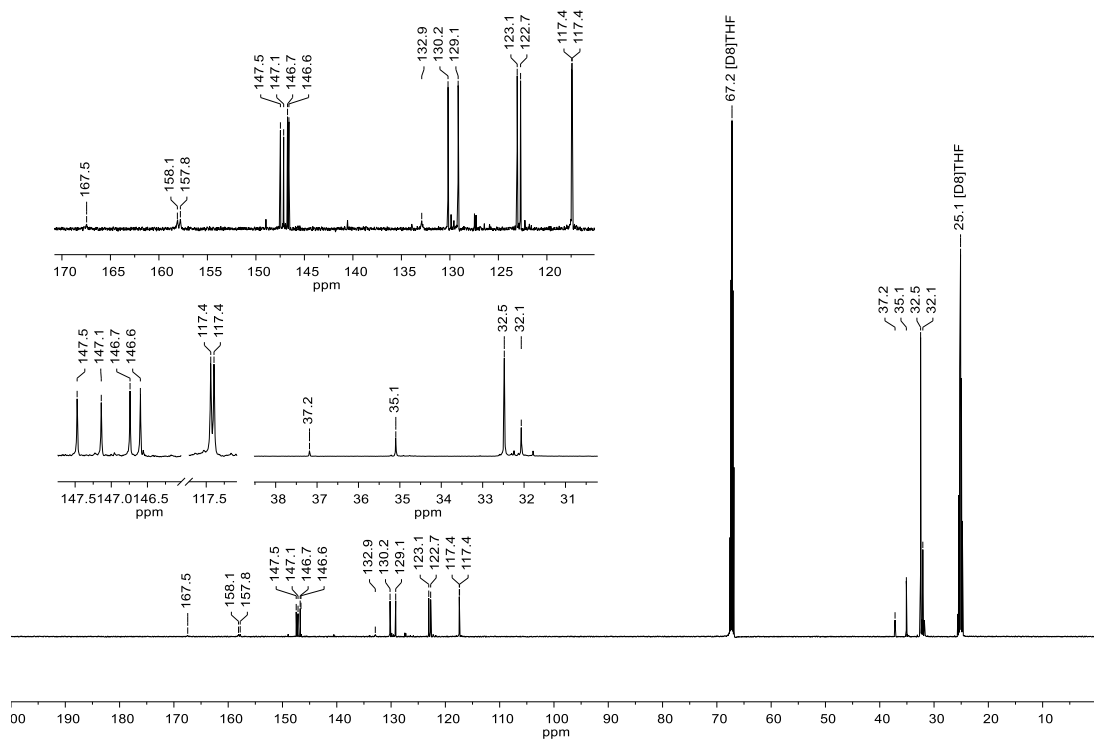


**Figure S23.**  $^{13}\text{C}$  NMR spectrum (125.8 MHz,  $\text{THF-d}_8$ ) of compound Li[16].

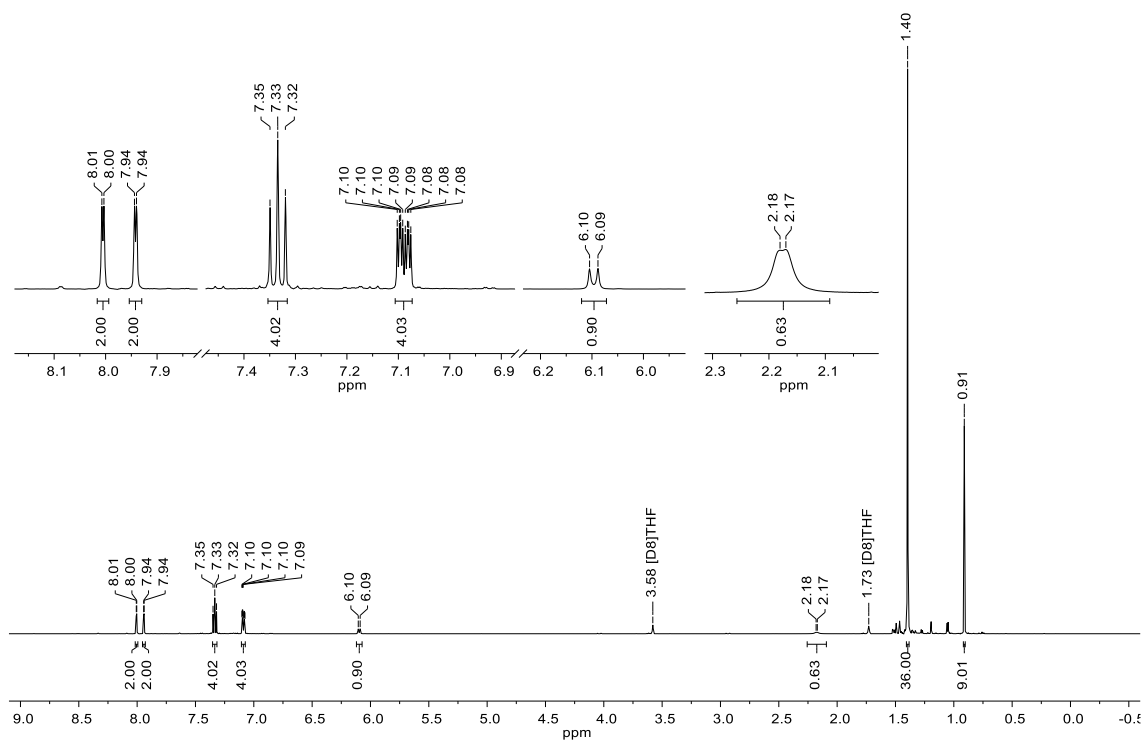


Figure S24.  $^1\text{H}$  NMR spectrum (500.2 MHz,  $\text{THF-}d_8$ ) of compound K[16].

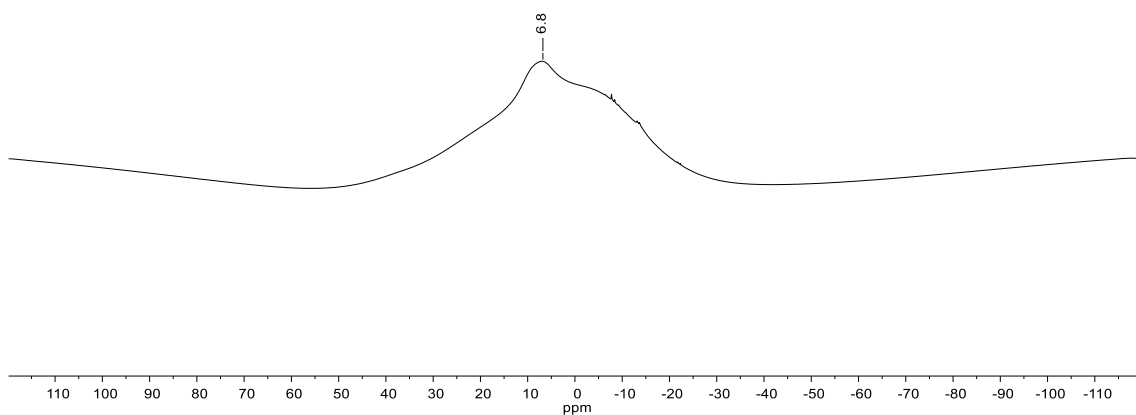
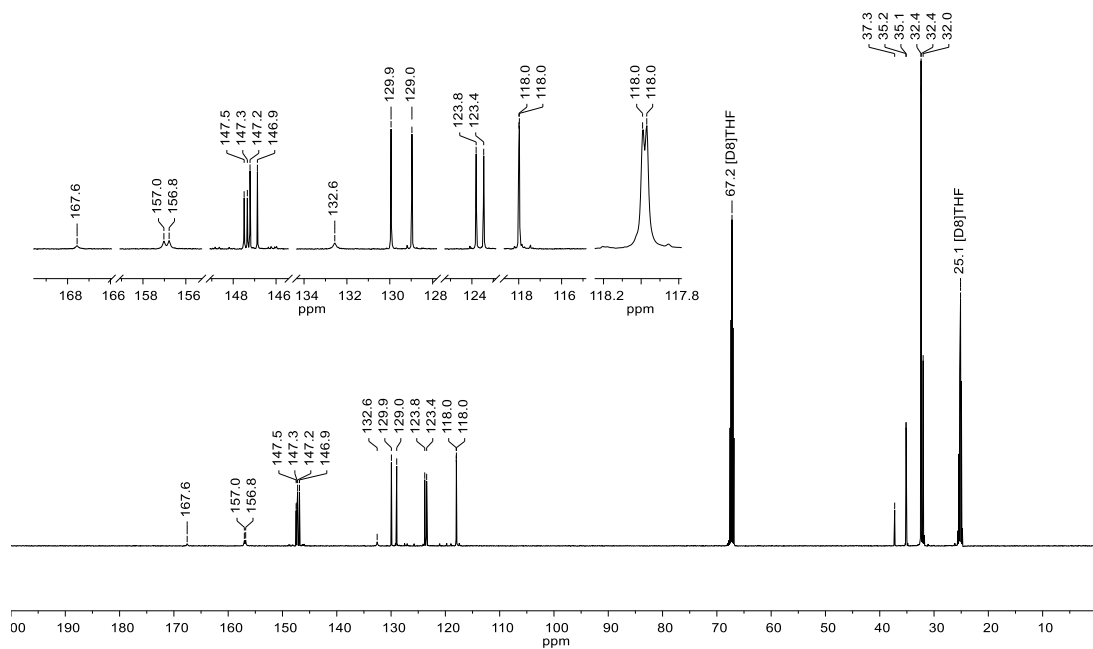
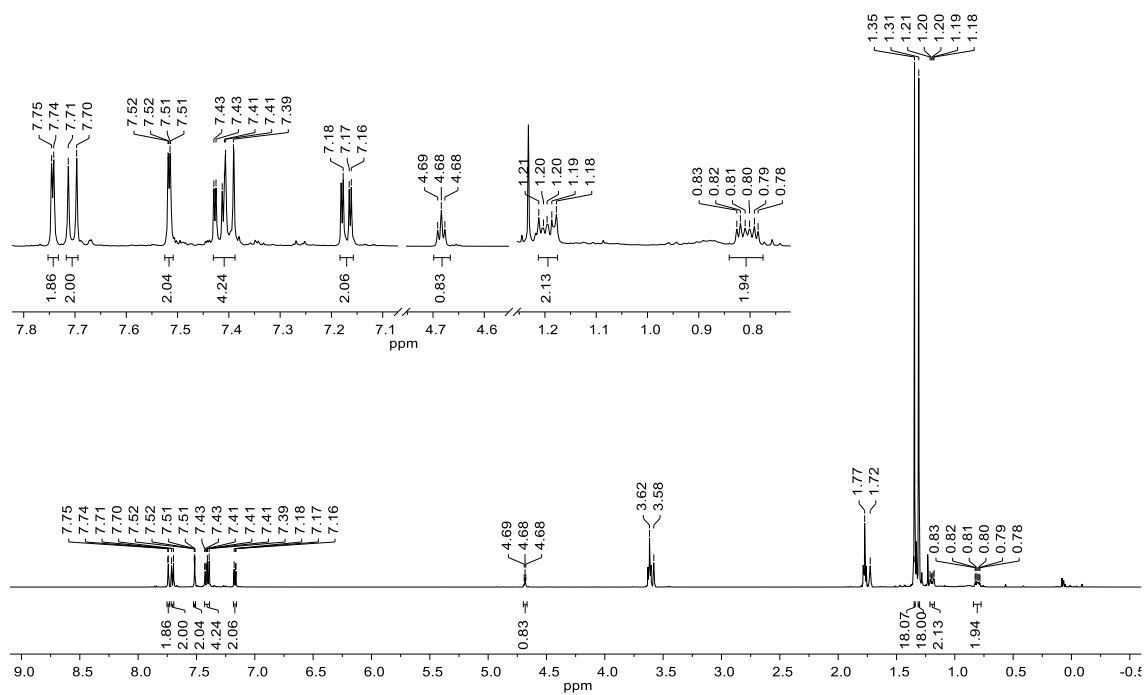


Figure S25.  $^{11}\text{B}$  NMR spectrum (160.5 MHz,  $\text{THF-}d_8$ ) of compound K[16].



**Figure S26.**  $^{13}\text{C}$  NMR spectrum (125.8 MHz,  $\text{THF-}d_8$ ) of compound K[16].



**Figure S27.**  $^1\text{H}$  NMR spectrum (500.2 MHz,  $\text{THF-d}_8$ ) of compound **6**(thf).

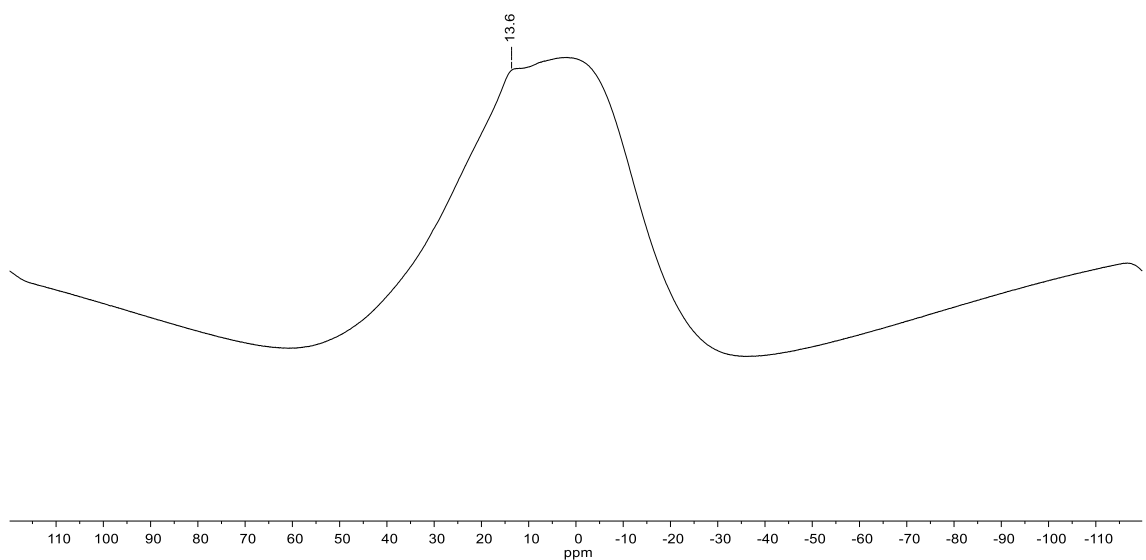


**Figure S28.**  $^{11}\text{B}$  NMR spectrum (160.5 MHz,  $\text{THF-d}_8$ ) of compound **6**(thf).

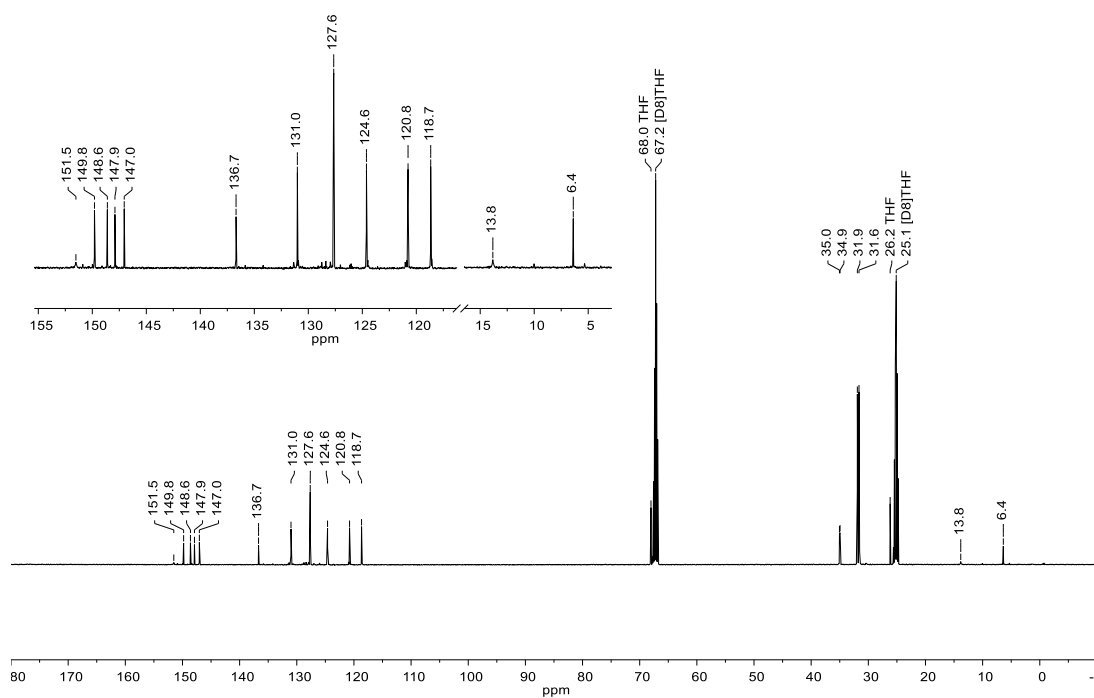


**Figure S29.**  $^{13}\text{C}$  NMR spectrum (125.8 MHz,  $\text{THF-}d_8$ ) of compound **6**(thf).

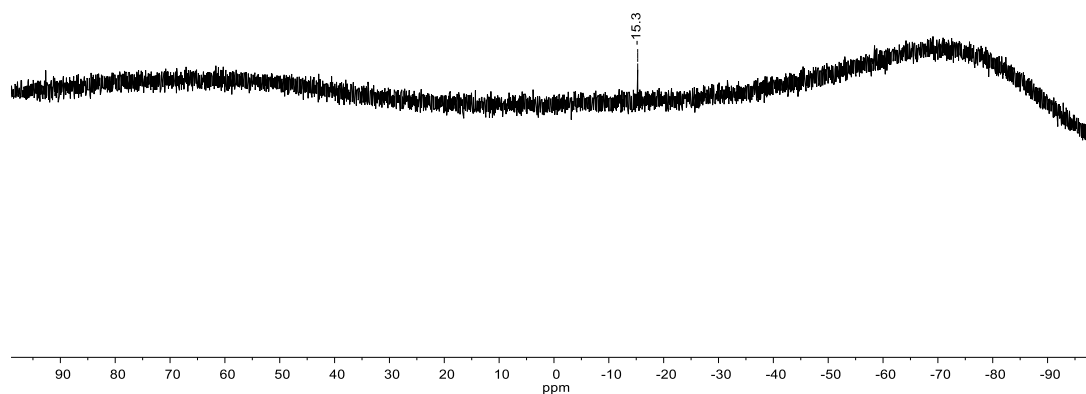


**Figure S30.**  $^{29}\text{Si}\{^1\text{H}\}$  NMR spectrum (99.4 MHz,  $\text{THF-}d_8$ ) of compound **6**(thf).

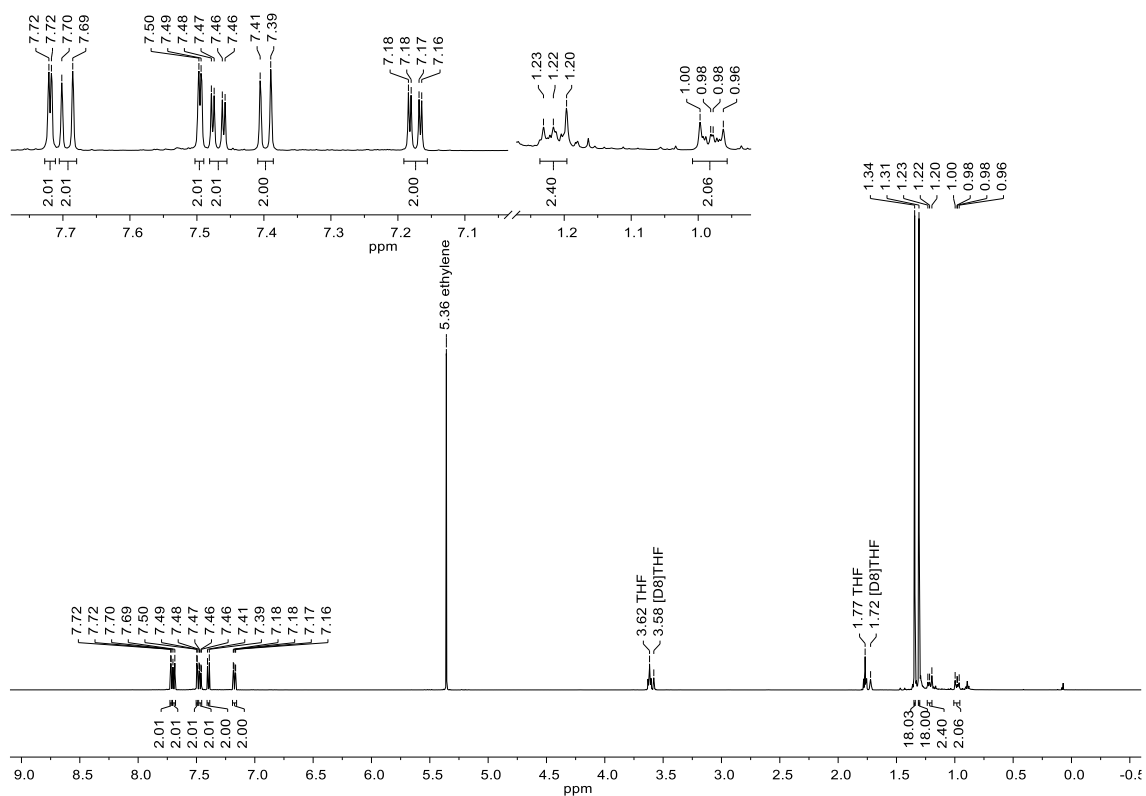


Figure S31.  $^1\text{H}$  NMR spectrum (500.2 MHz,  $\text{THF-}d_8$ ) of compound **10**(thf).

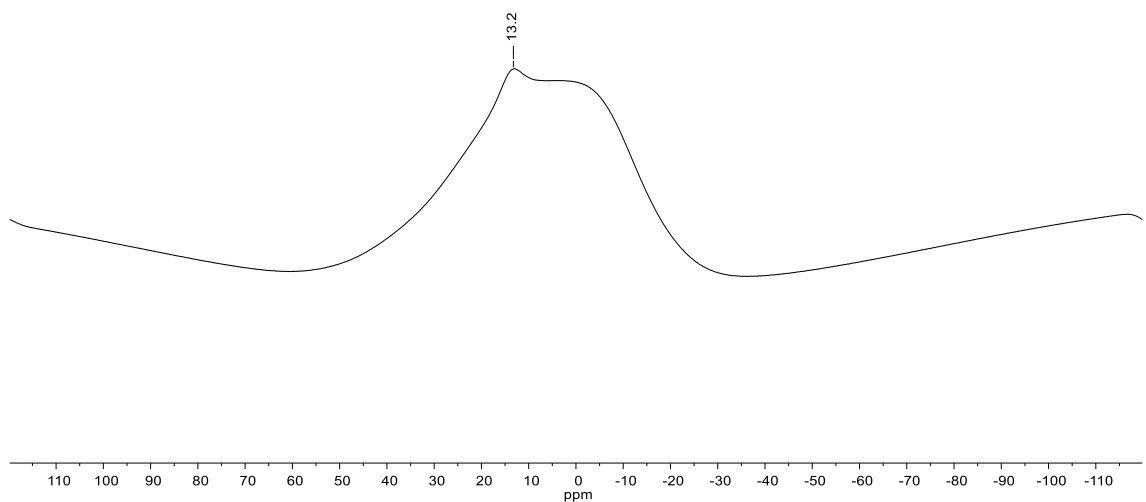
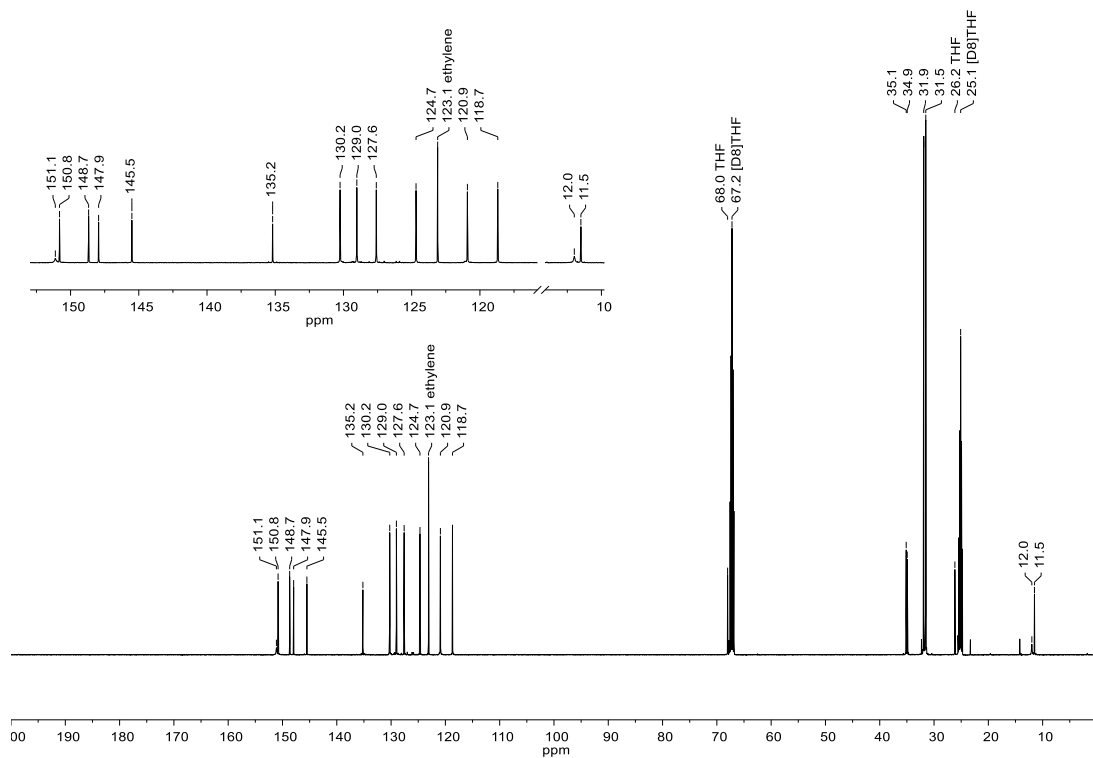
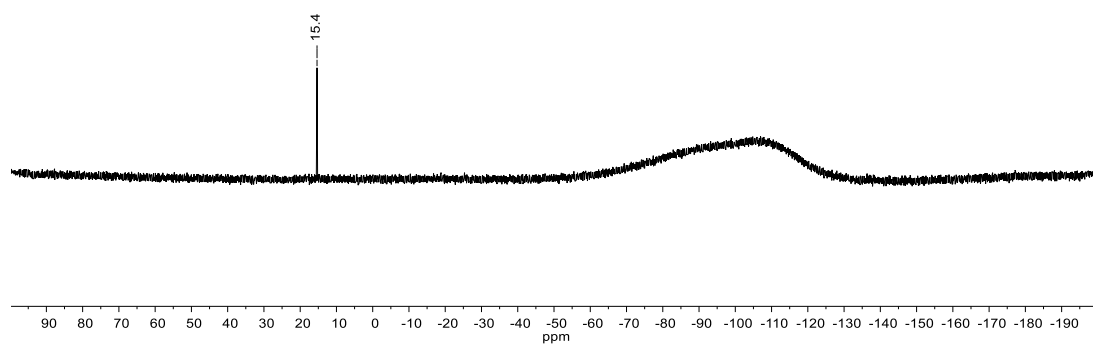


Figure S32.  $^{11}\text{B}$  NMR spectrum (160.5 MHz,  $\text{THF-}d_8$ ) of compound **10**(thf).



**Figure S33.**  $^{13}\text{C}$  NMR spectrum (125.8 MHz,  $\text{THF-}d_8$ ) of compound **10**(thf).



**Figure S34.**  $^{29}\text{Si}\{^1\text{H}\}$  NMR spectrum (99.4 MHz,  $\text{THF-}d_8$ ) of compound **10**(thf).

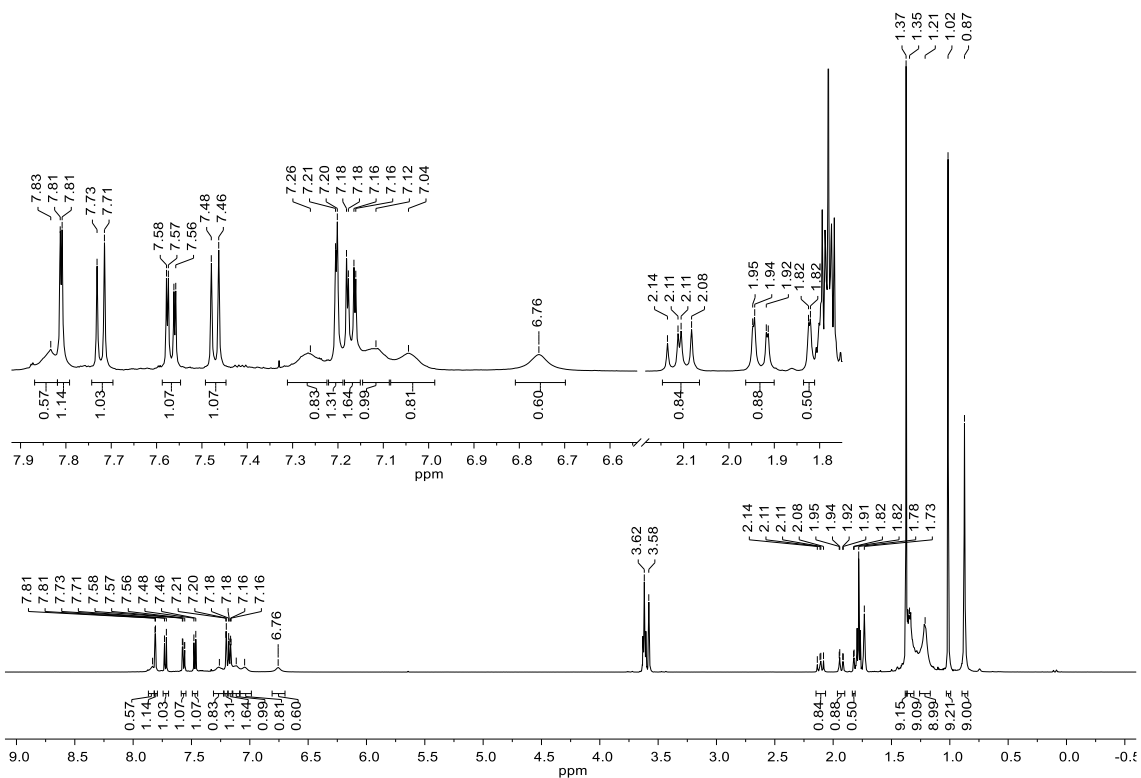


Figure S35.  $^1\text{H}$  NMR spectrum (500.2 MHz,  $\text{THF-}d_8$ , 243 K) of compound **13**.

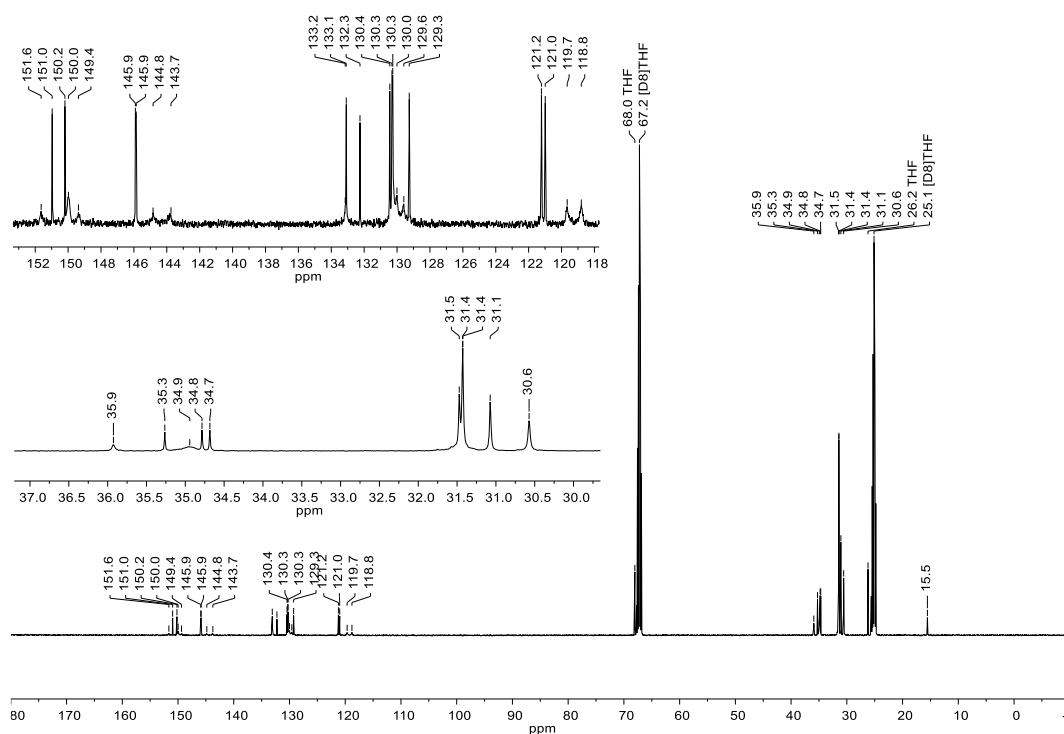
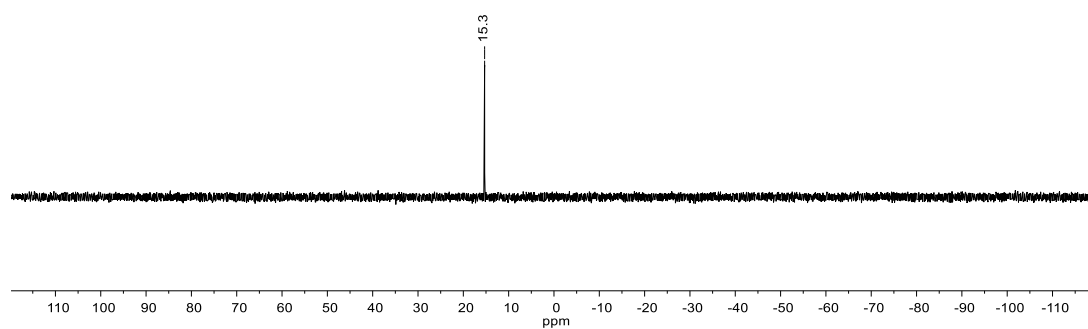


Figure S36.  $^{13}\text{C}$  NMR spectrum (125.8 MHz,  $\text{THF-}d_8$ , 243 K) of compound **13**.



**Figure S37.**  $^{29}\text{Si}\{^1\text{H}\}$  NMR spectrum (99.4 MHz,  $\text{THF-}d_8$ , 243 K) of compound **13**.

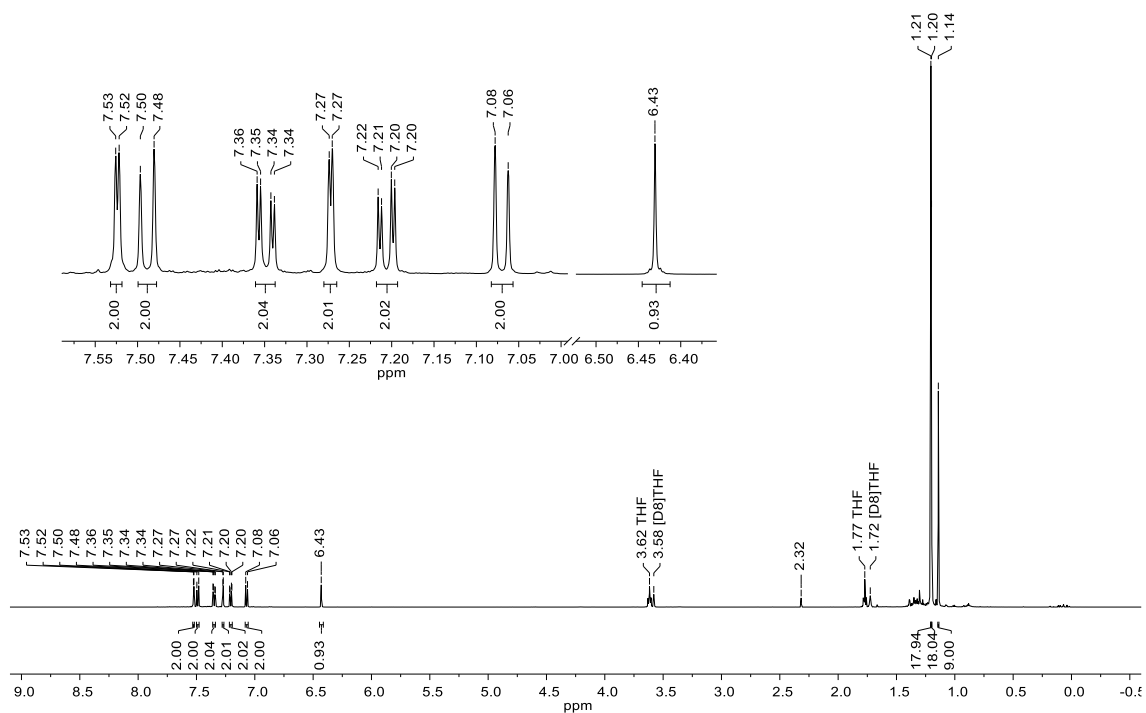


Figure S38.  $^1\text{H}$  NMR spectrum (500.2 MHz,  $\text{THF-}d_8$ ) of compound **17**.

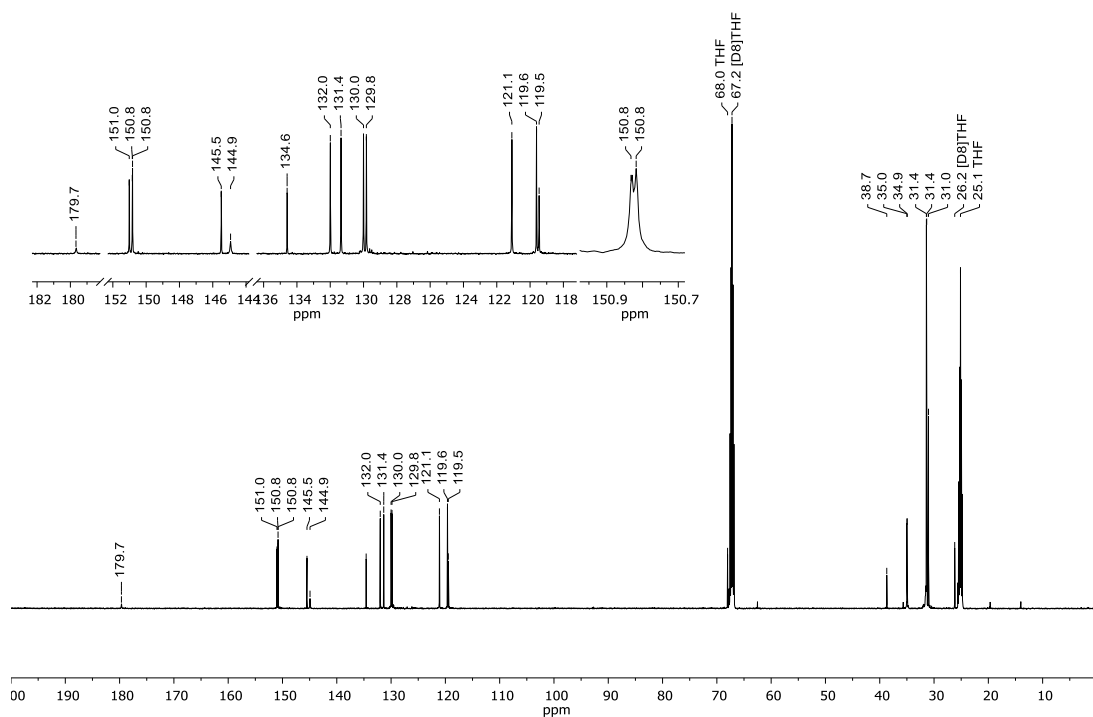
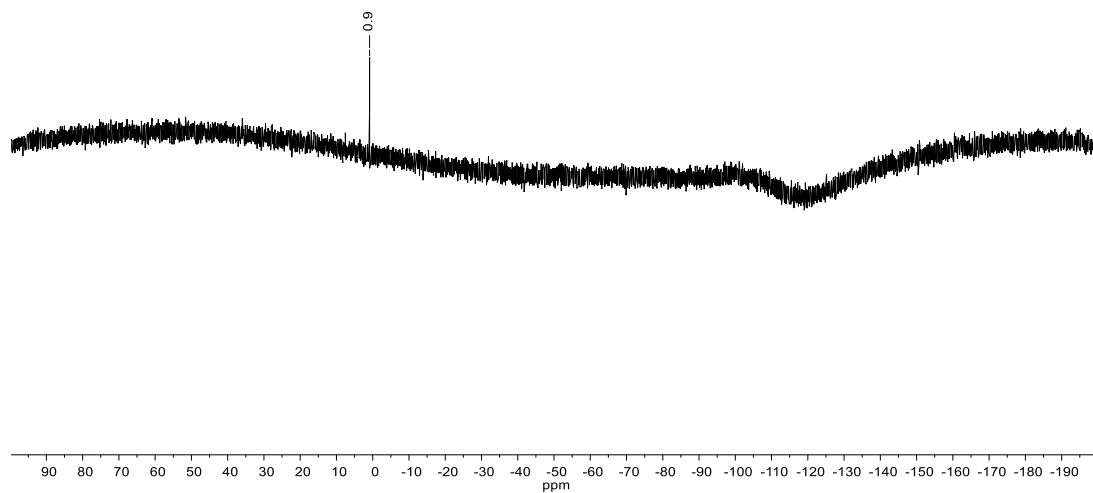
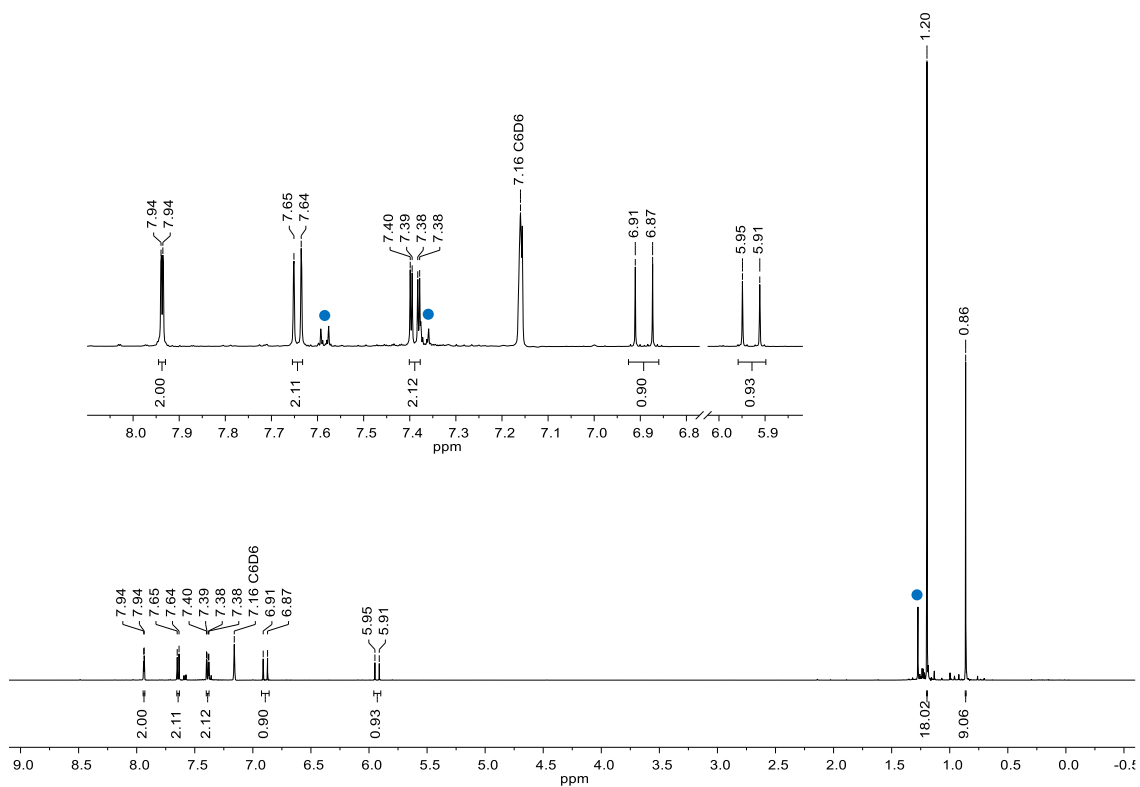


Figure S39.  $^{13}\text{C}$  NMR spectrum (125.8 MHz,  $\text{THF-}d_8$ ) of compound **17**.



**Figure S40.**  $^{29}\text{Si}\{^1\text{H}\}$  NMR spectrum (99.4 MHz,  $\text{THF-}d_8$ ) of compound **17**.



**Figure S41.**  $^1\text{H}$  NMR spectrum (500.2 MHz,  $\text{C}_6\text{D}_6$ ) of compound **S2**. Observed minor component: 4,4'-Di-*tert*-butyl-biphenyl (●).

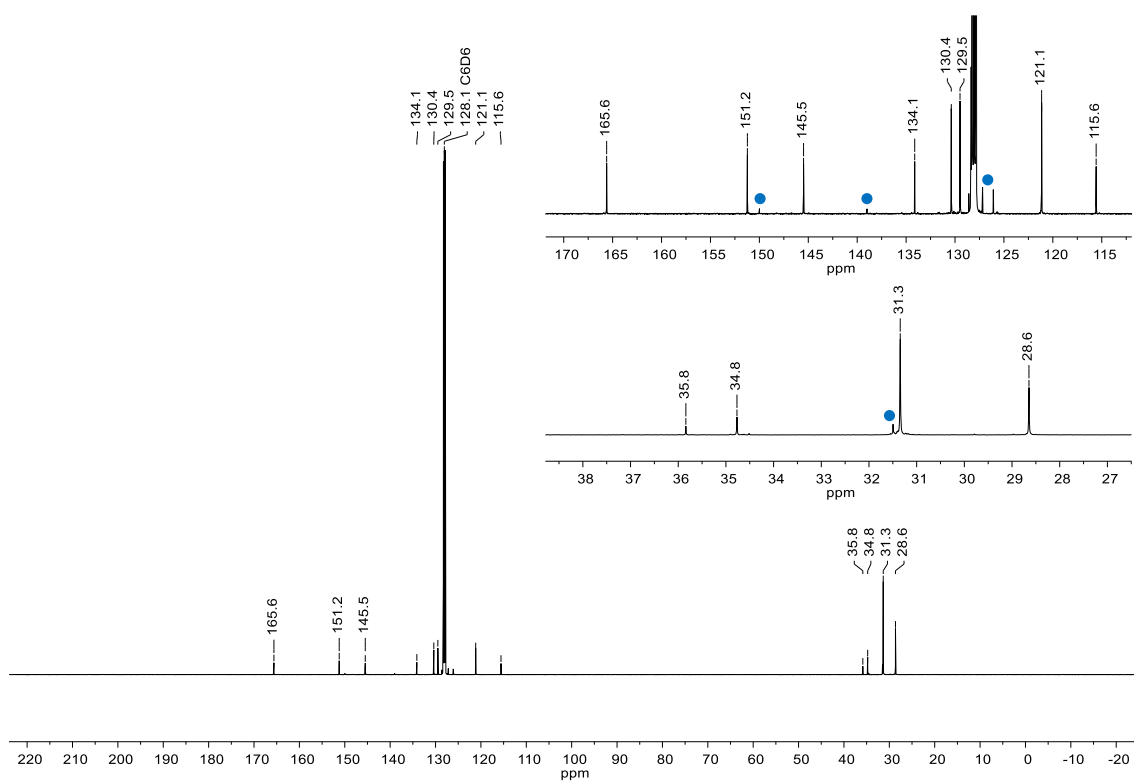


**Figure S42.**  $^{13}\text{C}$  NMR spectrum (125.8 MHz,  $\text{C}_6\text{D}_6$ ) of compound **S2**. Observed minor component: 4,4'-Di-*tert*-butyl-biphenyl (●).

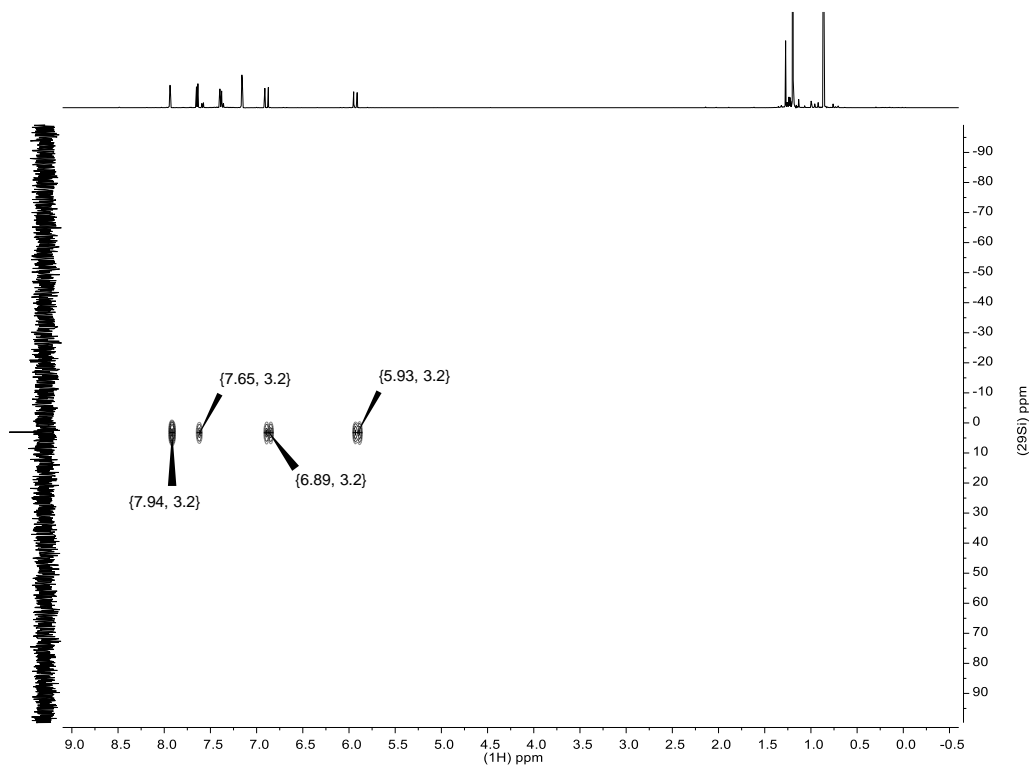


**Figure S43.**  $^1\text{H}$ - $^{29}\text{Si}$ -HMBC NMR spectrum ( $^1\text{H}$ : 500.2 MHz,  $^{29}\text{Si}$ : 99.4 MHz,  $\text{C}_6\text{D}_6$ ) of compound **S2**.

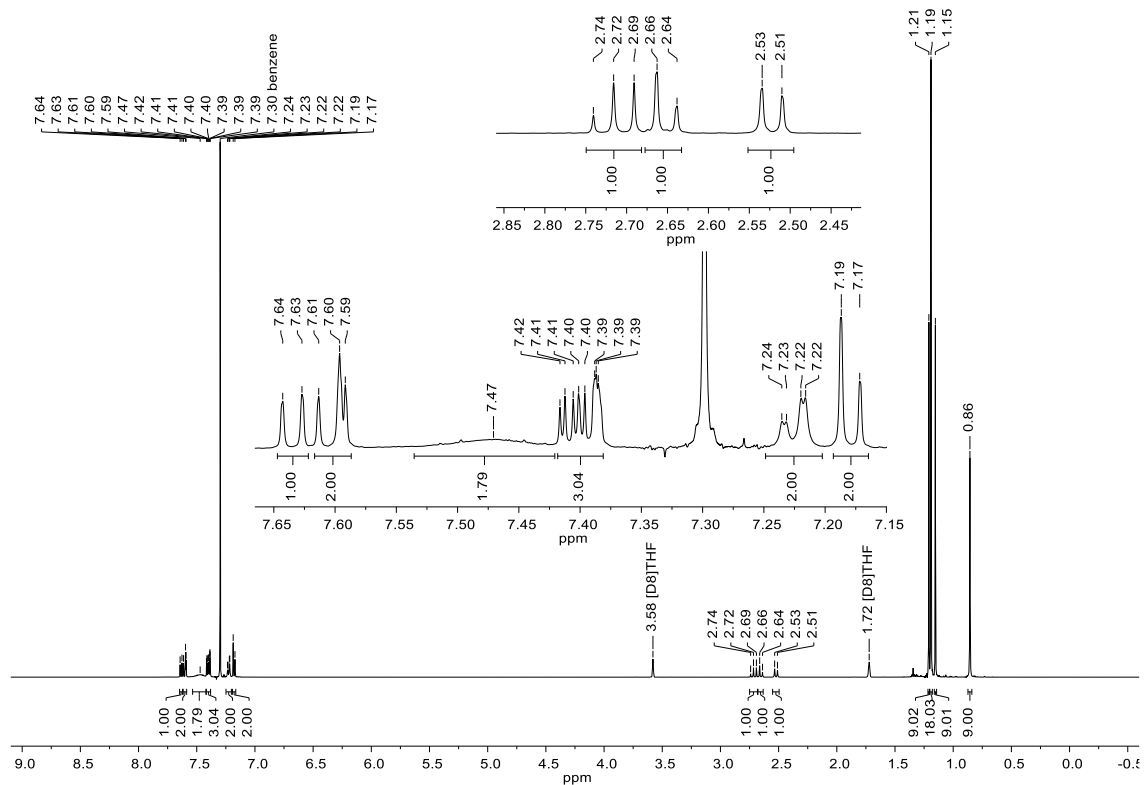


Figure S44.  $^1\text{H}$  NMR spectrum (500.2 MHz,  $\text{THF-}d_8$ ) of compound **14**.

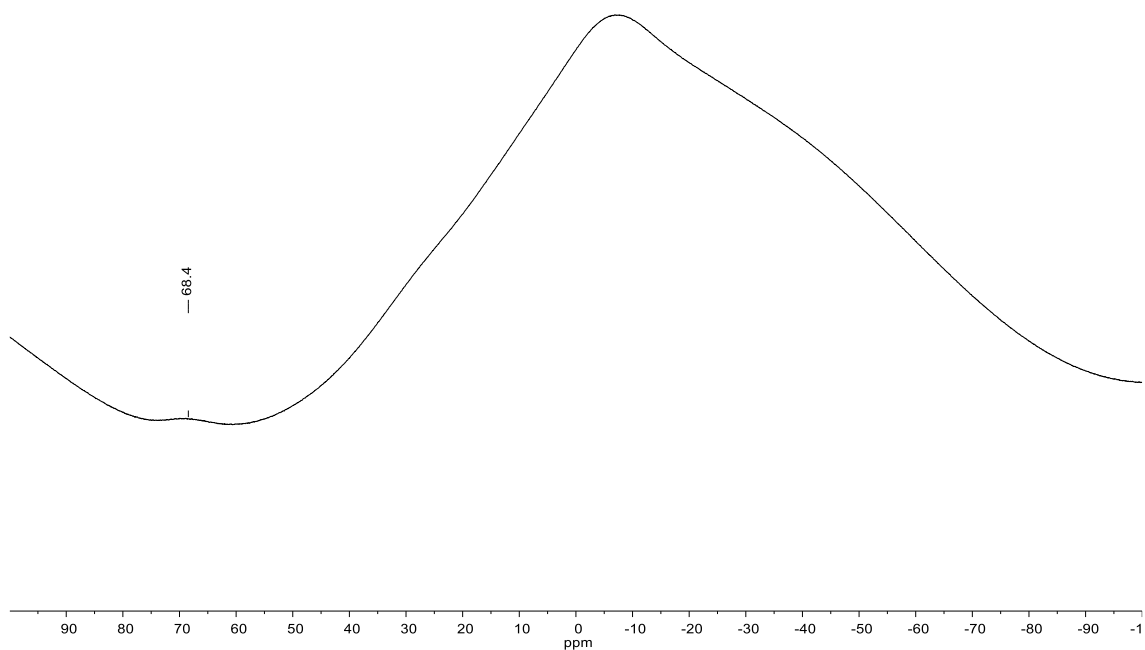


Figure S45.  $^{11}\text{B}$  NMR spectrum (96.3 MHz,  $\text{THF-}d_8$ ) of compound **14**.

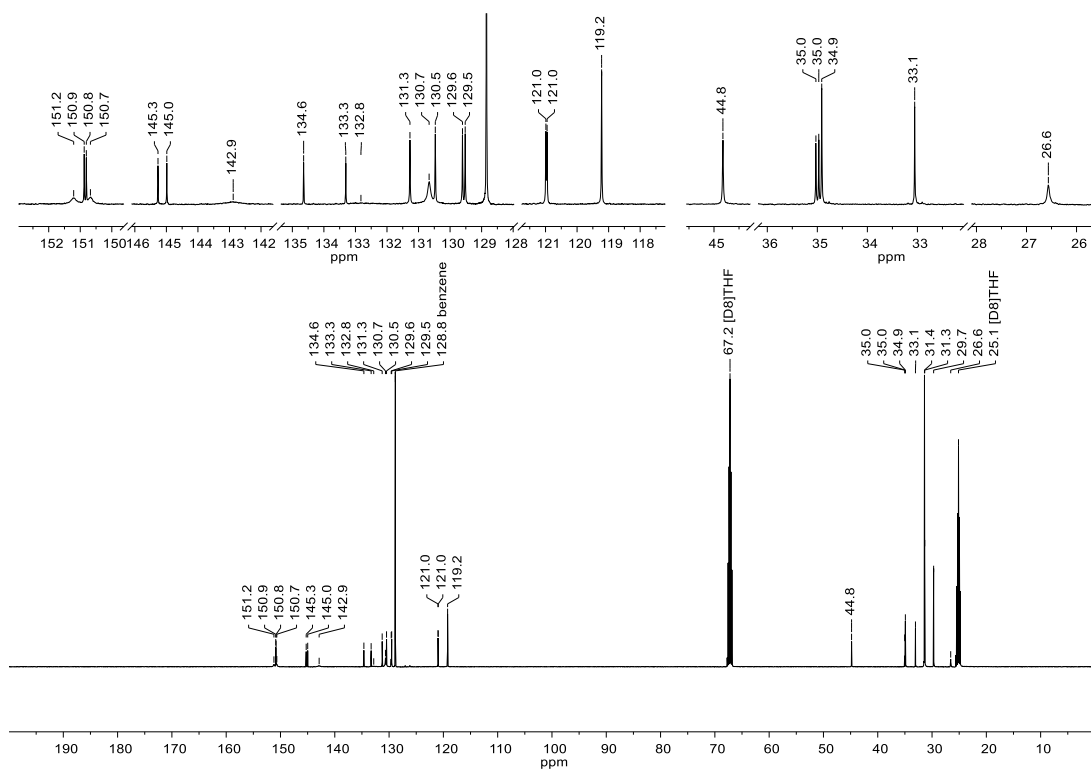


Figure S46.  $^{13}\text{C}$  NMR spectrum (125.8 MHz,  $\text{THF-}d_8$ ) of compound **14**.

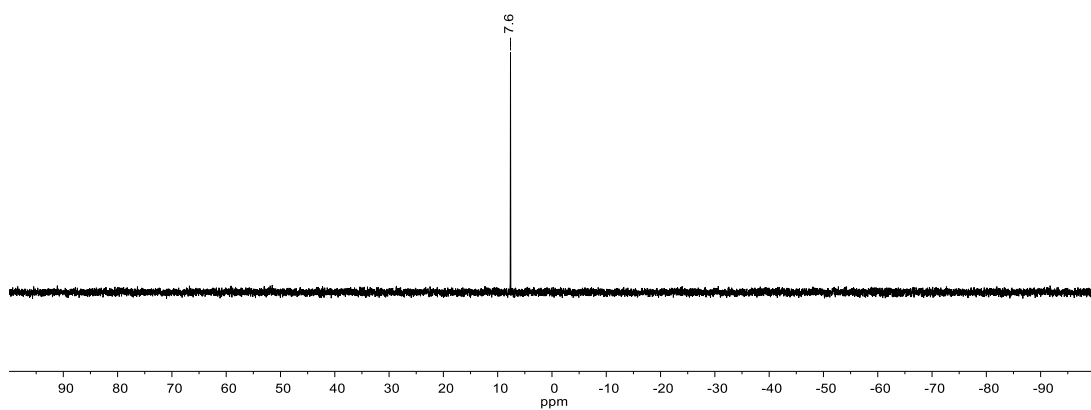
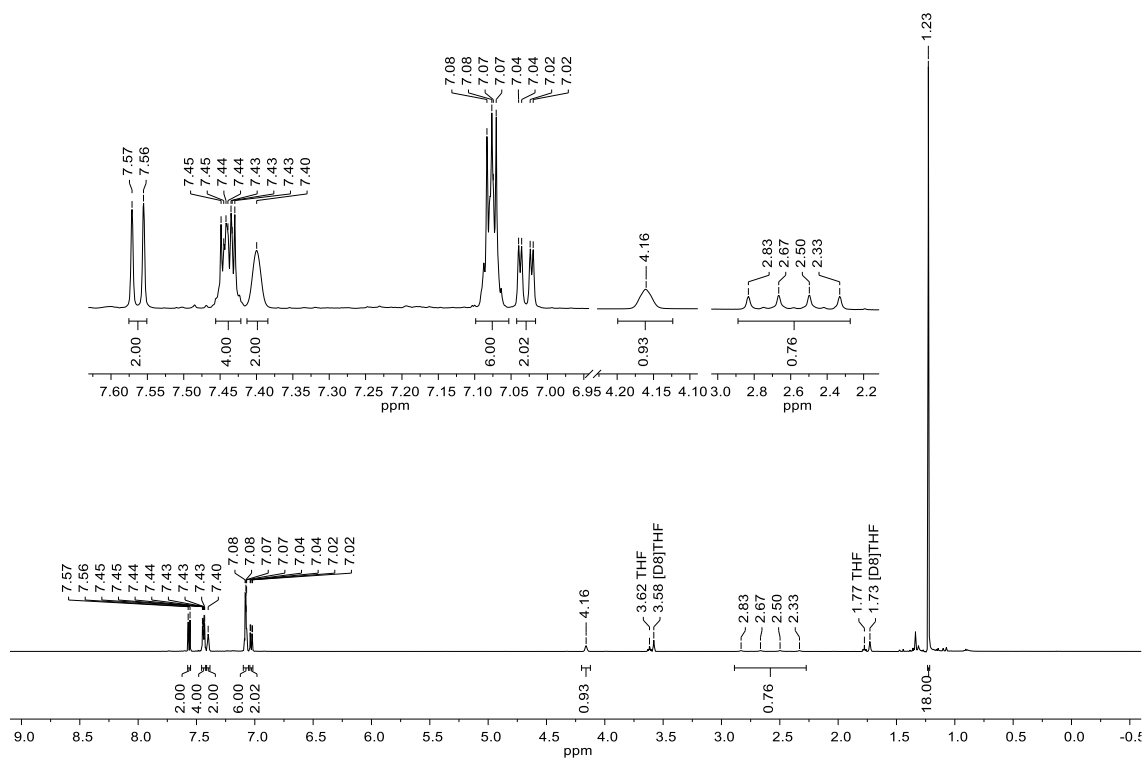
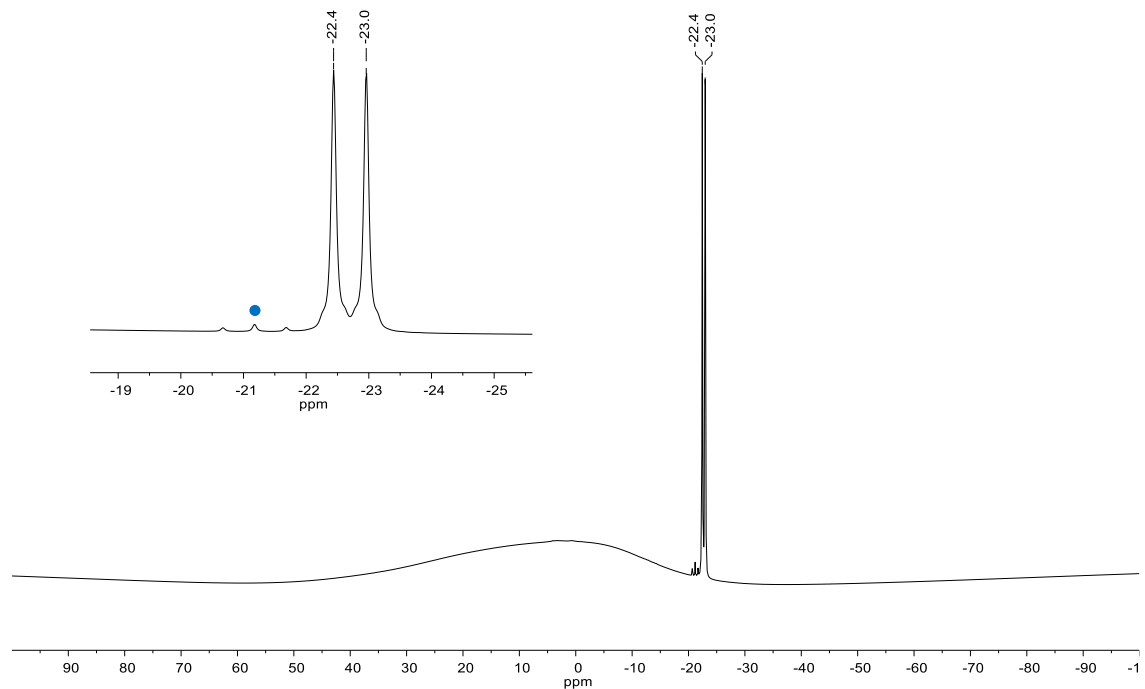


Figure S47.  $^{29}\text{Si}\{^1\text{H}\}$  NMR spectrum (99.4 MHz,  $\text{THF-}d_8$ ) of compound **14**.



**Figure S48.**  $^1\text{H}$  NMR spectrum (500.2 MHz,  $\text{THF-}d_8$ ) of compound  $\text{Na[S3]}$ .



**Figure S49.**  $^{11}\text{B}$  NMR spectrum (96.3 MHz,  $\text{THF-}d_8$ ) of compound  $\text{Na[S3]}$ . Observed minor component:  $\text{Li[H}_2\text{BFlu]}$  (●, triplet; BFlu = 2,7-di-*tert*-butyl-9-borabluorene)

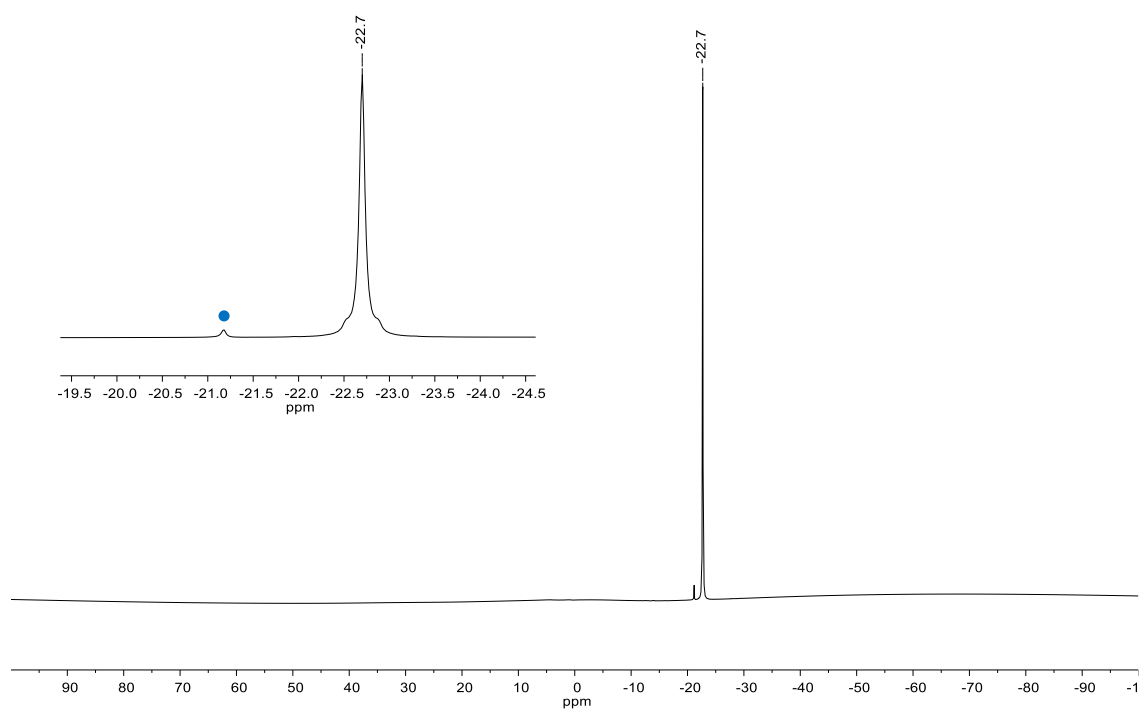


**Figure S50.**  $^{11}\text{B}\{^1\text{H}\}$  NMR spectrum (96.3 MHz,  $\text{THF-}d_8$ ) of compound  $\text{Na}[\text{S3}]$ . Observed minor component:  $\text{Li}[\text{H}_2\text{BFlu}]$  (●, singlet; BFlu = 2,7-di-*tert*-butyl-9-borafluorene)

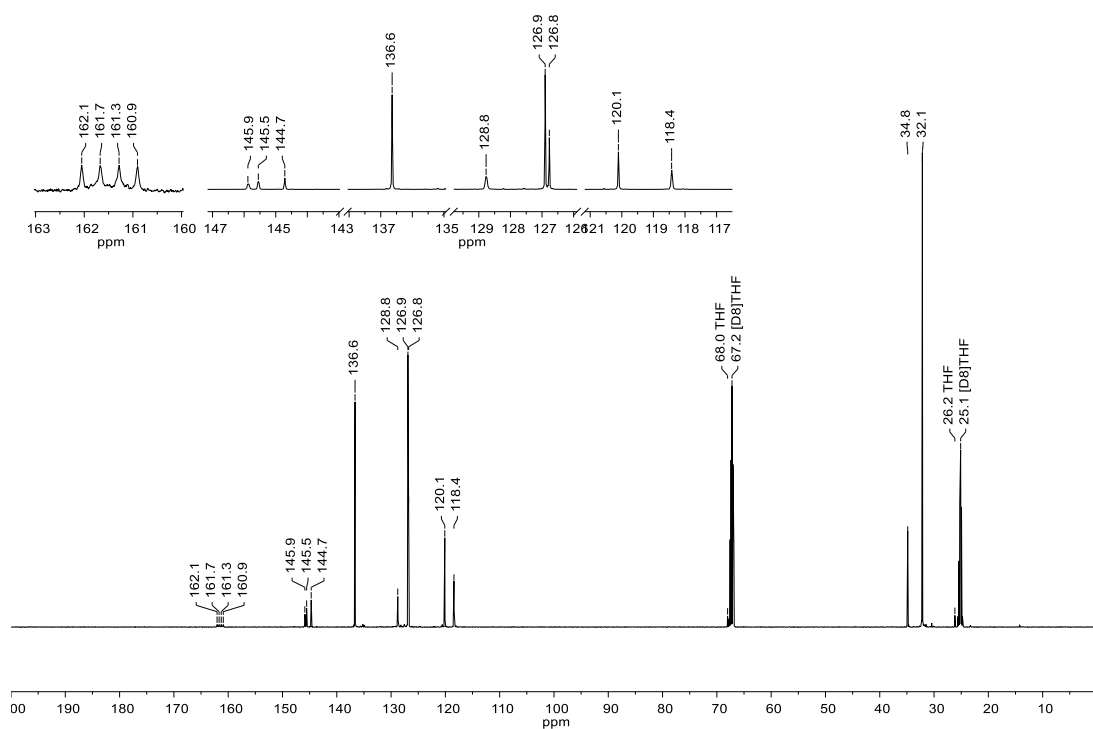


**Figure S51.**  $^{13}\text{C}$  NMR spectrum (125.8 MHz,  $\text{THF-}d_8$ ) of compound  $\text{Na}[\text{S3}]$ .

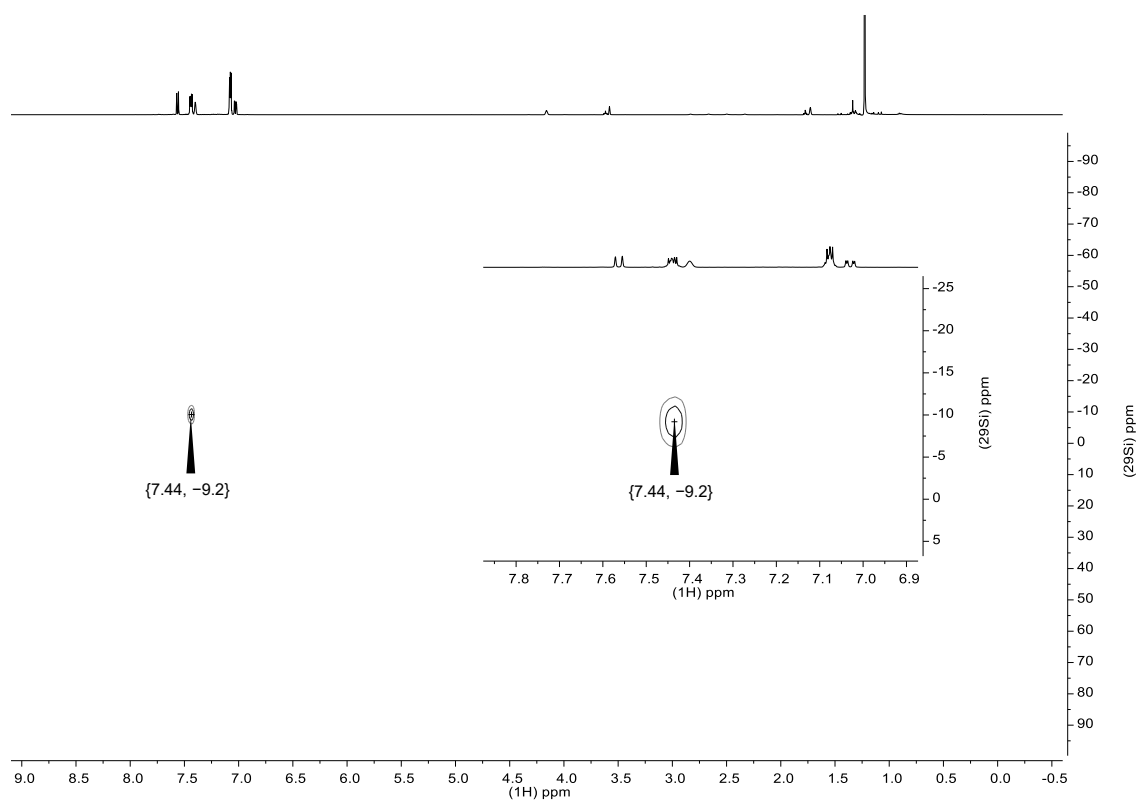


**Figure S52.**  $^1\text{H}$ - $^{29}\text{Si}$ -HMBC NMR spectrum ( $^1\text{H}$ : 500.2 MHz,  $^{29}\text{Si}$ : 99.4 MHz,  $\text{THF-}d_8$ ) of compound Na[S3].

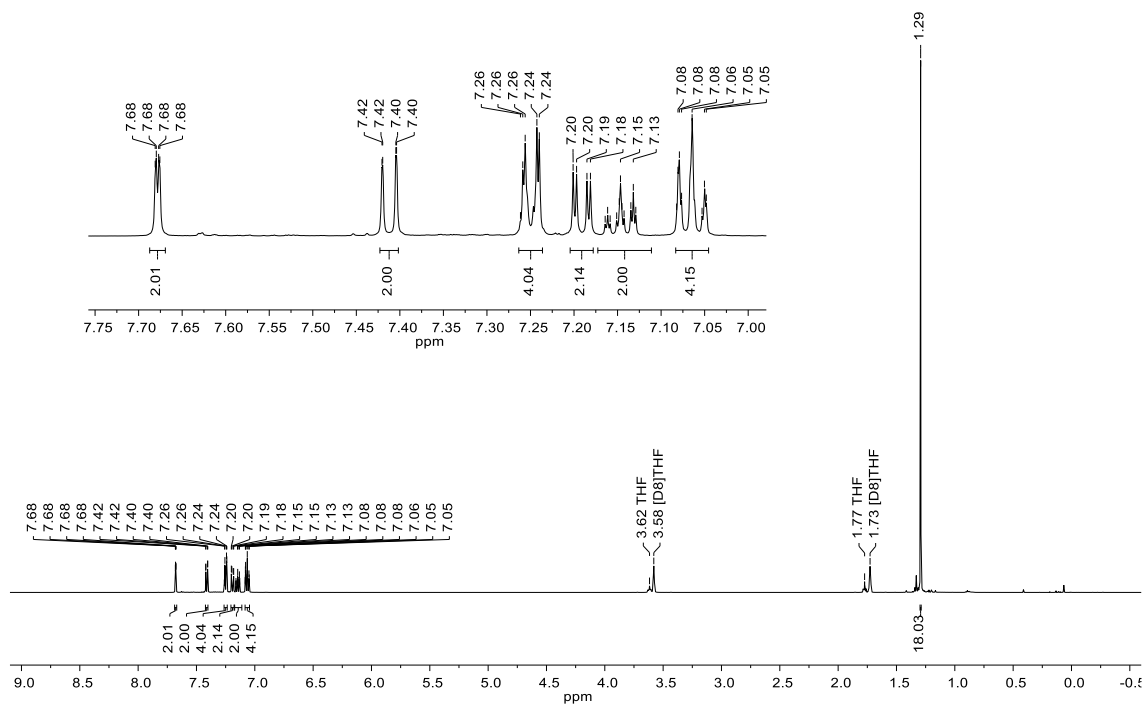


**Figure S53.**  $^1\text{H}$  NMR spectrum (500.2 MHz,  $\text{THF-}d_8$ ) of compound **18**(thf).

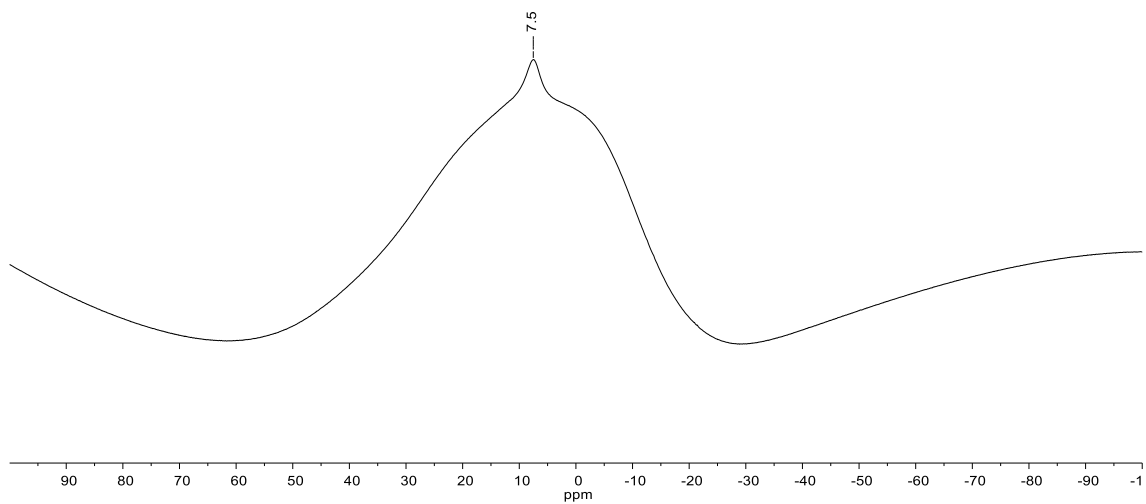


**Figure S54.**  $^{11}\text{B}$  NMR spectrum (96.3 MHz,  $\text{THF-}d_8$ ) of compound **18**(thf).



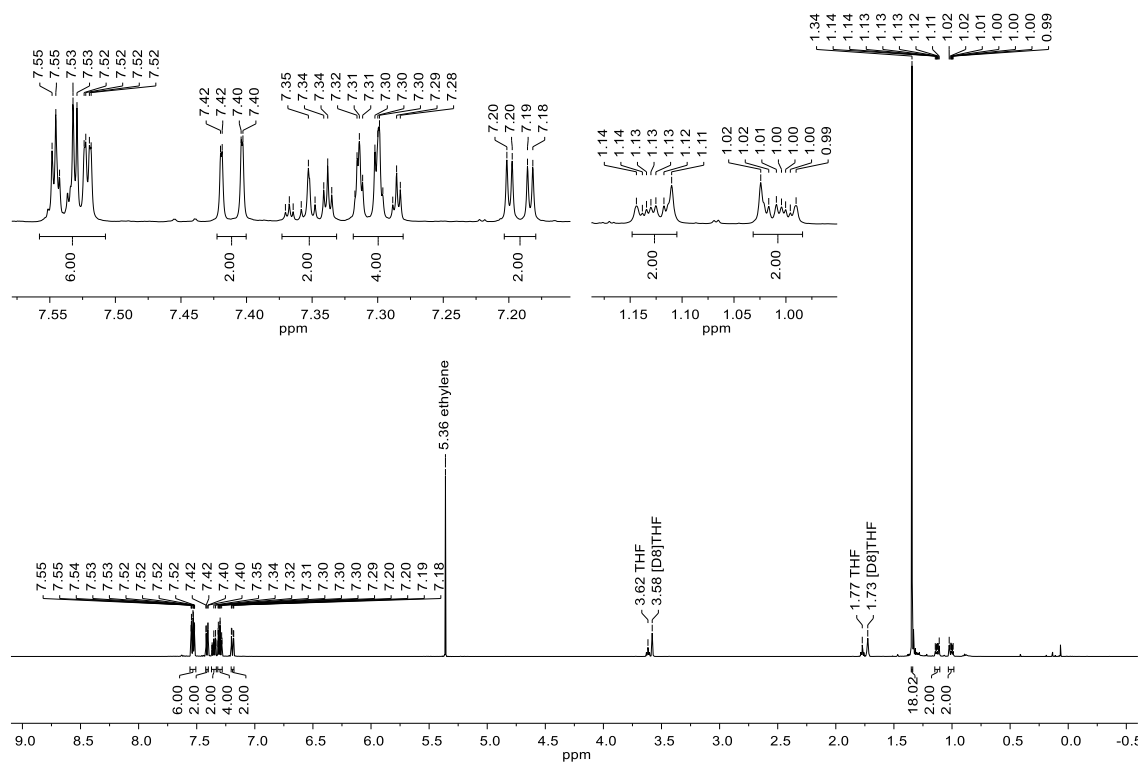


Figure S57.  $^1\text{H}$  NMR spectrum (500.2 MHz,  $\text{THF-}d_8$ ) of compound **19**(thf).

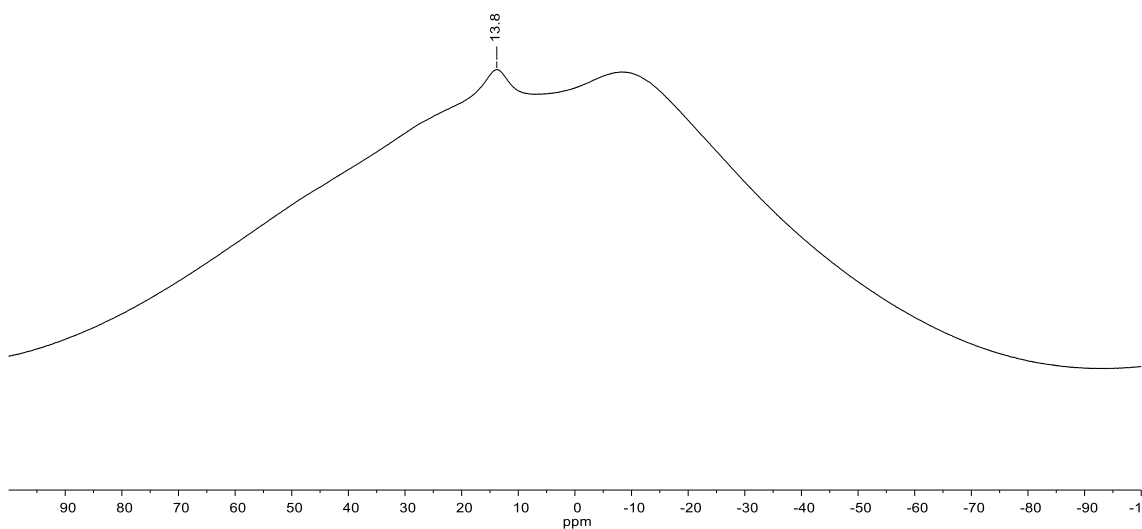
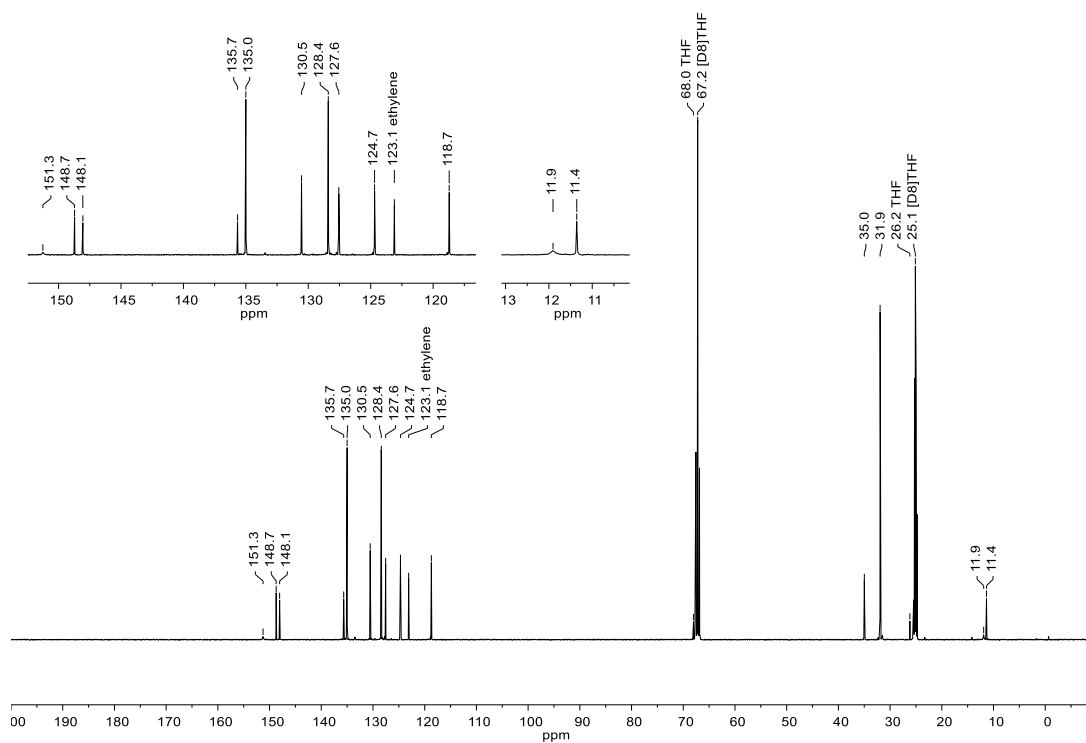
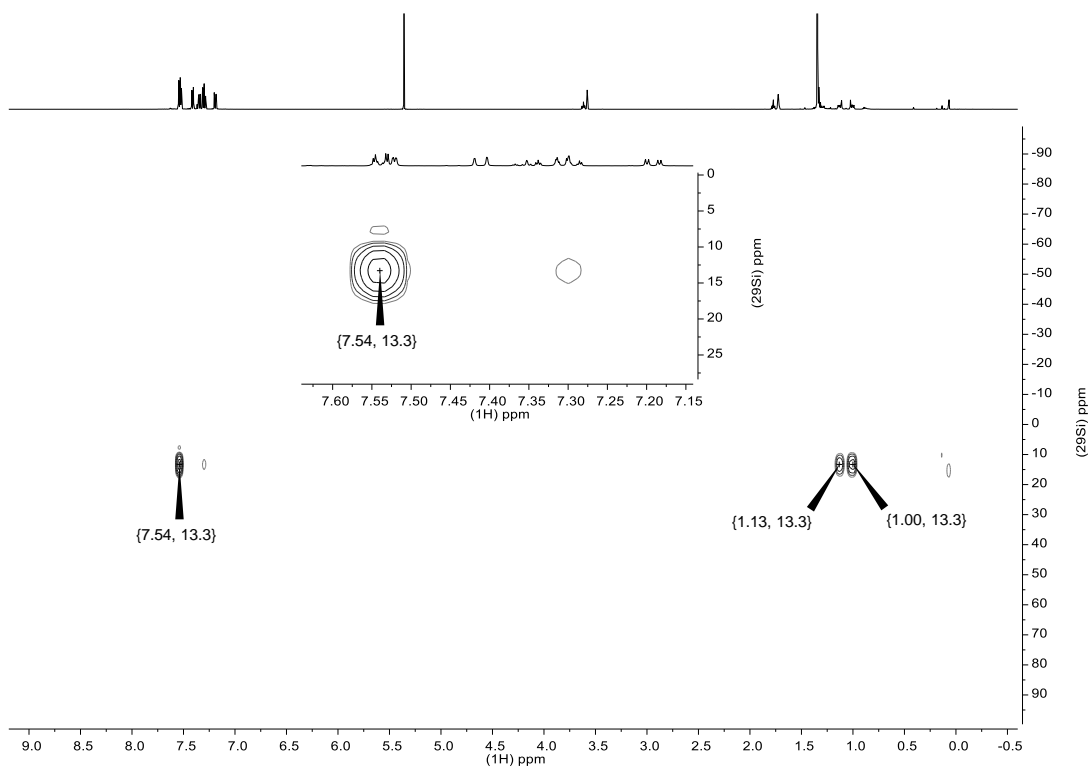


Figure S58.  $^{11}\text{B}$  NMR spectrum (96.3 MHz,  $\text{THF-}d_8$ ) of compound **19**(thf).



**Figure S59.** <sup>13</sup>C NMR spectrum (125.8 MHz, THF-*d*<sub>8</sub>) of compound **19**(thf).



**Figure S60.** <sup>1</sup>H-<sup>29</sup>Si-HMBC NMR spectrum (<sup>1</sup>H: 500.2 MHz, <sup>29</sup>Si: 99.4 MHz, THF-*d*<sub>8</sub>) of compound **19**(thf).

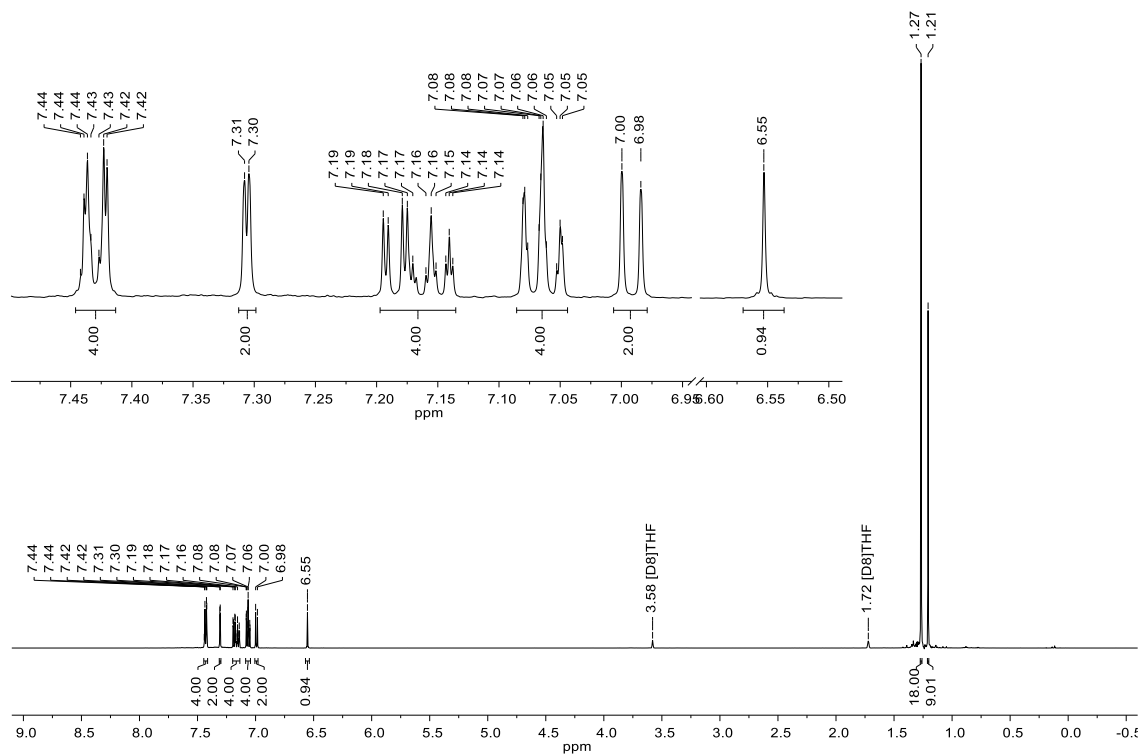


**Figure S61.**  $^1\text{H}$  NMR spectrum (500.2 MHz,  $\text{THF-}d_8$ ) of compound **20**.

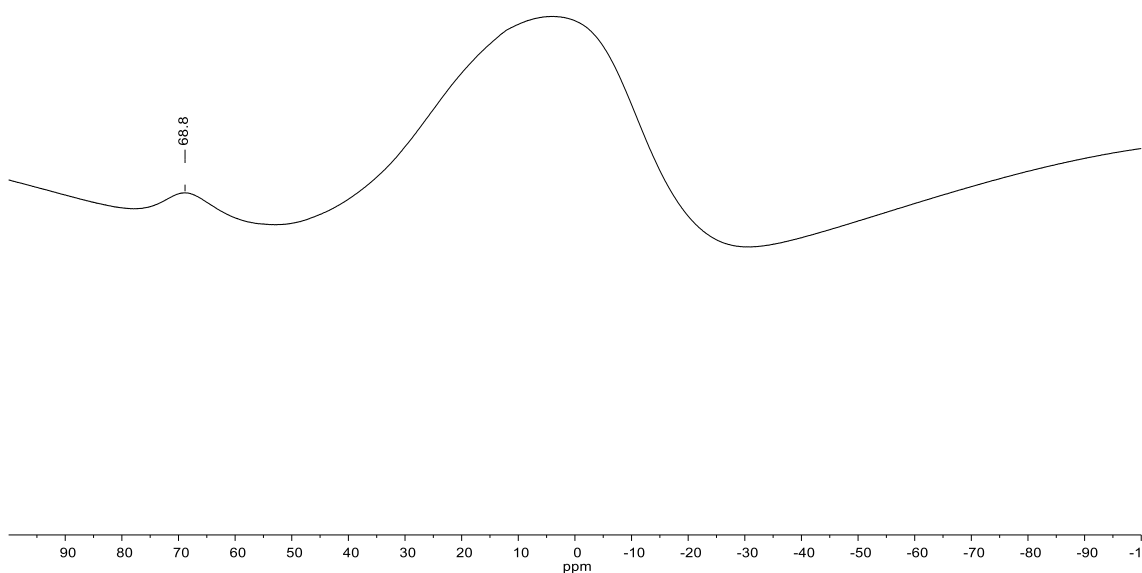


**Figure S62.**  $^{11}\text{B}$  NMR spectrum (96.3 MHz,  $\text{THF-}d_8$ ) of compound **20**.

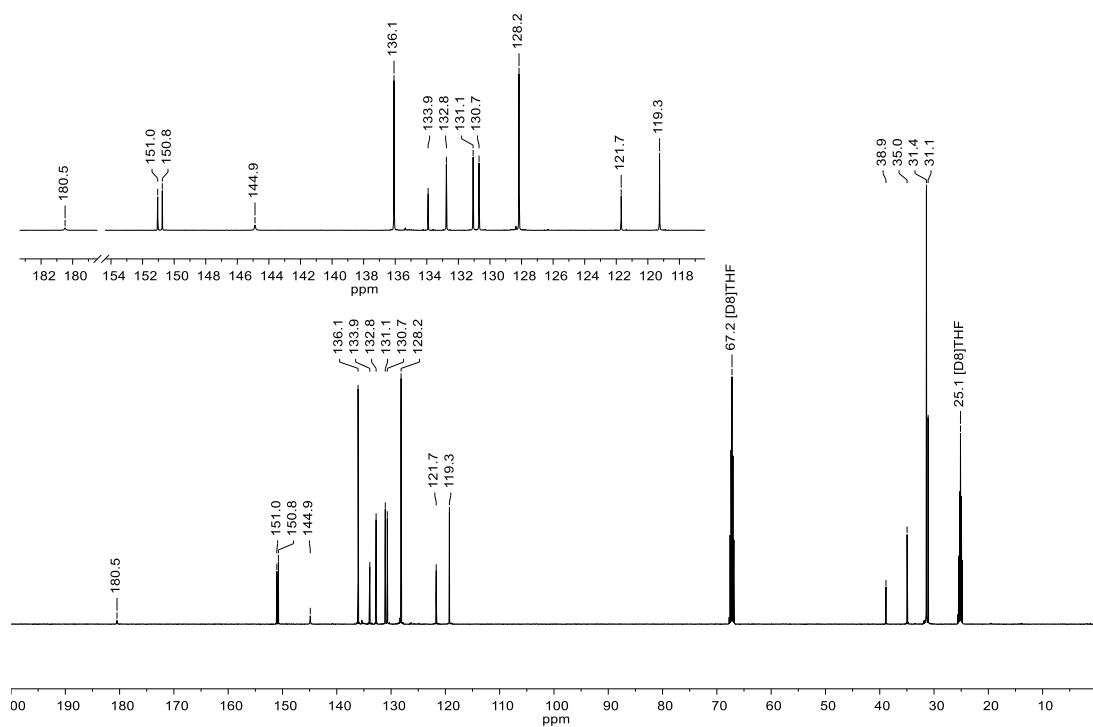


Figure S63.  $^{13}\text{C}$  NMR spectrum (125.8 MHz,  $\text{THF-}d_8$ ) of compound **20**.

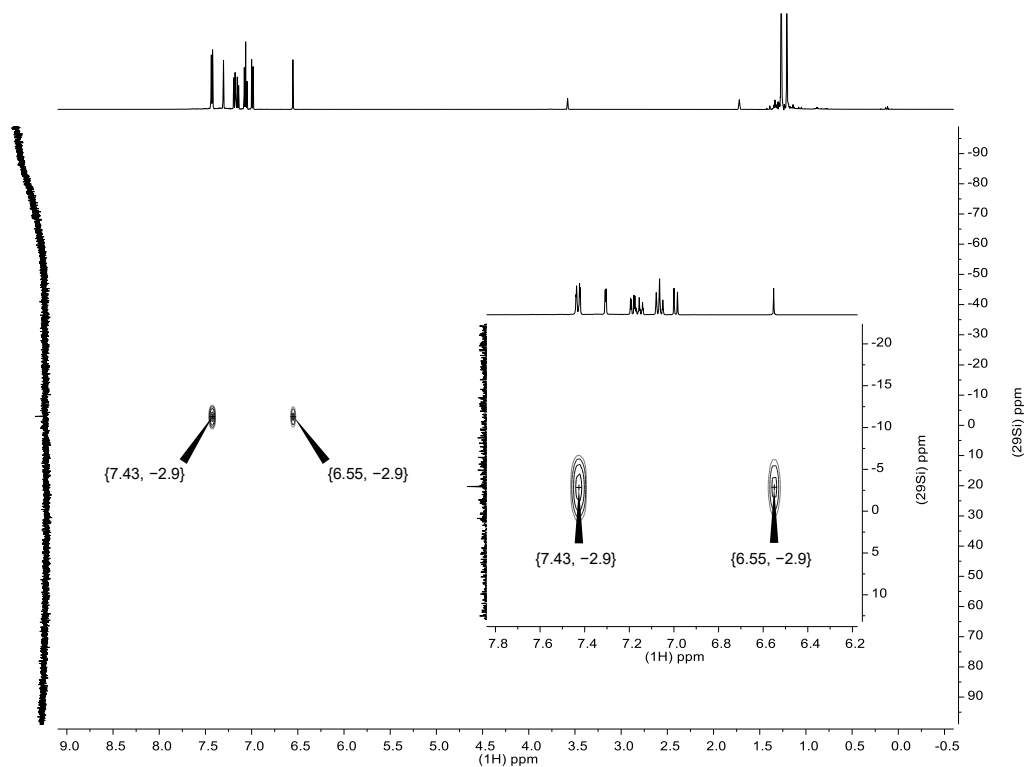


Figure S64.  $^1\text{H-}^{29}\text{Si}$ -HMBC NMR spectrum ( $^1\text{H}$ : 500.2 MHz,  $^{29}\text{Si}$ : 99.4 MHz,  $\text{THF-}d_8$ ) of compound **20**.

### 3. X-ray crystal structure determinations

Single-crystal diffraction data were collected at 173 K on a *STOE IPDS II* two-circle diffractometer equipped with a *Genix 3D HS* microfocus  $\text{MoK}_\alpha$  X-ray source ( $\lambda = 0.71073 \text{ \AA}$ ). The finalizations of the data, including empirical absorption corrections, was done using the X-Area program set v.1.50 (Stoe & Cie, 2006; for  $[\text{K}(\text{thf})_2]\{[\mathbf{11}]_{0.73}[\mathbf{12}]_{0.27}\}$  and  $\mathbf{10}(\text{thf})$ ) or the *CrysAlisPro* software v.1.171.42.43a (Rigaku Oxford Diffraction, 2022; for all other samples). In some cases the crystals scattered weakly and therefore showed almost no reflections at high  $2\Theta$  (see below for details). In these cases, the data above certain  $d_{hkl}$  limits were discarded from consideration. The structures were solved using the programs SHELXS or SHELXT and refined against  $|F|^2$  with full-matrix least-squares techniques using the program *SHELXL-2018/3*.<sup>S6</sup> Most hydrogen atoms were located geometrically and refined riding on the pivot atom; some B( $\mu$ -H)B or SiH-hydrogen atoms were freely refined (see below for details).

CIF files containing the crystallographic information were deposited with the Cambridge Crystallographic Data Centre under the deposition codes 2247211 – 2247221 and can be obtained free of charge via [www.ccdc.cam.ac.uk/data\\_request/cif](http://www.ccdc.cam.ac.uk/data_request/cif). Crystallographic data and parameters of the diffraction experiments are given in Tables S1-S6.

**Table S1.** Selected crystallographic data for [K(thf)<sub>2</sub>][**5**] and [K(thf)<sub>2</sub>][K(thf)<sub>3</sub>][FluB( $\mu$ -CH<sub>2</sub>CH<sub>2</sub>)( $\mu$ OH)BFlu]<sub>2</sub> · C<sub>6</sub>H<sub>14</sub>.

	[K(thf) <sub>2</sub> ][ <b>5</b> ]	[K(thf) <sub>2</sub> ][K(thf) <sub>3</sub> ][FluB( $\mu$ -CH <sub>2</sub> CH <sub>2</sub> )( $\mu$ -OH)BFlu] <sub>2</sub> · C <sub>6</sub> H <sub>14</sub>
CCDC code	2247211	2247212
Chemical formula	C <sub>50</sub> H <sub>69</sub> B <sub>2</sub> KO <sub>2</sub>	C <sub>104</sub> H <sub>146</sub> B <sub>4</sub> K <sub>2</sub> O <sub>7</sub> · C <sub>6</sub> H <sub>14</sub>
<i>M<sub>r</sub></i>	762.77	1715.81
Crystal system, space group	Monoclinic, <i>P</i> 2 <sub>1</sub> / <i>c</i>	Monoclinic, <i>P</i> 2 <sub>1</sub> / <i>n</i>
Temperature (K)	173	173
<i>a</i> , <i>b</i> , <i>c</i> (Å)	9.5248 (4), 27.3332 (15), 17.6167 (12)	17.7590 (9), 21.4676 (11), 28.6119 (16)
$\alpha$ , $\beta$ , $\gamma$ (°)	90, 91.785 (5), 90	90, 104.031 (6), 90
<i>V</i> (Å <sup>3</sup> )	4584.2 (4)	10582.6 (10)
<i>Z</i>	4	4
<i>F</i> (000)	1656	3736
<i>D<sub>x</sub></i> (Mg m <sup>-3</sup> )	1.105	1.077
Radiation type	Mo <i>K</i> $\alpha$	Mo <i>K</i> $\alpha$
$\mu$ (mm <sup>-1</sup> )	0.15	0.14
Crystal shape	Block	Needle
Color	Colorless	Colorless
Crystal size (mm)	0.18 × 0.12 × 0.09	0.15 × 0.10 × 0.05
Absorption correction	Multi-scan	Multi-scan
<i>T<sub>min</sub></i> , <i>T<sub>max</sub></i>	0.685, 1.000	0.951, 1.000
No. of measured, independent and observed [ <i>I</i> > 2 <i>s</i> ( <i>I</i> )] reflections	28566, 9347, 6058	80744, 8257, 5794
<i>R<sub>int</sub></i>	0.088	0.110
$\Theta_{\max}$ (°)	26.4	18.9
Range of <i>h</i> , <i>k</i> , <i>l</i>	<i>h</i> = -11 → 11, <i>k</i> = -34 → 34, <i>l</i> = -22 → 19	<i>h</i> = -16 → 16, <i>k</i> = -19 → 19, <i>l</i> = -26 → 26
<i>R</i> [ <i>F</i> <sup>2</sup> > 2 <i>s</i> ( <i>F</i> <sup>2</sup> )], <i>wR</i> ( <i>F</i> <sup>2</sup> ), <i>S</i>	0.061, 0.169, 1.01	0.082, 0.248, 1.02
No. of reflections	9347	8257
No. of parameters	542	1078
No. of restraints	33	15
$\Delta\rho_{\max}$ , $\Delta\rho_{\min}$ (e Å <sup>-3</sup> )	0.53, -0.29	0.67, -0.31

**Table S2.** Selected crystallographic data for  $[\text{K}(\text{thf})_2]\{[\mathbf{11}]_{0.73}[\mathbf{12}]_{0.27}\}$  and  $[\text{Li}(\text{thf})_4][\mathbf{12}]$ .

	$[\text{K}(\text{thf})_2]\{[\mathbf{11}]_{0.73}[\mathbf{12}]_{0.27}\}$	$[\text{Li}(\text{thf})_4][\mathbf{12}]$
CCDC code	2247213	2247214
Chemical formula	$\text{C}_{54}\text{H}_{77}\text{B}_2\text{KO}_2$	$\text{C}_{62}\text{H}_{93}\text{B}_2\text{LiO}_4$
$M_r$	818.87	930.92
Crystal system, space group	Monoclinic, $P2_1/n$	Monoclinic, $P2_1$
Temperature (K)	173	173
$a, b, c$ (Å)	14.9715 (5), 21.0575 (4), 17.4635 (5)	11.9232 (8), 19.4217 (13), 25.512 (2)
$\alpha, \beta, \gamma$ (°)	90, 114.563 (4), 90	90, 91.836 (8), 90
$V$ (Å <sup>3</sup> )	5007.4 (3)	5904.8 (7)
$Z$	4	4
$F(000)$	1784	2040
$D_x$ (Mg m <sup>-3</sup> )	1.086	1.047
Radiation type	Mo $K\alpha$	Mo $K\alpha$
$\mu$ (mm <sup>-1</sup> )	0.14	0.06
Crystal shape	Plate	Block
Color	Colorless	Colorless
Crystal size (mm)	0.29 × 0.28 × 0.14	0.29 × 0.27 × 0.24
Absorption correction	Multi-scan	Multi-scan
$T_{\min}, T_{\max}$	0.493, 1.000	0.265, 1.000
No. of measured, independent and observed [ $I > 2s(I)$ ] reflections	88021, 9514, 7942	23899, 23899, 9092
$R_{\text{int}}$	0.052	0.097
$\Theta_{\text{max}}$ (°)	25.7	25.4
Range of $h, k, l$	$h = -18 \rightarrow 18, k = -25 \rightarrow 25,$ $l = -21 \rightarrow 21$	$h = -14 \rightarrow 12, k = -23 \rightarrow 23,$ $l = -30 \rightarrow 30$
$R[F^2 > 2s(F^2)], wR(F^2), S$	0.055, 0.148, 1.05	0.062, 0.121, 0.75
No. of reflections	9514	23899
No. of parameters	690	1300
No. of restraints	18	25
$\Delta\rho_{\text{max}}, \Delta\rho_{\text{min}}$ (e Å <sup>-3</sup> )	0.33, -0.27	0.17, -0.16
Absolute structure (Flack) parameter	-	0.3(10)

**Table S3.** Selected crystallographic data for [K(thf)<sub>2</sub>][**16**] and **6**(thf) · 2 THF.

	[K(thf) <sub>2</sub> ][ <b>16</b> ]	<b>6</b> (thf) · 2 THF
CCDC code	2247215	2247216
Chemical formula	C <sub>54</sub> H <sub>75</sub> B <sub>2</sub> KO <sub>2</sub>	C <sub>46</sub> H <sub>61</sub> BOSi · 2(C <sub>4</sub> H <sub>8</sub> O)
<i>M</i> <sub>r</sub>	816.86	813.05
Crystal system, space group	Monoclinic, <i>P</i> 2 <sub>1</sub> / <i>n</i>	Monoclinic, <i>P</i> 2 <sub>1</sub> / <i>n</i>
Temperature (K)	173	173
<i>a</i> , <i>b</i> , <i>c</i> (Å)	14.9707 (12), 21.1115 (13), 17.2101 (16)	17.8000 (7), 14.6788 (5), 19.2967 (7)
<i>α</i> , <i>β</i> , <i>γ</i> (°)	90, 113.427 (10), 90	90, 96.263 (3), 90
<i>V</i> (Å <sup>3</sup> )	4990.9 (8)	5011.8 (3)
<i>Z</i>	4	4
<i>F</i> (000)	1776	1776
<i>D</i> <sub>x</sub> (Mg m <sup>-3</sup> )	1.087	1.078
Radiation type	Mo <i>Kα</i>	Mo <i>Kα</i>
<i>μ</i> (mm <sup>-1</sup> )	0.14	0.09
Crystal shape	Block	Block
Color	Orange	Colorless
Crystal size (mm)	0.16 × 0.14 × 0.08	0.20 × 0.19 × 0.15
Absorption correction	Multi-scan	Multi-scan
<i>T</i> <sub>min</sub> , <i>T</i> <sub>max</sub>	0.978, 1.000	0.709, 1.000
No. of measured, independent and observed [ <i>I</i> > 2 <i>s</i> ( <i>I</i> )] reflections	16636, 5179, 3511	49839, 9473, 4615
<i>R</i> <sub>int</sub>	0.088	0.111
Θ <sub>max</sub> (°)	20.8	25.7
Range of <i>h</i> , <i>k</i> , <i>l</i>	<i>h</i> = -14 → 14, <i>k</i> = -21 → 20, <i>l</i> = -17 → 17	<i>h</i> = -21 → 21, <i>k</i> = -17 → 17, <i>l</i> = -23 → 23
<i>R</i> [ <i>F</i> <sup>2</sup> > 2 <i>s</i> ( <i>F</i> <sup>2</sup> )], <i>wR</i> ( <i>F</i> <sup>2</sup> ), <i>S</i>	0.055, 0.147, 0.99	0.065, 0.181, 0.86
No. of reflections	5179	9473
No. of parameters	611	547
No. of restraints	57	18
Δρ <sub>max</sub> , Δρ <sub>min</sub> (e Å <sup>-3</sup> )	0.31, -0.21	0.51, -0.32

**Table S4.** Selected crystallographic data for **10**(thf) · 1.5 Et<sub>2</sub>O and **13**.

	<b>10</b> (thf) · 1.5 Et <sub>2</sub> O	<b>13</b>
CCDC code	2247217	2247218
Chemical formula	C <sub>46</sub> H <sub>60</sub> BClOSi · 1.5(C <sub>4</sub> H <sub>10</sub> O)	C <sub>46</sub> H <sub>60</sub> BClSi
<i>M<sub>r</sub></i>	814.47	687.29
Crystal system, space group	Monoclinic, <i>P2<sub>1</sub>/c</i>	Monoclinic, <i>P2<sub>1</sub>/n</i>
Temperature (K)	173	173
<i>a</i> , <i>b</i> , <i>c</i> (Å)	14.8477 (7), 14.9915 (7), 22.6511 (12)	11.9435 (8), 24.517 (2), 15.0825 (12)
<i>α</i> , <i>β</i> , <i>γ</i> (°)	90, 100.094 (4), 90	90, 103.854 (8), 90
<i>V</i> (Å <sup>3</sup> )	4963.9 (4)	4288.0 (6)
<i>Z</i>	4	4
<i>F</i> (000)	1772	1488
<i>D<sub>x</sub></i> (Mg m <sup>-3</sup> )	1.090	1.065
Radiation type	Mo <i>Kα</i>	Mo <i>Kα</i>
<i>μ</i> (mm <sup>-1</sup> )	0.14	0.15
Crystal shape	Block	Block
Colour	Colorless	Yellow
Crystal size (mm)	0.32 × 0.31 × 0.26	0.21 × 0.14 × 0.13
Absorption correction	Multi-scan	Multi-scan
<i>T<sub>min</sub></i> , <i>T<sub>max</sub></i>	0.497, 1.000	0.908, 1.000
No. of measured, independent and observed [ <i>I</i> > 2 <i>s</i> ( <i>I</i> )] reflections	30219, 9272, 7369	17034, 6106, 3610
<i>R<sub>int</sub></i>	0.045	0.126
<i>Θ<sub>max</sub></i> (°)	25.7	23.3
Range of <i>h</i> , <i>k</i> , <i>l</i>	<i>h</i> = -17 → 18, <i>k</i> = -18 → 18, <i>l</i> = -27 → 27	<i>h</i> = -13 → 13, <i>k</i> = -24 → 27, <i>l</i> = -16 → 16
<i>R</i> [ <i>F</i> <sup>2</sup> > 2 <i>s</i> ( <i>F</i> <sup>2</sup> )], <i>wR</i> ( <i>F</i> <sup>2</sup> ), <i>S</i>	0.071, 0.191, 1.16	0.058, 0.127, 0.96
No. of reflections	9272	6106
No. of parameters	576	487
No. of restraints	70	36
<i>Δρ<sub>max</sub></i> , <i>Δρ<sub>min</sub></i> (e Å <sup>-3</sup> )	0.59, -0.44	0.24, -0.27

**Table S5.** Selected crystallographic data for **14** · 1.5 C<sub>6</sub>H<sub>6</sub> and **17**.

	<b>14</b> · 1.5 C <sub>6</sub> H <sub>6</sub>	<b>17</b>
CCDC code	2247219	2247220
Chemical formula	C <sub>46</sub> H <sub>60</sub> BClSi · 1.5(C <sub>6</sub> H <sub>6</sub> )	C <sub>46</sub> H <sub>58</sub> BClSi
<i>M<sub>r</sub></i>	804.45	685.27
Crystal system, space group	Triclinic, <i>P</i> -1	Triclinic, <i>P</i> -1
Temperature (K)	173	173
<i>a</i> , <i>b</i> , <i>c</i> (Å)	9.8384 (7), 14.6699 (11), 17.4340 (13)	9.8879 (12), 14.446 (2), 16.292 (3)
<i>α</i> , <i>β</i> , <i>γ</i> (°)	92.485 (6), 98.376 (6), 102.215 (6)	115.332 (15), 91.157 (11), 102.693 (11)
<i>V</i> (Å <sup>3</sup> )	2425.9(3)	2034.6 (6)
<i>Z</i>	2	2
<i>F</i> (000)	870	740
<i>D<sub>x</sub></i> (Mg m <sup>-3</sup> )	1.101	1.119
Radiation type	Mo <i>Kα</i>	Mo <i>Kα</i>
<i>μ</i> (mm <sup>-1</sup> )	0.14	0.15
Crystal shape	Block	Plate
Color	Colorless	Yellow
Crystal size (mm)	0.21 × 0.12 × 0.09	0.24 × 0.22 × 0.06
Absorption correction	Multi-scan	Multi-scan
<i>T<sub>min</sub></i> , <i>T<sub>max</sub></i>	0.507, 1.000	0.126, 1.000
No. of measured, independent and observed [ <i>I</i> > 2 <i>s</i> ( <i>I</i> )] reflections	23285, 9058, 5163	8415, 4168, 2608
<i>R<sub>int</sub></i>	0.075	0.076
<i>Θ<sub>max</sub></i> (°)	25.7	20.8
Range of <i>h</i> , <i>k</i> , <i>l</i>	<i>h</i> = -11→11, <i>k</i> = -17→17, <i>l</i> = -21→20	<i>h</i> = -9→9, <i>k</i> = -14→14, <i>l</i> = -16→16
<i>R</i> [ <i>F</i> <sup>2</sup> > 2 <i>s</i> ( <i>F</i> <sup>2</sup> )], <i>wR</i> ( <i>F</i> <sup>2</sup> ), <i>S</i>	0.055, 0.147, 0.99	0.071, 0.201, 1.03
No. of reflections	0.075, 0.189, 1.01	4168
No. of parameters	9058	511
No. of restraints	523	55
<i>Δρ<sub>max</sub></i> , <i>Δρ<sub>min</sub></i> (e Å <sup>-3</sup> )	0.47, -0.24	0.64, -0.30

**Table S6.** Selected crystallographic data for **20**.

<b>20</b>	
CCDC code	2247221
Chemical formula	C <sub>38</sub> H <sub>44</sub> BClSi
$M_r$	575.08
Crystal system, space group	Monoclinic, $P2_1/n$
Temperature (K)	173
$a, b, c$ (Å)	9.6488 (4), 12.5511 (5), 27.859 (1)
$\alpha, \beta, \gamma$ (°)	90, 96.072 (4), 90
$V$ (Å <sup>3</sup> )	3354.9 (2)
$Z$	4
$F(000)$	1232
$D_x$ (Mg m <sup>-3</sup> )	1.139
Radiation type	Mo $K\alpha$
$\mu$ (mm <sup>-1</sup> )	0.17
Crystal shape	Needle
Color	Yellow
Crystal size (mm)	0.25 × 0.13 × 0.13
Absorption correction	Multi-scan
$T_{\min}, T_{\max}$	0.765, 1.000
No. of measured, independent and observed [ $I > 2s(I)$ ] reflections	38252, 6600, 4728
$R_{\text{int}}$	0.112
$\Theta_{\text{max}}$ (°)	26.0
Range of $h, k, l$	$h = -11 \rightarrow 11, k = -15 \rightarrow 15,$ $l = -34 \rightarrow 34$
$R[F^2 > 2s(F^2)], wR(F^2), S$	0.048, 0.122, 1.01
No. of reflections	6600
No. of parameters	379
No. of restraints	0
$\Delta\rho_{\text{max}}, \Delta\rho_{\text{min}}$ (e Å <sup>-3</sup> )	0.31, -0.30

### 3.1 Single-crystal X-ray analysis of [K(thf)<sub>2</sub>][5]

Compound [K(thf)<sub>2</sub>][5] crystallizes in the monoclinic space group *P*2<sub>1</sub>/*c* (No. 14). The position of the  $\mu$ -H atom between the two boron atoms was localized in the residual density map and freely refined by applying isotropic approximation. One of the terminal *tert*-butyl groups was found to be rotationally disordered over two positions with the relative weights refined as 78:22 %. Both the anion and the [K(thf)<sub>2</sub>]<sup>+</sup> cation occupy general crystallographic positions, and the coordination sphere of the potassium atom is completed by carbon atoms belonging to aromatic rings as well as by two thf molecules. The specific mutual arrangement of the [K(thf)<sub>2</sub>]<sup>+</sup> and the B( $\mu$ -H)( $\mu$ -CH<sub>2</sub>CH<sub>2</sub>)B fragment leads to the formation of a K $\cdots$ ( $\mu$ -H) contact of 2.73(2) Å.

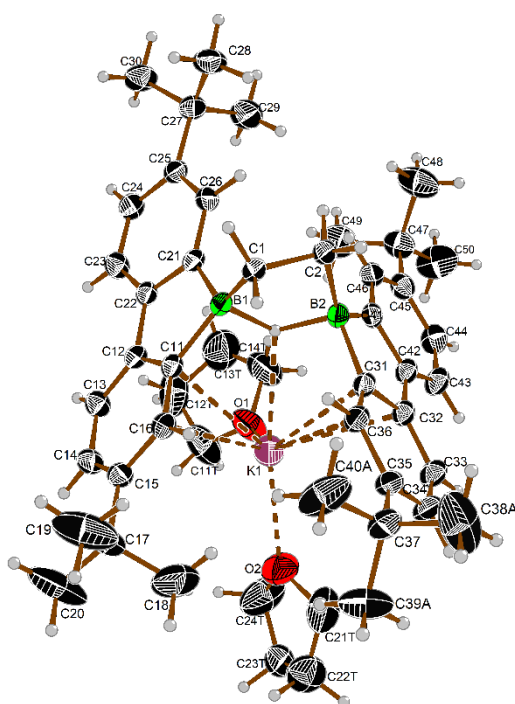


**Figure S65.** Molecular structure of [K(thf)<sub>2</sub>][5] in the solid state. Displacement ellipsoids are drawn at the 50 % probability level. Only the atoms with the occupancy >50 % are depicted.

### 3.2 Single-crystal X-ray analysis of $[\text{K}(\text{thf})_2][\text{K}(\text{thf})_3][\text{FluB}(\mu\text{-CH}_2\text{CH}_2)(\mu\text{-OH})\text{BFlu}]_2$

Compound  $[\text{K}(\text{thf})_2][\text{K}(\text{thf})_3][\text{FluB}(\mu\text{-CH}_2\text{CH}_2)(\mu\text{-OH})\text{BFlu}]_2$  crystallizes in the monoclinic space group  $P2_1/n$  (No. 14) with one *n*-hexane solvent molecule per two crystallographically unique  $[\text{K}(\text{thf})_n]^+$  ( $n = 2$  or 3) cations and  $[\text{FluB}(\mu\text{-CH}_2\text{CH}_2)(\mu\text{-OH})\text{BFlu}]^-$  anions. The single crystal scattered rather weakly, showing almost no reflections above  $d_{hkl} = 1.1 \text{ \AA}$ . Therefore, all data above this diffraction limit were discarded from the refinement. Both H atoms of the two OH groups were found in the residual density map and refined riding on the corresponding oxygen atoms. Both  $[\text{K}(\text{thf})_n]^+$  cations coordinate the organic anions via their carbon  $\pi$ -systems, thereby forming infinite chains along the *a* axis (Figure S67).

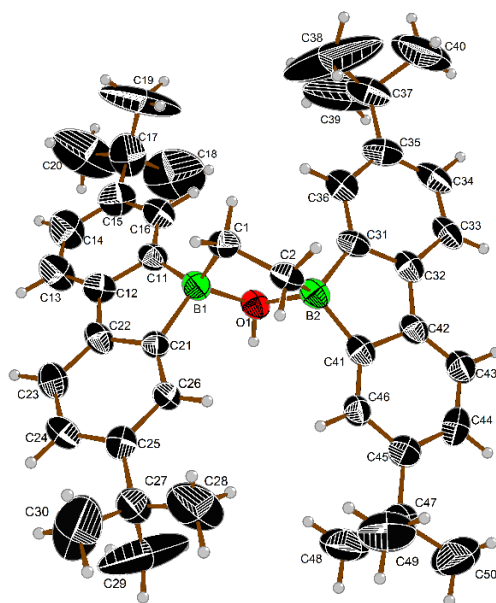


**Figure S66.** Molecular structure of  $[\text{K}(\text{thf})_2][\text{K}(\text{thf})_3][\text{FluB}(\mu\text{-CH}_2\text{CH}_2)(\mu\text{-OH})\text{BFlu}]_2$  in the solid state (only one of the two independent anions within the asymmetric unit is shown; the complex cations  $[\text{K}(\text{thf})_n]^+$  ( $n = 2$  or 3) and the non-coordinating *n*-hexane molecule are omitted for clarity. Displacement ellipsoids are drawn at the 50 % probability level.

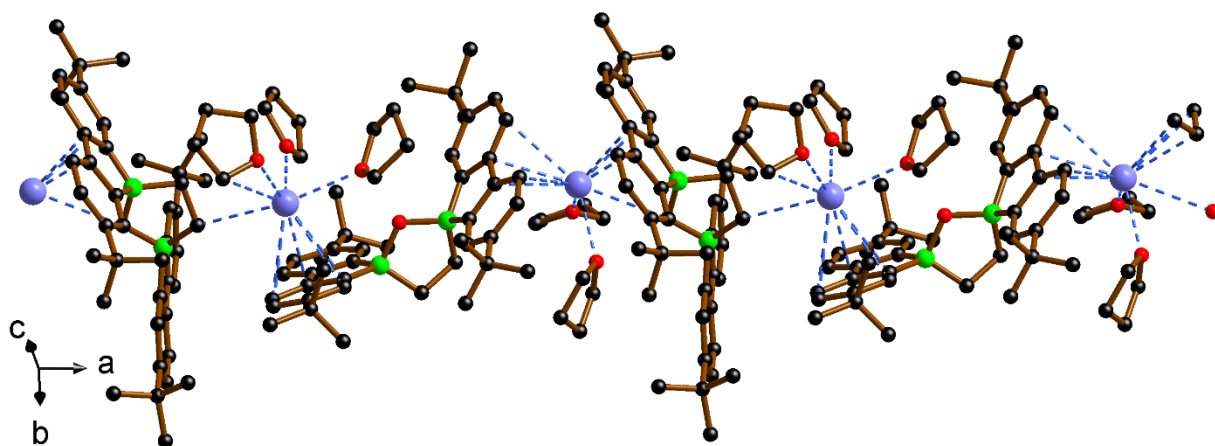


**Figure S67.** Infinite chains along the *a* axis in  $[\text{K}(\text{thf})_2][\text{K}(\text{thf})_3][\text{FluB}(\mu\text{-CH}_2\text{CH}_2)(\mu\text{-OH})\text{BFlu}]_2$ . H atoms are omitted for clarity.

### 3.3 Single-crystal X-ray analysis of $[\text{K}(\text{thf})_2]\{[\mathbf{11}]_{0.73}[\mathbf{12}]_{0.27}\}$

Compound  $[\text{K}(\text{thf})_2]\{[\mathbf{11}]_{0.73}[\mathbf{12}]_{0.27}\}$  crystallizes in the monoclinic space group  $P2_1/n$  (No. 14). The structure is disordered in a peculiar way pointing to the overlap of two species (Figure S68). Almost all atoms of both species coincide except for their  $\{\text{B}_2(\mu\text{-H})(\mu\text{-CH}_2\text{CH}t\text{Bu})\}$  and  $\{\text{B}_2(\mu\text{-H})(\mu\text{-CHCH}_2t\text{Bu})\}$  fragments, which overlap partly. The ratio of both species is 73:27 % (Figure S69). The position of the  $\mu\text{-H}$  atom which is shared by both species was found in the residual density map and freely refined. The coordination sphere of the complex  $\text{K}^+$  cation includes the anion ( $\pi$ -system) as well as two thf ligands. The  $[\text{K}(\text{thf})_2]^+$  cations link with the anions to form an infinite chain along  $[101]$  (Figure S70).

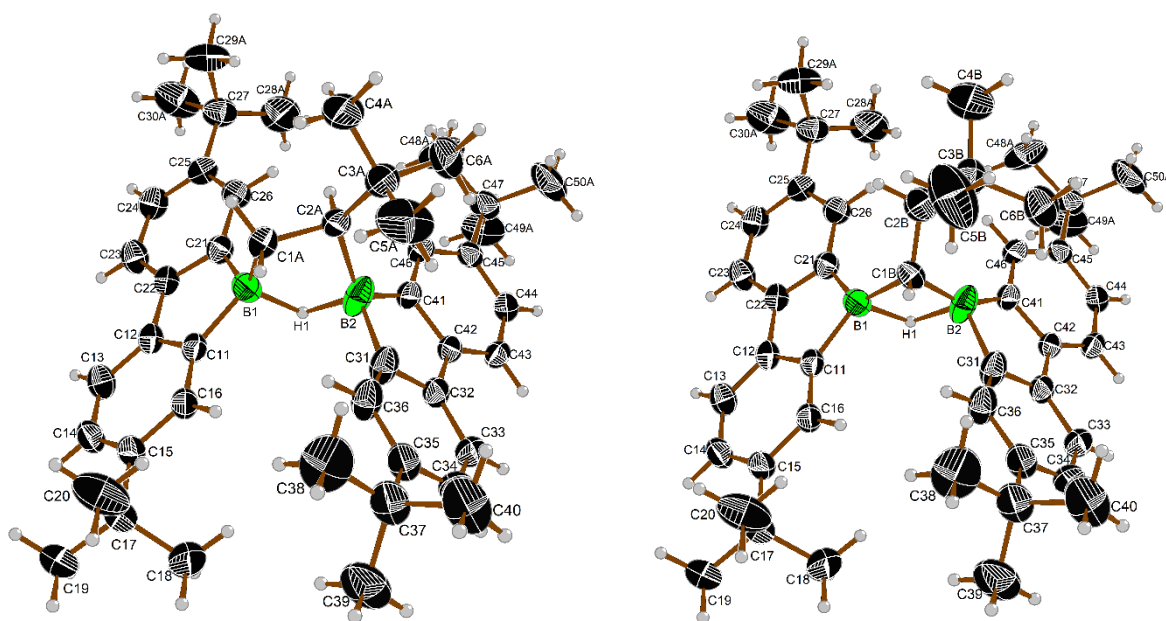


**Figure S68.** Molecular structure of  $[\text{K}(\text{thf})_2]\{[\mathbf{11}]_{0.73}[\mathbf{12}]_{0.27}\}$  in the solid state. Left:  $[\mathbf{11}]^-$  anion; right:  $[\mathbf{12}]^-$  anion. The coordinating complex cation  $[\text{K}(\text{thf})_2]^+$  is omitted for clarity. Displacement ellipsoids are drawn at the 50 % probability level.

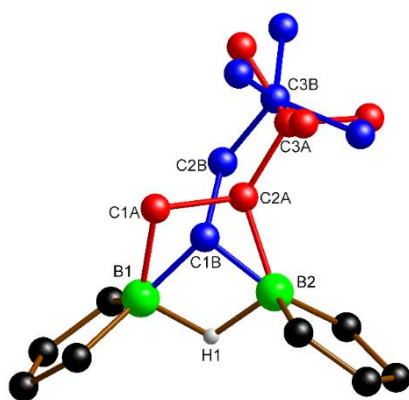


**Figure S69.** Overlap of the  $\{\text{B}(\mu\text{-H})(\mu\text{-CH}_2\text{CH}(t\text{Bu})\text{B})$  ( $\sim 73$  %, red) and  $\{\text{B}(\mu\text{-H})(\mu\text{-CHCH}_2(t\text{Bu})\text{B})$  ( $\sim 27$  %, blue) fragments in the crystal of  $[\text{K}(\text{thf})_2]\{[\mathbf{11}]_{0.73}[\mathbf{12}]_{0.27}\}$ .

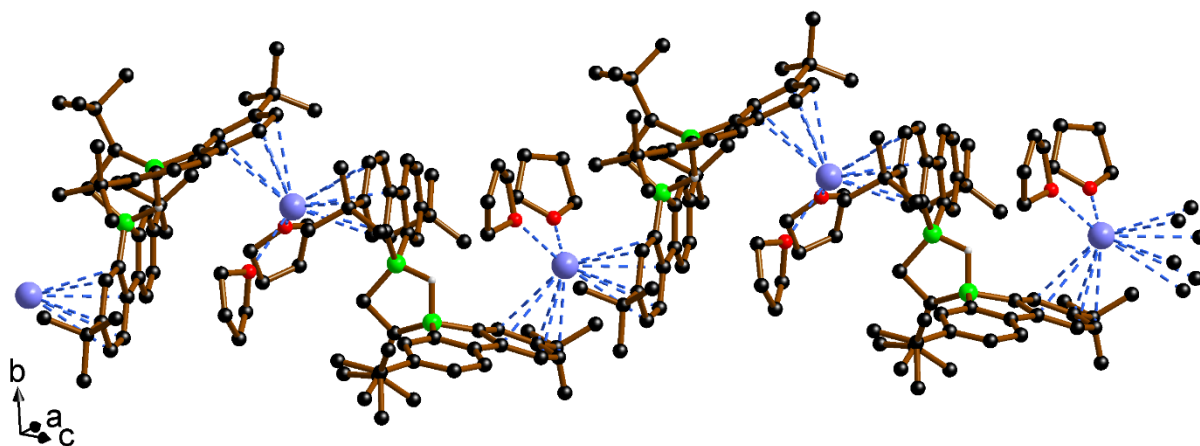


**Figure S70.** Infinite chains along  $[101]$  in  $[K(thf)_2]\{[11]_{0.73}[12]_{0.27}\}$ . C-bonded H atoms are omitted for clarity. Only the atoms with the occupancy  $>50\%$  are depicted.

### 3.4 Single-crystal X-ray analysis of [Li(thf)<sub>4</sub>][12]

Compound [Li(thf)<sub>4</sub>][12] crystallizes in the chiral polar monoclinic space group  $P2_1$  (No. 4). It was not possible to determine the absolute configuration of the crystal because the compound does not exhibit anomalous scattering effects due to the absence of heavy atoms. The measured crystal was twinned, with the second domain rotated by  $\sim 180^\circ$  around the [100] direct axis. The relative weight of the domains was about 60:40 %. The crystal structure consists of two crystallographically unique complex tetracoordinated [Li(thf)<sub>4</sub>]<sup>+</sup> cations and two organic anions occupying general crystallographic positions. The positions of the  $\mu$ -H atoms within the B( $\mu$ -H)B fragments were found in the residual density map and refined without constraints.

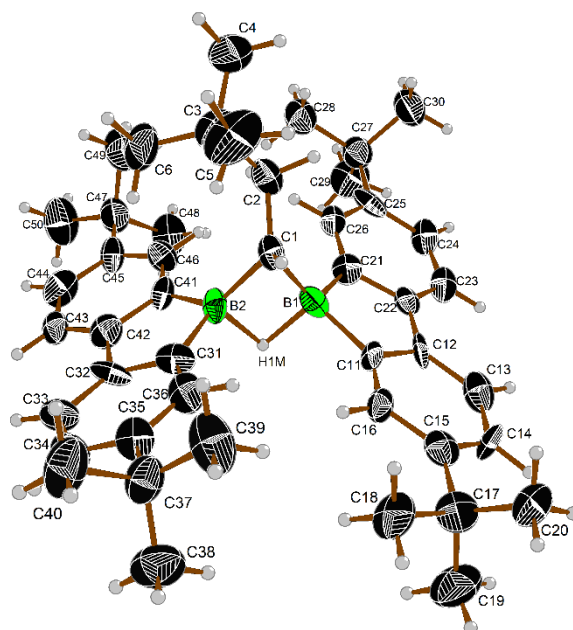


**Figure S71.** Molecular structure of [Li(thf)<sub>4</sub>][12] in the solid state. Shown is one of the two crystallographically unique organic anions. The non-coordinating complex cation [Li(thf)<sub>4</sub>]<sup>+</sup> is omitted for clarity. Displacement ellipsoids are drawn at the 50 % probability level.

### 3.5 Single-crystal X-ray analysis of $[\text{K}(\text{thf})_2][\mathbf{16}]$

Compound  $[\text{K}(\text{thf})_2][\mathbf{16}]$  crystallizes in the monoclinic space group  $P2_1/n$  (No. 14). The single crystal scattered rather weakly, showing almost no reflections above  $d_{hkl} = 1.0 \text{ \AA}$ . Therefore, all data above this diffraction limit were discarded from the refinement. The position of the  $\mu\text{-H}$  atom between the two boron atoms was found in the residual density map and freely refined by applying isotropic approximation. Two of the terminal *tert*-butyl groups are rotationally disordered over two positions, each with the relative weights refined as 58:42 % and 76:24 %. Both the anion and the complex  $[\text{K}(\text{thf})_2]^+$  cation occupy general crystallographic positions. Along with its two thf ligands, the  $\text{K}^+$  cation coordinates also the  $\pi$ -systems of neighboring anions to form infinite chains along  $[101]$  (Figure S73).

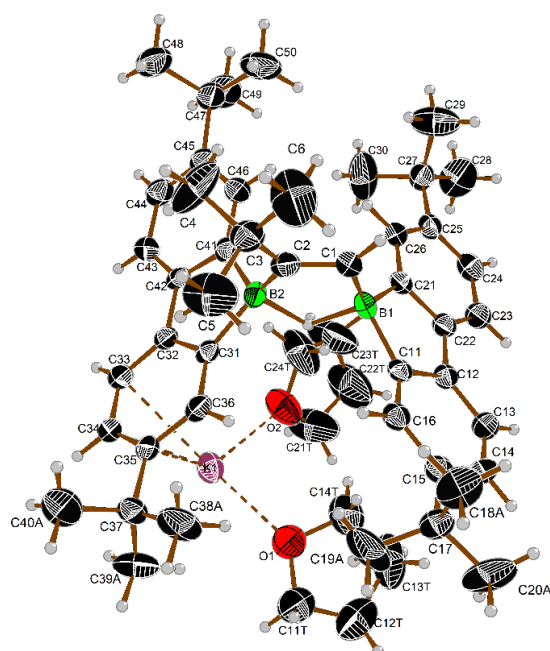


**Figure S72.** Molecular structure of  $[\text{K}(\text{thf})_2][\mathbf{16}]$  in the solid state. Displacement ellipsoids are drawn at the 50 % probability level. Only the atoms with the occupancy  $>50\%$  are depicted.

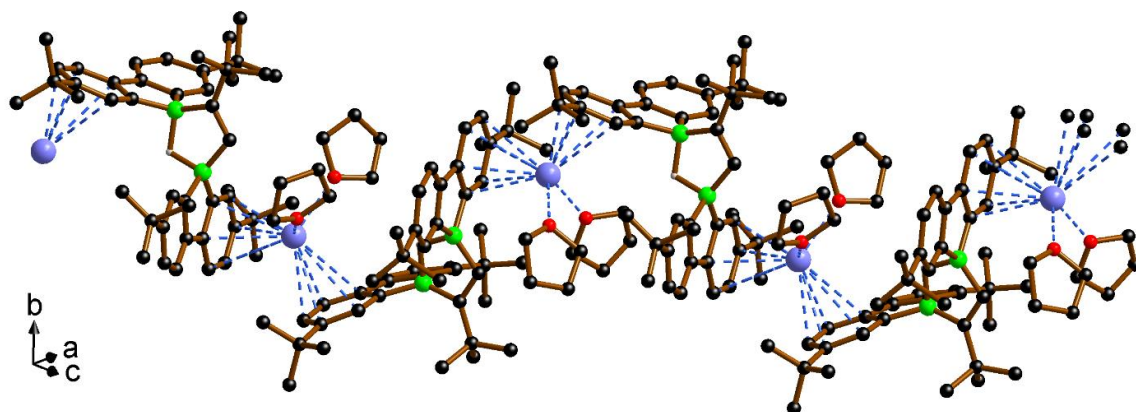


**Figure S73.** Infinite chains along  $[101]$  in  $[\text{K}(\text{thf})_2][\mathbf{16}]$ . C-bonded H atoms are omitted for clarity. Only the atoms with the occupancy  $>50\%$  are depicted.

### 3.6 Single-crystal X-ray analysis of 6(thf)

Compound **6**(thf) crystallizes together with two THF solvent molecules in the monoclinic space group  $P2_1/n$  (No. 14). The only crystallographically unique molecule lies, fully ordered, in the general crystallographic position. The terminal H atom at the Si1 atom was localized in the residual density map and refined freely with  $U_{iso}$  equal to the equivalent atomic displacement parameter of the Si1 atom.

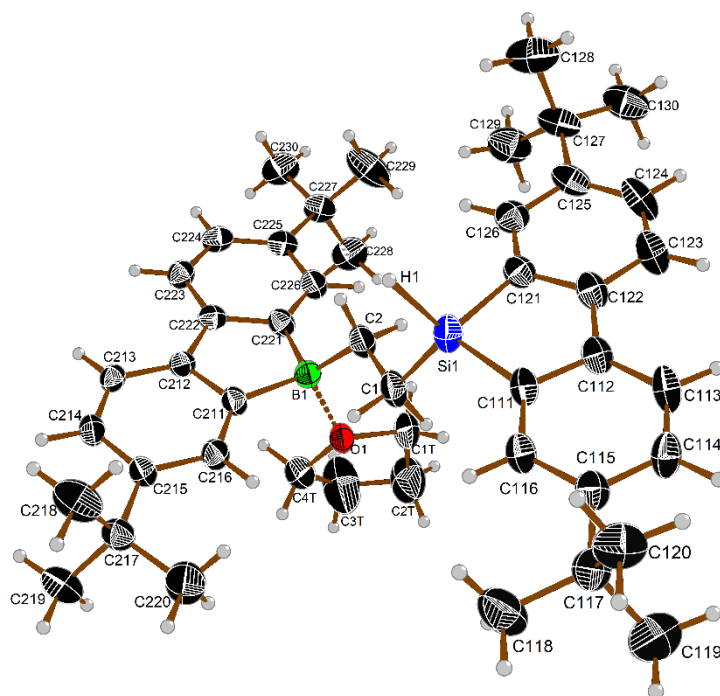


**Figure S74.** Molecular structure of **6**(thf) in the solid state. Two non-coordinating THF molecules are omitted for clarity. Displacement ellipsoids are drawn at the 50 % probability level.

### 3.7 Single-crystal X-ray analysis of 10(thf)

Compound **10**(thf) crystallizes in the monoclinic space group  $P2_1/c$  (No. 14) with 1.5 solvent molecules of  $\text{Et}_2\text{O}$  per formula unit. One of these molecules occupies the inversion center, while the second  $\text{Et}_2\text{O}$  molecule lies in the general crystallographic position. Two of the four terminal *tert*-butyl groups are rotationally disordered over two positions with the relative weights refined as 83:17 % and 85:15 %.

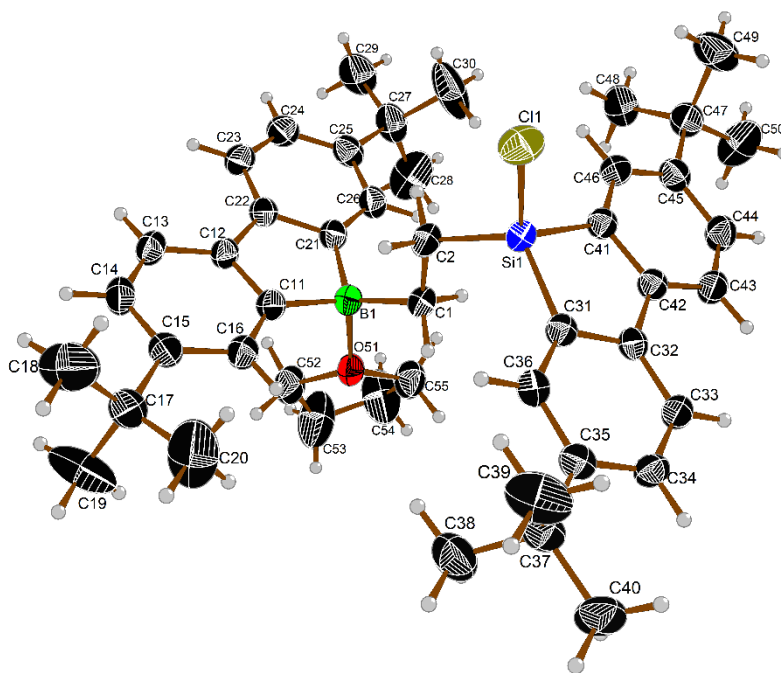


**Figure S75.** Molecular structure of **10**(thf) in the solid state. All non-coordinating  $\text{Et}_2\text{O}$  molecules are omitted for clarity. Displacement ellipsoids are drawn at the 50 % probability level. Only the atoms with the occupancy >50 % are depicted.

### 3.8 Single-crystal X-ray analysis of 13

Compound **13** crystallizes in the monoclinic space group  $P2_1/n$  (No. 14). The single crystal scattered rather weakly, showing almost no reflections above  $d_{hkl} = 0.9 \text{ \AA}$ . Therefore, all data above this diffraction limit were discarded from the refinement. The molecule lies in the general crystallographic position. One of the terminal *tert*-butyl groups is rotationally disordered over two positions with the relative weights refined as 75:25 %.

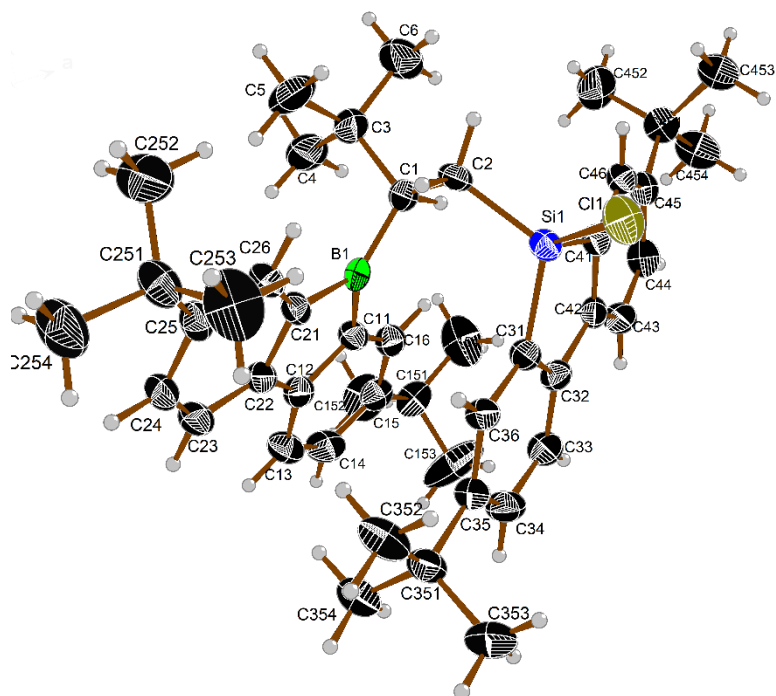


**Figure S76.** Molecular structure of **13** in the solid state. Displacement ellipsoids are drawn at the 50 % probability level. Only the atoms with the occupancy >50 % are depicted.

### 3.9 Single-crystal X-ray analysis of **14**

Compound **14** crystallizes with 1.5 C<sub>6</sub>H<sub>6</sub> molecules in the triclinic space group *P1* (No. 2). The molecule **14** occupies the general crystallographic position, while two crystallographically unique C<sub>6</sub>H<sub>6</sub> solvent molecules occupy the general position and the inversion center, respectively.

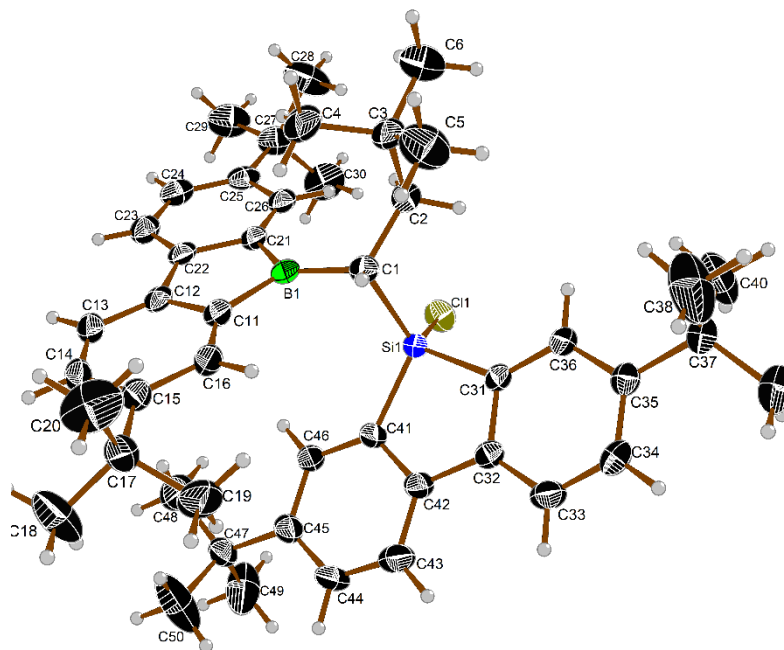


**Figure S77.** Molecular structure of **14** in the solid state. All non-coordinating C<sub>6</sub>H<sub>6</sub> molecules are omitted for clarity. Displacement ellipsoids are drawn at the 50 % probability level.

### 3.10 Single-crystal X-ray analysis of 17

Compound **17** crystallizes in the triclinic space group *P1* (No. 2). The single crystal scattered rather weakly, showing almost no reflections above  $d_{hkl} = 1.0 \text{ \AA}$ . Therefore, all data above this diffraction limit were discarded from the refinement. The only crystallographically unique molecule lies in the general crystallographic position, with one of the terminal *tert*-butyl groups being rotationally disordered over three positions with the relative weights refined as 59:27:14 %.

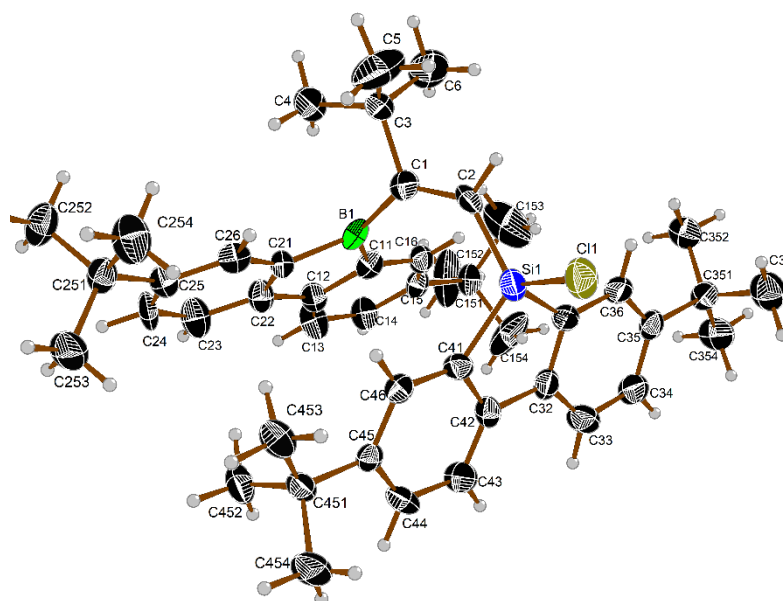


**Figure S78.** Molecular structure of **17** in the solid state. Displacement ellipsoids are drawn at the 50 % probability level. Only the atoms with the occupancy >50 % are depicted.

### 3.11 Single-crystal X-ray analysis of **20**

Compound **20** crystallizes in the monoclinic space group  $P2_1/n$  (No. 14). The molecule lies on the general position showing no disorder.

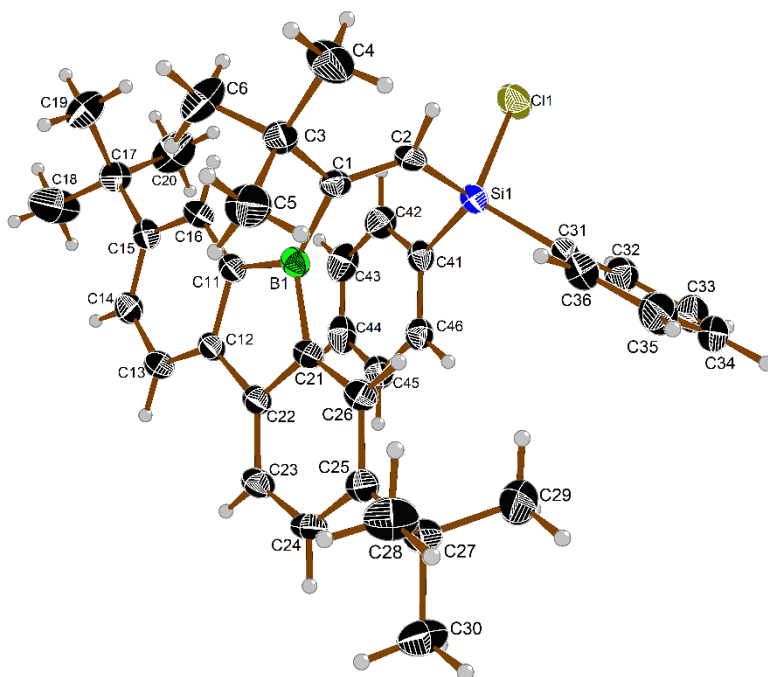


**Figure S79.** Molecular structure of **20** in the solid state. Displacement ellipsoids are drawn at the 50 % probability level.

## 4. Computational details

All DFT calculations were performed using *Gaussian 16, Revision B.01*,<sup>S7</sup> while coupled cluster calculations were done in *ORCA 5.0.3*.<sup>S8</sup> IBO calculations were carried out with *IBOview*.<sup>S9</sup> The NBO analyses were performed with *NBO 7.0*.<sup>S10</sup> Graphical representations of molecular geometries were produced with the *CYLVIEW20* software.<sup>S11</sup>

To determine appropriate methods for optimizing the structures investigated herein, we performed geometry optimizations of **[3]<sup>-</sup>** and **9(thf)** considering five distinct DFT functionals, namely B3LYP-D3<sup>S12</sup>(BJ)<sup>S13</sup>, BP86<sup>S14</sup>-D3(BJ), M06-2X<sup>S15</sup>-D3, PBE0<sup>S16</sup>-D3(BJ), and  $\omega$ B97XD<sup>S17</sup>. Pople's 6-31+G\*\* basis set was used in these calculations.<sup>S18</sup> The optimized results were compared to the respective X-ray crystal structures **[K(thf)<sub>2</sub>][3]** (CCDC code: 1456614)<sup>S19</sup> and **9(thf)** (CCDC code: 2203995).<sup>S2</sup> A comparison of the root-mean-square deviation (RMSD) values, which were obtained excluding hydrogen atoms and *tert*-butyl groups, are shown in Table S7. Our results show that, on average,  $\omega$ B97XD provided the least RMSD values, closely followed by M06-2X-D3. Based on these results, we investigated the impact on the RMSD values of including implicit solvation by the solvent model based on density (SMD; solvent = THF;  $\epsilon = 7.4257$ ),<sup>S20</sup> the more diffuse 6-31++G\*\* Pople basis set, as well as both in combination (Table S8). The use of the more diffuse basis set showed almost no effect, whereas the use of the SMD model led to significantly lower RMSD values. Overall, SMD(THF)/ $\omega$ B97XD/6-31+G\*\* performed best among the tested theory levels. Optimized geometries were confirmed to be the desired minimum energy structures or transition states by vibrational frequency analysis.

**Table S7.** Root-mean-square deviation (RMSD) values for each functional in combination with Pople's 6-31+G\*\* basis set. RMSD values are reported excluding hydrogen atoms and *tert*-butyl groups.

Compound	B3LYP-D3(BJ)	BP86-D3(BJ)	M06-2X-D3	PBE0-D3(BJ)	$\omega$ B97XD
<b>[3]<sup>-</sup></b>	0.1303	0.1293	0.1259	0.1378	0.1265
<b>9(thf)</b>	0.3027	0.3719	0.2881	0.3157	0.2873
<b>Avg.</b>	<b>0.2165</b>	<b>0.2506</b>	<b>0.2070</b>	<b>0.2267</b>	<b>0.2069</b>

**Table S8.** Root-mean-square deviation (RMSD) values observed with the functional  $\omega$ B97XD in combination with the basis sets 6-31+G\*\* or 6-31++G\*\*, each without and with the SMD(THF) model.

Compound	6-31+G** <i>No SMD</i>	6-31+G** SMD(THF)	6-31++G** <i>No SMD</i>	6-31++G** SMD(THF)
<b>[3]<sup>-</sup></b>	0.1265	0.1005	0.1253	0.0992
<b>9(thf)</b>	0.2873	0.2670	0.2885	0.2711
<b>Avg.</b>	<b>0.2069</b>	<b>0.1838</b>	<b>0.2069</b>	<b>0.1851</b>

In the following benchmark study and all calculated mechanistic scenarios, the aryl-bonded *tert*-butyl groups were substituted by hydrogen atoms (corresponding compound numbers are denoted with a superscript C), since this drastically reduced the CPU time. This is justified by the neglectable influence of the *tert*-butyl groups on the conformation of the individual compounds as depicted in Figure S80 (RMSD values:  $[3]^-$  vs.  $[3^C]^-$  = 0.06;  $[5]^-$  vs.  $[5^C]^-$  = 0.18; **2** vs. **2<sup>C</sup>** = 0.15; *anti*-**6** vs. *anti*-**6<sup>C</sup>** = 0.23; excluding C-bonded H atoms and *tert*-butyl groups).

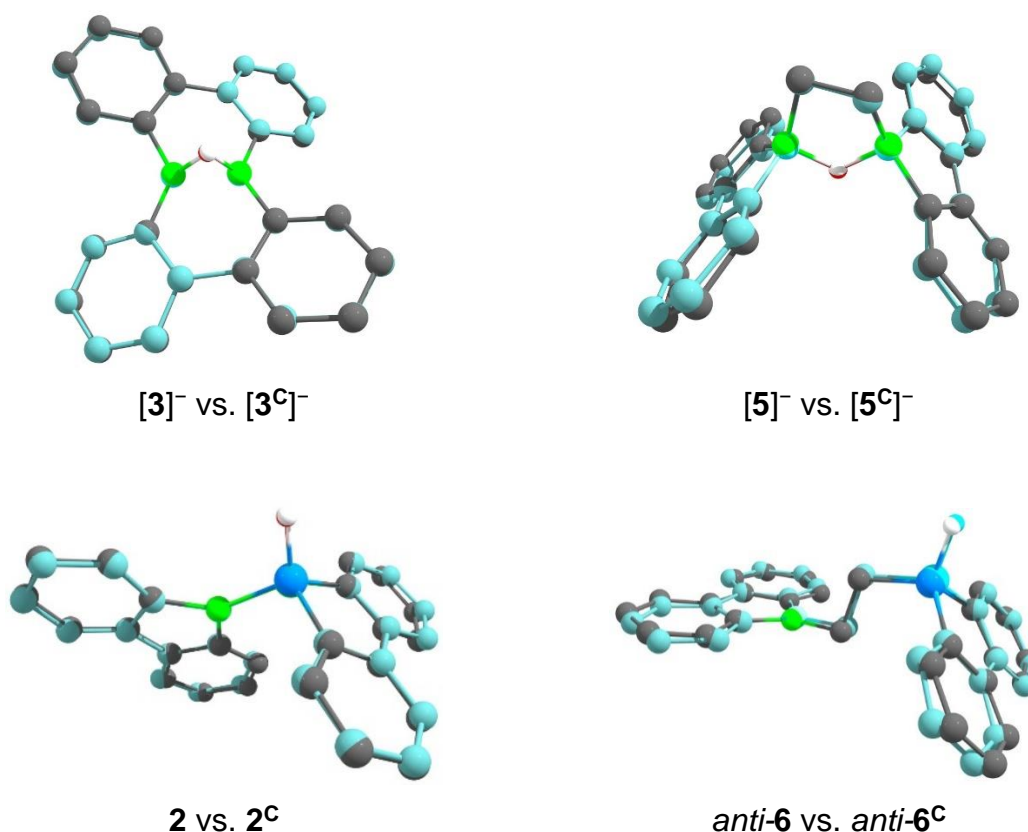
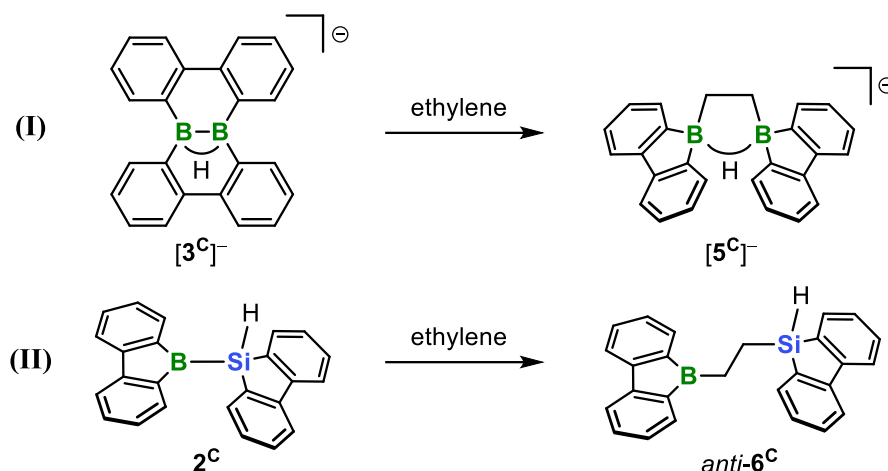


**Figure S80.** Superpositions of the calculated structures  $[3]^-$ ,  $[5]^-$ , **2**, and *anti*-**6**, with *tert*-butyl groups (cyan) or H atoms (normal color code) in fluorene positions 2 and 7. *tert*-Butyl groups and C-bonded H atoms are omitted for clarity.

To select a suitable method to calculate the final energies of the optimized structures we calculated the free energy values of the reactions (**I**) and (**II**) depicted in Scheme S1 using the five above mentioned functionals in combination with the SMD(THF) model and either Popel's 6-311++G\*\* or Alrich's def2-QZVPP<sup>S21</sup> basis set. These free energies were in turn compared with the energies obtained from high-level SMD(THF)/DLPNO-CCSD(T)<sup>S11</sup>/cc-pVDZ<sup>S22</sup> calculations (Table S9; DLPNO-CCSD(T) free energies:  $\Delta G_{298}(\text{I}) = -25.1 \text{ kcal mol}^{-1}$ ;  $\Delta G_{298}(\text{II}) = -26.3 \text{ kcal mol}^{-1}$ ). The combination SMD(THF)/ $\omega$ B97XD/def2-QZVPP showed the smallest average of absolute deviation from the high-level computed free energies and is therefore the most appropriate method among the tested ones. All free energy values were calculated for the corresponding experimental temperature and included a

concentration correction<sup>S23</sup> accounting for the change in standard states going from gas phase to condensed phase.



**Scheme S1.** The diboration and silaboration reactions (I) and (II) used for benchmarking the theory level for the calculation of the final energies.

**Table S9.**  $\Delta G_{298}(\text{I/II})$  values considering the different theory levels. In addition, the averaged absolute deviation from  $\Delta G_{298}(\text{I/II})$  obtained from high-level DLPNO-CCSD(T) calculations is given.

Reaction	Level of theory	B3LYP-D3(BJ)	BP86-D3(BJ)	M06-2X-D3	PBE0-D3(BJ)	$\omega$ B97XD
(I)	6-311++G**	-20.3	-21.1	-23.4	-27.0	-28.1
	def2-QZVPP	-19.5	-20.2	-21.8	-25.6	-27.0
(II)	6-311++G**	-24.2	-24.7	-28.9	-29.4	-28.4
	def2-QZVPP	-24.2	-24.7	-28.6	-29.4	-28.2
Avg. abs. dev. to CCSD	6-311++G**	<b>3.5</b>	<b>2.8</b>	<b>2.1</b>	<b>2.5</b>	<b>2.5</b>
	def2-QZVPP	<b>3.9</b>	<b>3.2</b>	<b>2.8</b>	<b>1.9</b>	<b>1.8</b>

<sup>13</sup>C NMR isotropic shielding tensors (IST) were computed using the continuous set of gauge transformation (CSGT)<sup>S24</sup> method with the SMD(THF)/LC-TPSSTPSS<sup>S25</sup>/cc-pVTZ<sup>S26</sup> level of theory, as this combination was shown to deliver reliable results in a recent benchmark study.<sup>S27</sup> Since the experimentally observed NMR-shift values are the result of a dynamic process, the computed ISTs were averaged over all symmetry-related positions for the nuclei under consideration in each molecule. <sup>13</sup>C NMR resonances were referenced against SiMe<sub>4</sub> (IST = 196.8 ppm; formula (III)), for which optimization and chemical shielding was calculated in the same manner.

$$\delta_{\text{calc}}(E) = \text{IST}(\text{SiMe}_4) - \text{IST}(E) \quad (\text{III})$$

$$\delta_{\text{corr}}(E) = 0.921 \cdot \delta_{\text{calc}}(E) - 0.0606 \quad (\text{IV})$$

The calculated NMR-shift values  $\delta(E)$  were further corrected by applying a compensating linear scaling approach using formula (IV). The correction factors were determined using known K[3] as a benchmark molecule (Figure S82), which is a constitutionally comparable compound with a comparatively weak coordinating cation (Table S10).<sup>S1</sup> Figure S81 shows the calculated uncorrected <sup>13</sup>C NMR-shift values of the benchmark molecule (x-axis) plotted against the experimentally observed NMR shifts (y-axis).

**Table S10.** Calculated isotropic shielding tensors (avg. IST), calculated NMR-shift value  $\delta_{\text{calc}}(^{13}\text{C})$ , and experimental NMR-shift value  $\delta_{\text{exp}}(^{13}\text{C})$  (bottom; as its K<sup>+</sup> salt) in ppm for all <sup>13</sup>C nuclei of the benchmark molecule [3]<sup>-</sup>.

Carbon atom	avg. IST / ppm	$\delta_{\text{calc}}(^{13}\text{C})$ / ppm	$\delta_{\text{exp}}(^{13}\text{C})$ / ppm
1	57.6	139.2	127.8
2	36.2	160.6	156.0
3	61.2	135.6	121.4
4	56.7	140.2	125.9
5	46.0	150.8	138.7
6	36.7	160.1	145.2
7	157.9	38.9	35.1
8	163.8	33.0	32.3

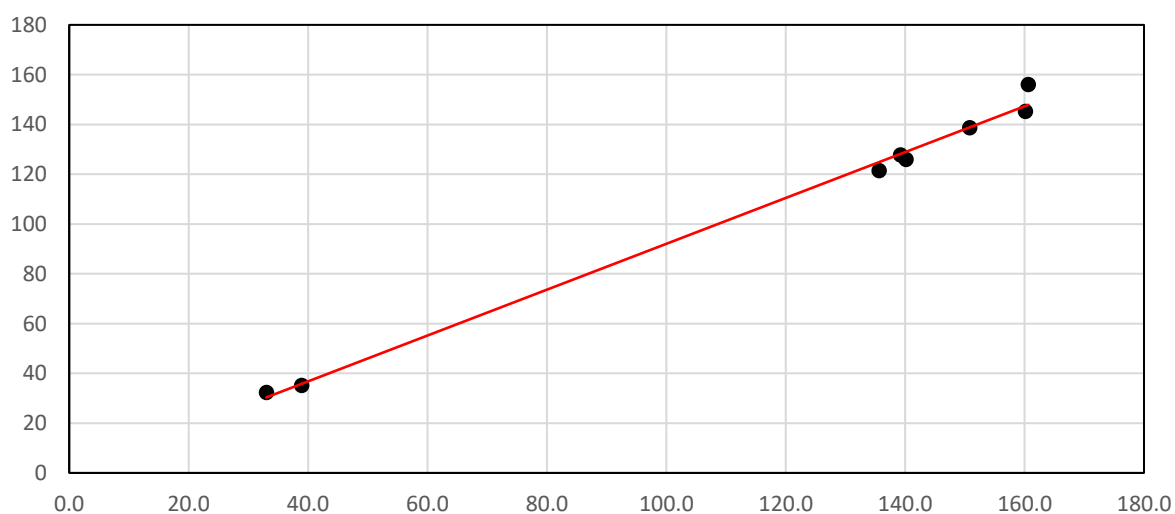


**Figure S81.** Plot of the calculated <sup>13</sup>C NMR-shift values (x-axis, ppm) of the benchmark molecule [3]<sup>-</sup> against the corresponding reported experimentally determined shift values (y-axis, ppm; as its K<sup>+</sup> salt). The linear regression is  $f(x) = 0.921x - 0.0606$  with a certainty of  $R^2 = 0.994$ .

#### 4.1 $^{13}\text{C}$ NMR-shift calculations of $[\mathbf{5}]^-$ and $[\mathbf{S4}]^-$

To further verify that the product of the reaction of  $\text{M}[\mathbf{3}]$  ( $\text{M} = \text{Li}, \text{K}$ ) with ethylene has (also in solution) two borafluorene moieties and not a dibenzo[*g,p*]chrysene-like framework as in the starting material, we calculated the  $^{13}\text{C}$  NMR-shift values of  $[\mathbf{5}]^-$  and  $[\mathbf{S4}]^-$  (Figure S82) and compared them to the experimentally observed values of the weakly interacting  $\text{K}[\mathbf{5}]$  salt. Only those carbon atoms with calculated NMR-shift values differing  $> 1.0$  ppm for  $[\mathbf{5}]^-$  and  $[\mathbf{S4}]^-$  were considered (Table S11).  $[\mathbf{5}]^-$  exhibits the smallest variation from the experimentally observed NMR shift values with an average absolute deviation of 1.8 ppm (Table S12). The averaged absolute deviation from  $[\mathbf{S4}]^-$  is 4.8 ppm and thus significantly higher.

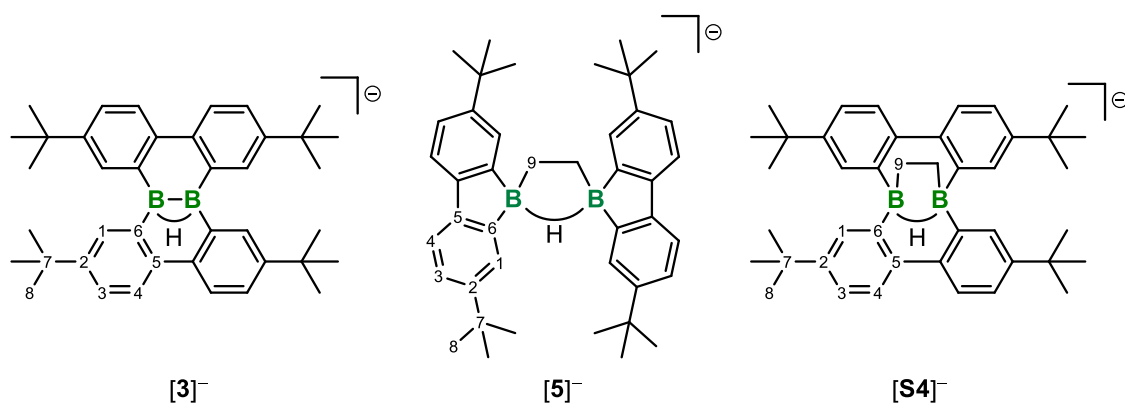


**Figure S82.** Optimized structures for  $^{13}\text{C}$  NMR-shift calculations and the underlying numbering scheme for the assignment.

**Table S11.** Calculated isotropic shielding tensors (IST in ppm), calculated NMR-shift values  $\delta_{\text{calc}}(^{13}\text{C})$ , and the corrected NMR-shift values  $\delta_{\text{corr}}(^{13}\text{C})$  in ppm for all carbon atoms in  $[\mathbf{5}]^-$  and  $[\mathbf{S4}]^-$ . The last column shows the absolute difference of the computed chemical-shift values of both derivatives; carbon atoms whose chemical-shift value differs by more than 1.0 ppm are marked in yellow.

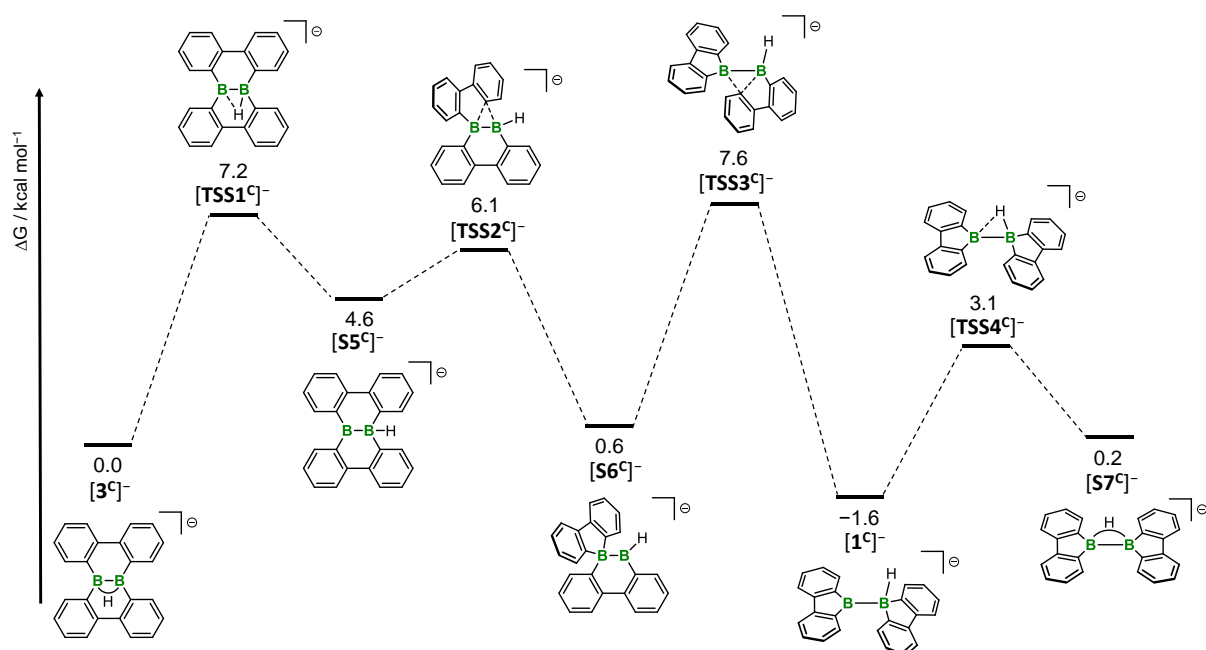
Carbon atom	$[\mathbf{5}]^-$			$[\mathbf{S4}]^-$			Abs. Diff. / ppm
	IST / ppm	$\delta_{\text{calc}}(^{13}\text{C})$ / ppm	$\delta_{\text{corr}}(^{13}\text{C})$ / ppm	IST / ppm	$\delta_{\text{calc}}(^{13}\text{C})$ / ppm	$\delta_{\text{corr}}(^{13}\text{C})$ / ppm	
1	53.3489	143.5	132.1	52.7203	144.1	132.7	0.6
2	34.3229	162.5	149.6	34.7172	162.1	149.2	0.4
3	62.1004	134.7	124.0	64.0019	132.8	122.3	1.8
4	65.5591	131.3	120.8	54.5403	142.3	131.0	10.1
5	37.5161	159.3	146.7	41.3798	155.4	143.1	3.6
6	25.7307	171.1	157.5	28.9808	167.8	154.5	3.0
7	157.8808	38.9	35.8	158.3615	38.5	35.4	0.4
8	163.6472	33.2	30.5	164.4140	32.4	29.8	0.7
9	185.1254	11.7	10.7	183.2377	13.6	12.5	1.7

**Table S12.** Comparison of the calculated  $^{13}\text{C}$  NMR shifts of  $[\mathbf{5}]^-$  and  $[\mathbf{S4}]^-$  and the experimentally observed shifts of the product derived from reaction of  $\text{K}[\mathbf{3}]$  with ethylene in  $\text{THF-}d_8$ . Only the resonances of the carbon atoms for which the calculated shifts of  $[\mathbf{5}]^-$  and  $[\mathbf{S4}]^-$  differ  $> 1.0$  ppm are considered.

Carbon atom	$\delta_{\text{exp}}(^{13}\text{C})$ / ppm	$[\mathbf{5}]^-$		$[\mathbf{S4}]^-$	
		$\delta_{\text{corr}}(^{13}\text{C})$ / ppm	$\Delta (\delta_{\text{corr}} - \delta_{\text{exp}})$ / ppm	$\delta_{\text{corr}} (^{13}\text{C})$ / ppm	$\Delta (\delta_{\text{corr}} - \delta_{\text{exp}})$ / ppm
<b>3</b>	123.1	124.0	0.9	122.3	-0.8
<b>4</b>	117.7	120.8	3.1	131.0	13.3
<b>5</b>	146.9	146.7	-0.2	143.1	-3.8
<b>6</b>	157.7	157.5	-0.3	154.5	-3.2
<b>9</b>	15.2	10.7	-4.5	12.5	-2.7
<b>Avg. abs. <math>\Delta</math> / ppm</b>		<b>1.8</b>		<b>4.8</b>	

## 4.2 Rearrangement mechanism of the anion $[3^C]^-$

The rearrangement of the dibenzo[*g,p*]chrysene-like structure in  $[3^C]^-$  to the bis(9-borabluorene) structure in  $[S7^C]^-$  is possible within a maximum energy range of  $9.0 \text{ kcal mol}^{-1}$  (Scheme S2). The rearrangement mechanism consists of a hydride shift of the boron-bonded hydrogen atom from a bridging to a terminal position, followed by two 1,2-phenyl shifts. Finally, the terminal B–H atom bridges the two boron atoms again. The corresponding thf adducts play a minor role as they are all higher in energy than their non-coordinated counterparts ( $[S5^C(\text{thf})]^-$ :  $+10.5 \text{ kcal mol}^{-1}$ ;  $[S6^C(\text{thf})]^-$ :  $+3.1 \text{ kcal mol}^{-1}$ ;  $[1^C(\text{thf})]^-$ :  $+3.3 \text{ kcal mol}^{-1}$ ; all values relative to their non-coordinated counterparts).



**Scheme S2.** Mechanism of the rearrangement of  $[3^C]^-$ .

Although the deviation is within the range of the uncertainty of DFT, the calculations suggest that  $[1^C]^-$  is  $1.6 \text{ kcal mol}^{-1}$  more stable than  $[3^C]^-$ , which contradicts the experimental findings identifying  $[3^C]^-$  unequivocally as the most energetically stable structure within this row. To tackle the discrepancy between calculation and experiment, we also calculated the two derivatives  $[3^C]^-$  and  $[1^C]^-$  in the presence of lithium cations as overall neutral compounds. The best position of the cation was determined by considering the molecular electrostatic potential of both anions (Figure S83). The compounds  $\text{Li}[3^C]$  and  $\text{Li}[1^C]$  have an energy difference of only  $0.1 \text{ kcal mol}^{-1}$ , with  $\text{Li}[1^C]$  still being calculated as more stable. Therefore, the influence of the THF-ligand sphere of the lithium cation on the relative energies was investigated, as it has recently been shown to have a notable influence.<sup>S28</sup> Both species show the most stable configuration with two THF ligands coordinating the lithium cation (Table S13). The comparison of  $[\text{Li}(\text{thf})_2][3^C]$  and  $[\text{Li}(\text{thf})_2][1^C]$  finally reveals that  $[\text{Li}(\text{thf})_2][3^C]$  is more stable than  $[\text{Li}(\text{thf})_2][1^C]$  by  $2.0 \text{ kcal mol}^{-1}$ , which is in good agreement with the experiment. In the following, however, the counterions are not considered, for the following reasons: (i) in our case observed energy

differences are close to the inaccuracy of DFT; (ii) the calculated energy barriers and spans of all described mechanisms are significantly larger, so that the overall picture remains unchanged.

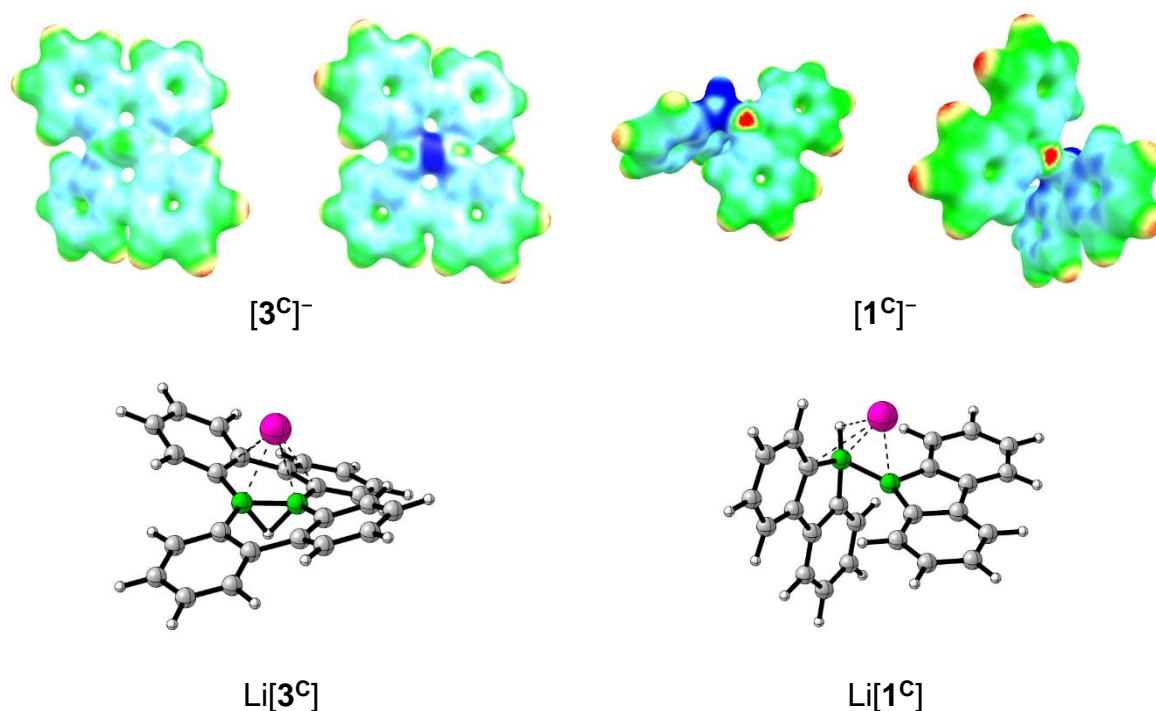


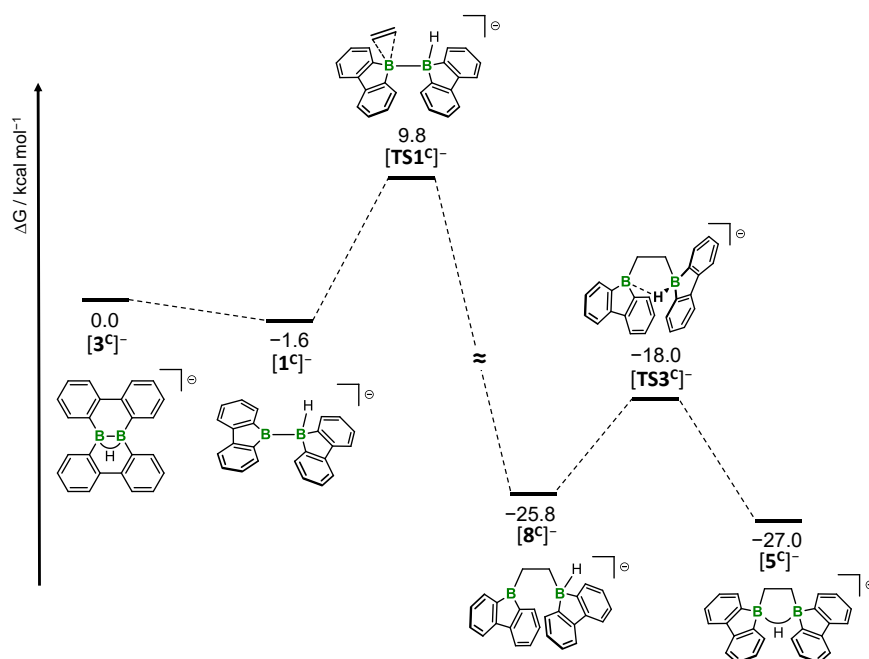
**Figure S83.** *Top:* Plots of the molecular electrostatic potential on the surface of  $[3C]^-$  and  $[1C]^-$  (interval range:  $-0.15$  to  $0.15$  (blue to red); isosurface value:  $0.03$ ). *Bottom:* Optimized structures of  $Li[3C]$  and  $Li[1C]$ .

**Table S13.** Absolute and relative free Gibbs energies of  $[Li(thf)_n][3C]$  and  $[Li(thf)_n][1C]$  ( $n = 0-3$ ).

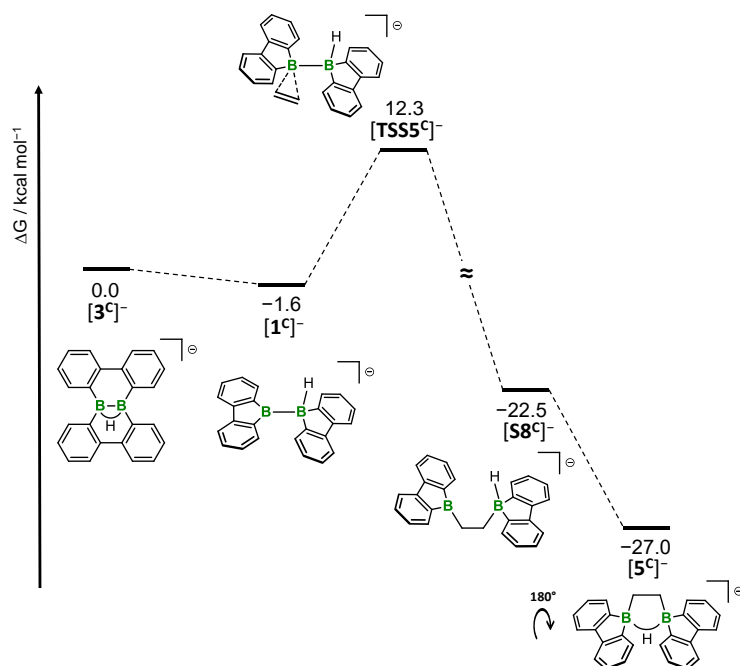
Compound	$n$	$\Delta G_{298}$ (relative to $G_{298}(Li[3C])$ )
$[Li(thf)_n][3C]$	0	0.0
	1	-10.9
	2	-19.8
	3	-19.5
$[Li(thf)_n][1C]$	0	-0.1
	1	-13.2
	2	-17.8
	3	-15.3

### 4.3 Diboration mechanisms of ethylene with $[3^C]^-$

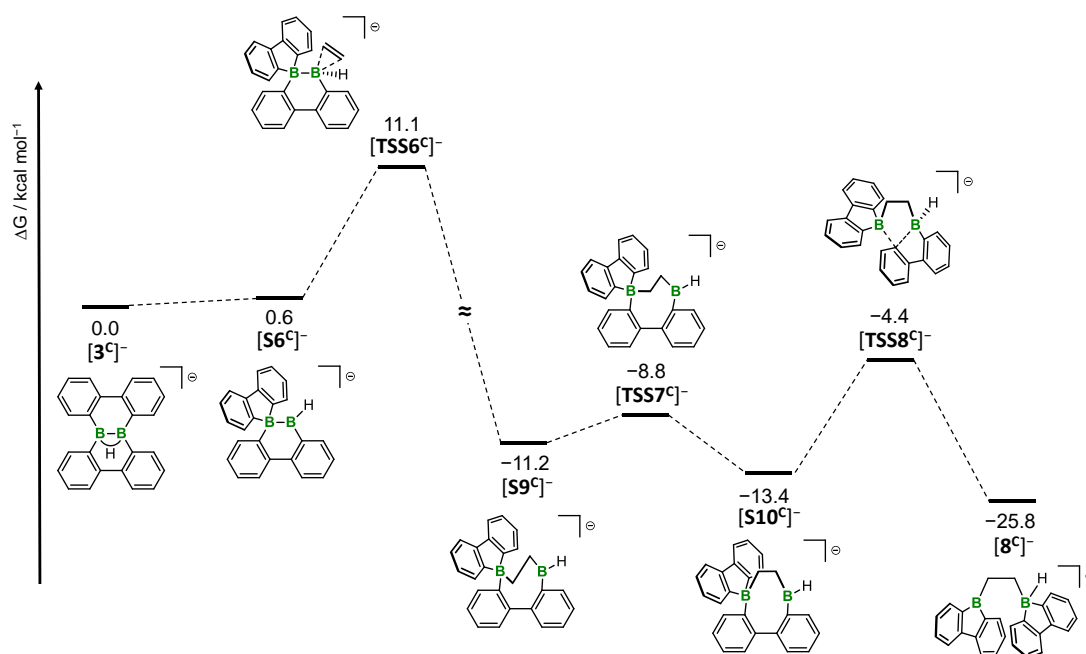
Several potential mechanisms for the diboration of ethylene with  $M[3]$  observed in this study were investigated. The different minimum structures with vacant  $p_z$  orbitals involved in the rearrangement mechanism of  $[3^C]^-$  (Scheme S2) served as starting points for the potential interaction with ethylene: Two different transition states for the interaction with ethylene were found for  $[1^C]^-$  and  $[S5^C]^-$ , respectively, and one transition state was found for  $[S6^C]^-$  (due to symmetry). All but one of the investigated mechanisms lead to the experimentally observed product, with all transition states being reachable at room temperature (mechanisms in Schemes S3, S4, S5, and S6 lead to the experimentally observed product  $[5^C]^-$ ; mechanism in Scheme S7 lead to  $[S4^C]^-$ ). The most energetically favorable mechanism ( $\Delta G^\ddagger(\text{max}) = 9.8 \text{ kcal mol}^{-1}$ ) is depicted in Scheme S3, in which ethylene interacts with the vacant  $B(p_z)$  orbital of  $[1^C]^-$  in a *cis* conformation relative to the B–H bond.



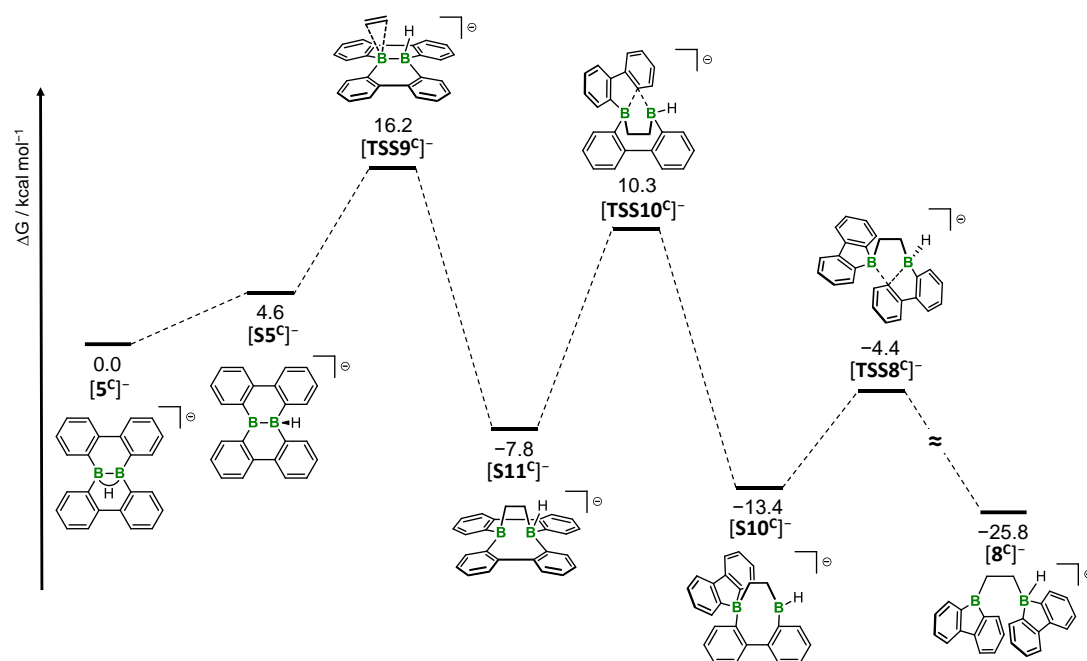
**Scheme S3.** Possible diboration mechanism of ethylene with  $[3^C]^-$  to give  $[5^C]^-$  considering  $[1^C]^-$  as diborane interacting with the double bond. The rearrangement from  $[3^C]^-$  to  $[1^C]^-$  is analogous to the mechanism depicted in Scheme S2 and is omitted for clarity (maximum barrier of rearrangement:  $7.6 \text{ kcal mol}^{-1}$ ). The initial interaction with ethylene is *cis* to the B–H bond in  $[TS1^C]^-$ .



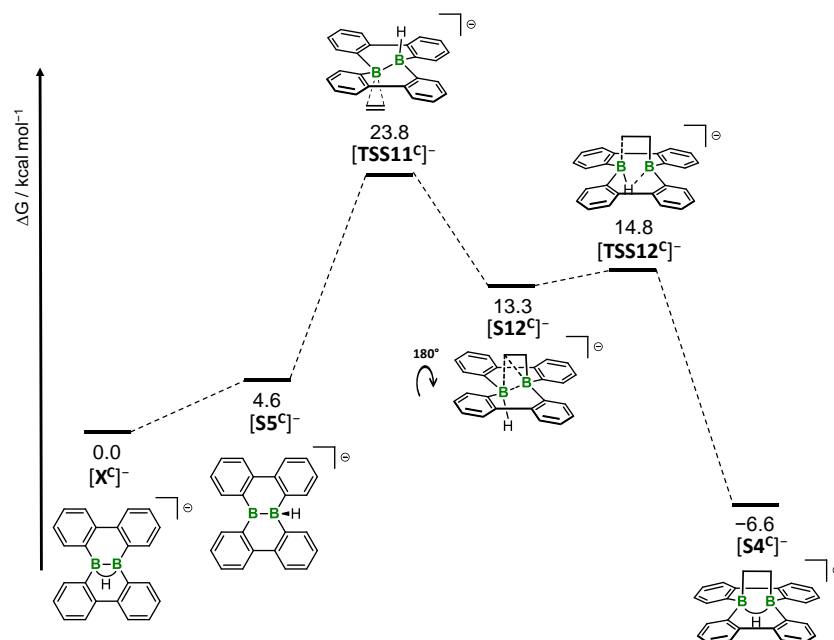
**Scheme S4.** Possible diboration mechanism of ethylene with  $[3^C]^-$  to give  $[5^C]^-$  considering  $[1^C]^-$  as diborane interacting with the double bond. The rearrangement from  $[3^C]^-$  to  $[1^C]^-$  is analogous to the mechanism depicted in Scheme S2 and is omitted for clarity (maximum barrier of rearrangement: 7.6 kcal mol<sup>-1</sup>). The initial interaction with ethylene is *trans* to the B–H bond in  $[TSS5^C]^-$ . As indicated by the curved arrow, structure  $[5^C]^-$  has been rotated for clarity.



**Scheme S5.** Possible diboration mechanism of ethylene with  $[3^C]^-$  to give  $[5^C]^-$  considering  $[S6^C]^-$  as diborane interacting with the double bond. The rearrangement from  $[3^C]^-$  to  $[S6^C]^-$  is analogous to the mechanism depicted in Scheme S2 and is omitted for clarity (maximum barrier of rearrangement: 7.2 kcal mol<sup>-1</sup>). The rearrangement of  $[8^C]^-$  to the final reaction product  $[5^C]^-$  is not depicted but proceeds analogously to the rearrangement in Scheme S3.



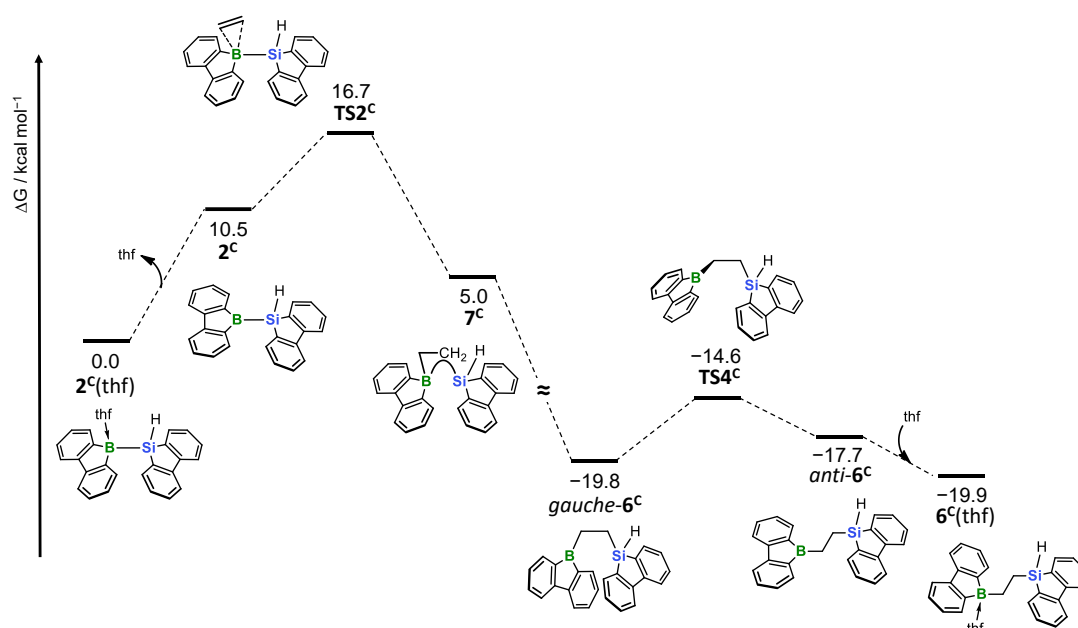
**Scheme S6.** Possible diboration mechanism of ethylene with  $[3^C]^-$  to give  $[5^C]^-$  considering  $[S5^C]^-$  as diborane interacting with the double bond. The rearrangement from  $[3^C]^-$  to  $[S5^C]^-$  is analogous to the mechanism depicted in Scheme S2 and is omitted for clarity (maximum barrier of rearrangement:  $7.2 \text{ kcal mol}^{-1}$ ). The initial interaction with ethylene is *cis* to the B–H bond in  $[TSS9^C]^-$ . The rearrangement of  $[8^C]^-$  to the final reaction product  $[5^C]^-$  is not depicted but proceeds analogously to the rearrangement in Scheme S3.



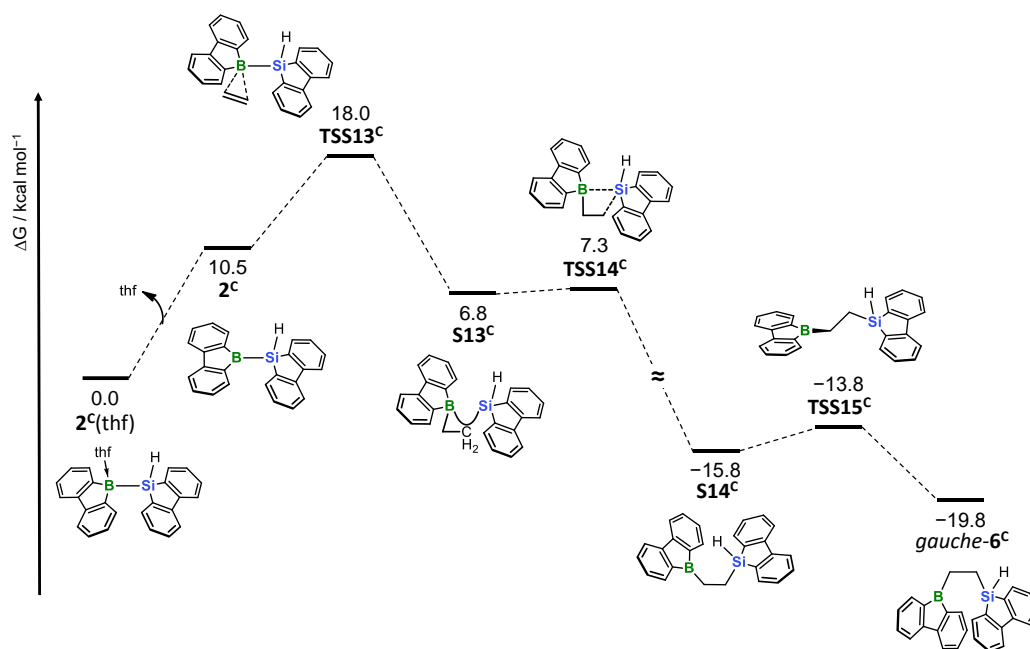
**Scheme S7.** Possible diboration mechanism of ethylene with  $[3^C]^-$  to give  $[4^C]^-$  (not the observed reaction product) considering  $[S5^C]^-$  as diborane interacting with the double bond. The rearrangement from  $[3^C]^-$  to  $[S5^C]^-$  is analogous to the mechanism depicted in Scheme S2 and is omitted for clarity (maximum barrier of rearrangement:  $7.2 \text{ kcal mol}^{-1}$ ). The initial interaction with ethylene is *trans* to the B–H bond in  $[TSS11^C]^-$ . As indicated by the curved arrow, the structures following  $[TSS11^C]^-$  have been rotated for clarity.

#### 4.4 Silaboration mechanisms of ethylene with 2(thf)

For the observed silaboration of ethylene with 2(thf), only structures with two heterofluorene scaffolds were considered, since there is no experimental evidence for the existence of dibenzo[*g,p*]chrysene-like structures. Two mechanisms were formulated in which ethylene interacts with the vacant  $p_z$  orbital of the boron atom either in *cis* or *trans* configuration relative to Si–H bond after thf dissociation. The most energetically favorable mechanism (*cis* configuration;  $\Delta G^\ddagger(\text{max}) = 16.7 \text{ kcal mol}^{-1}$ ) is depicted in Scheme S8.



**Scheme S8.** Possible silaboration mechanism of ethylene with  $2^{\text{C}}(\text{thf})$  to give  $6^{\text{C}}(\text{thf})$ . The initial interaction with ethylene is *cis* to the Si–H bond in  $\text{TS}2^{\text{C}}$ .



**Scheme S9.** Possible silaboration mechanism of ethylene with **2<sup>C</sup>(thf)** to give **6<sup>C</sup>(thf)**. The initial interaction with ethylene is *trans* to the Si–H bond in **TSS13<sup>C</sup>**. The rearrangement of *gauche-6<sup>C</sup>* and thf adduct formation to the final reaction product **6<sup>C</sup>(thf)** is not depicted but proceeds analogously to the rearrangement in Scheme S8.

## 4.5 Computed F<sup>-</sup>-ion affinities

For the structural optimization and enthalpy calculations, the analogous theory level was used as previously described in the benchmarking section. Thus, the F<sup>-</sup>-ion affinities (FIA) are calculated for the condensed phase in THF.

The following isodesmic reactions were calculated: {[LA]<sup>n-</sup> + [CF<sub>3</sub>O]<sup>-</sup> → [LA(F)]<sup>(n+1)-</sup> + CF<sub>2</sub>O} (LA = Lewis acid: [1<sup>C</sup>]<sup>-</sup>, n = 0; 2<sup>C</sup>, n = 1). Final FIAs were obtained by subtracting the experimentally determined FIA of CF<sub>2</sub>O (208.8 kJ mol<sup>-1</sup>) from the calculated reaction enthalpies.

**Table S14.** Lewis acidities assessed by F<sup>-</sup>-ion affinities; level of theory: SMD(THF)/ωB97XD/def2-QZVPP//SMD(THF)/ωB97XD/6-31+G\*\*.

Compound	n	[LA] <sup>n-</sup> / Hartree	[CF <sub>3</sub> O] <sup>-</sup> / Hartree	[LA(F)] <sup>(n+1)-</sup> / Hartree	CF <sub>2</sub> O / Hartree	FIA <sub>solv</sub> / kJ mol <sup>-1</sup>	FIA <sub>solv</sub> / kcal mol <sup>-1</sup>
[1 <sup>C</sup> ] <sup>-</sup>	1	-974.3543	-413.0893	-1074.3701	-313.0660	189	45
2 <sup>C</sup>	0	-1238.8987	-413.0893	-1338.9546	-313.0660	294	70

## 4.6 Intrinsic bond orbital calculations

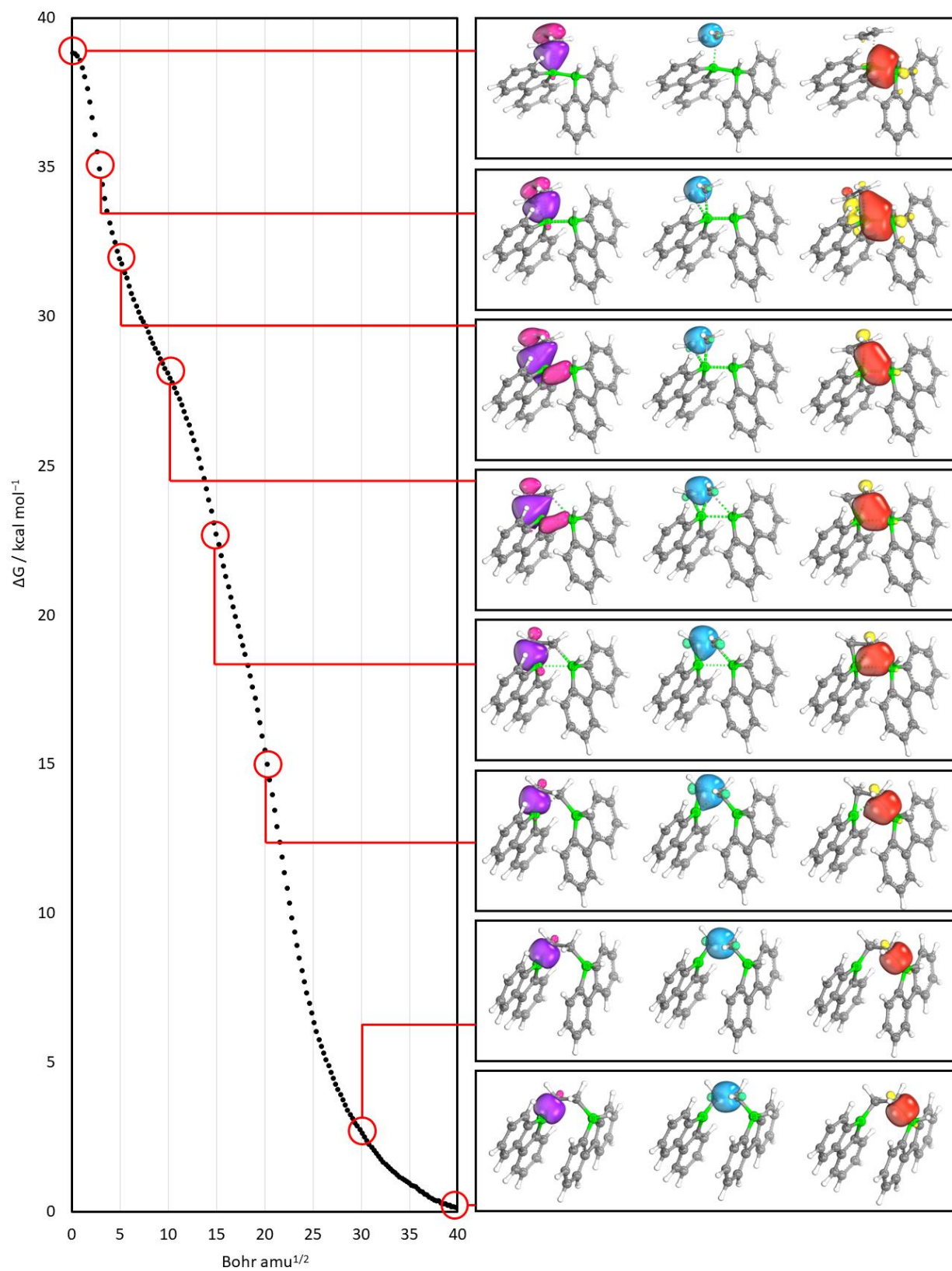


**Figure S84.** Transformations of selected intrinsic bond orbitals along the  $\text{IRC}([TS1^C]^- \rightarrow [8^C]^-)$  path.

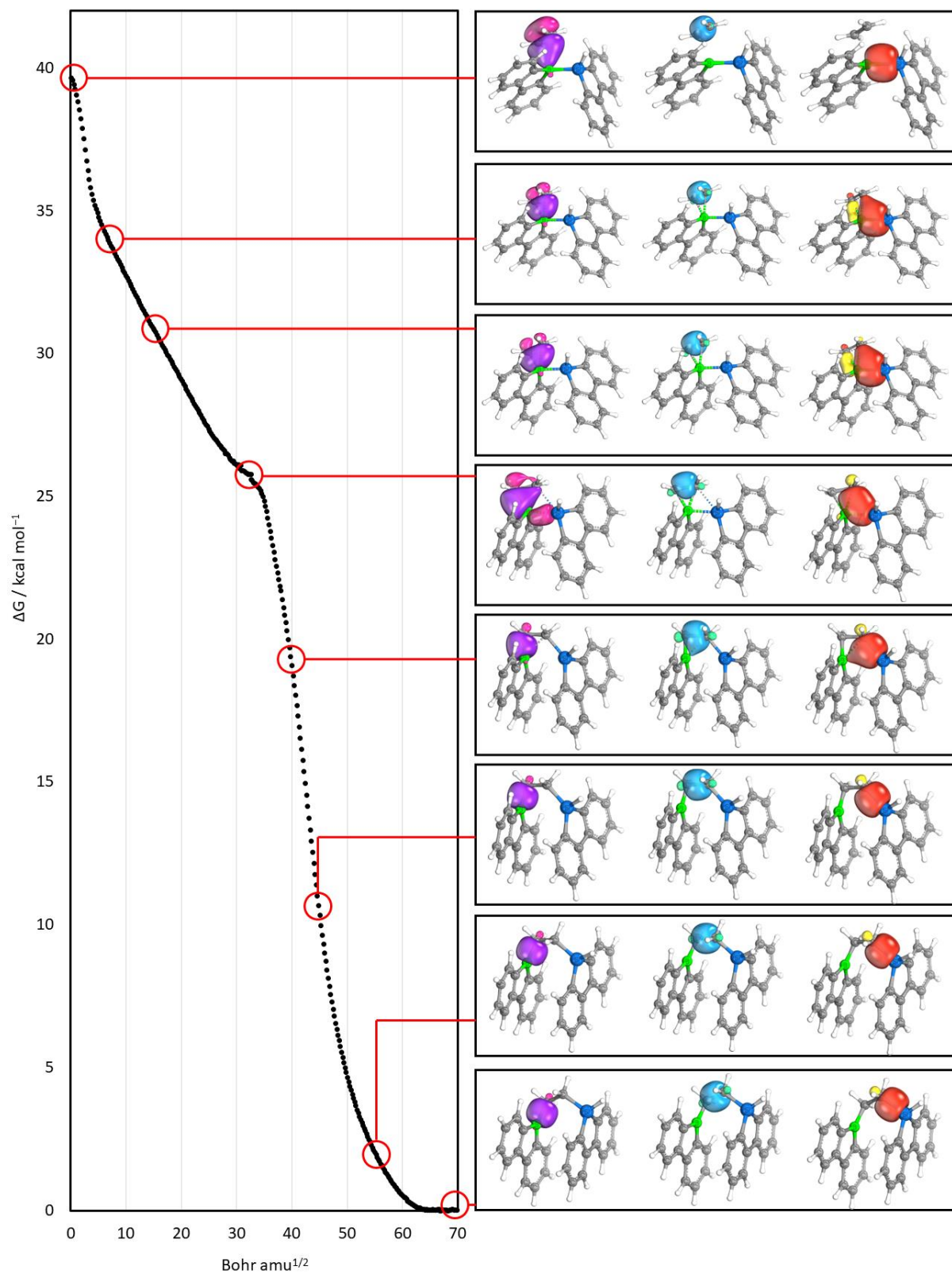
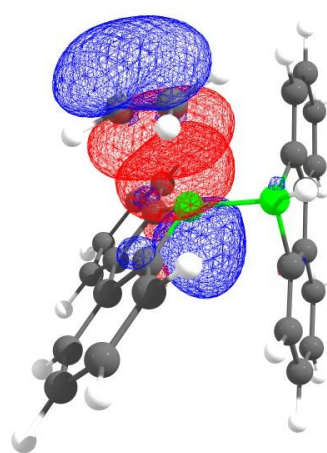


**Figure S85.** Transformations of selected intrinsic bond orbitals along the IRC( $\text{TS2}^{\text{C}} \rightarrow 7^{\text{C}} \rightarrow \text{gauche-6}^{\text{C}}$ ) path.

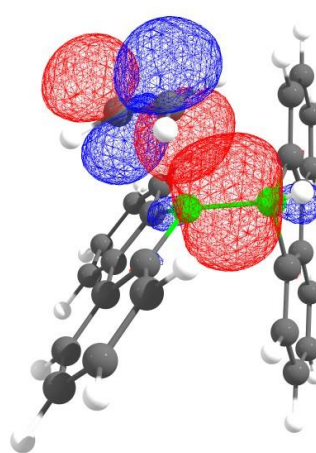
## 4.7 Natural bond orbital calculations

**Table S15.** The net charges ( $q$ ) of the natural population analysis (NPA) of both  $B(sp^2)$  and  $E(sp^3)$  ( $E = B, Si$ ) atoms derived from the NBO calculations on  $[1^C]^-$ ,  $[Li(thf)_2][1^C]$ ,  $[TS1^C]^-$ ,  $2^C$ , and  $TS2^C$ . Level of theory:  $\omega B97XD/def2-TZVPP//SMD(THF)/\omega B97XD/6-31+G^{**}$ .

Compound	$E(sp^3)$	$q[B(sp^2)] / e$	$q[E(sp^3)] / e$	$\Delta q / e$
$[1^C]^-$	B	0.75	-0.40	1.15
$[Li(thf)_2][1^C]$	B	0.50	-0.30	0.80
$[TS1^C]^-$	B	0.71	-0.35	1.06
$2^C$	Si	0.44	1.03	-0.59
$TS2^C$	Si	0.42	1.06	-0.64

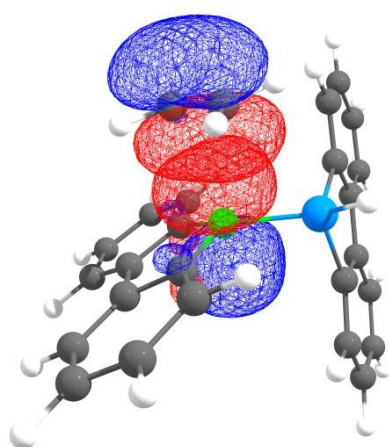


ethylene( $\pi$ )  $\rightarrow$  B( $p_z$ )  
60.8 kcal mol $^{-1}$

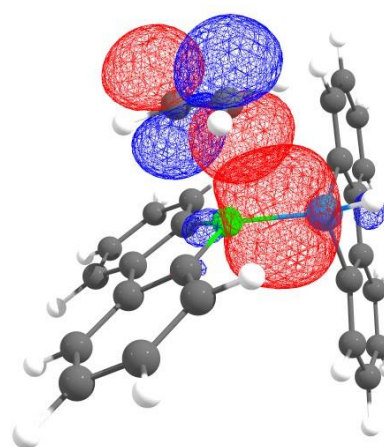


B-B( $\sigma$ )  $\rightarrow$  ethylene( $\pi^*$ )  
8.2 kcal mol $^{-1}$

**Figure S86.** Dominant NBO orbitals of  $[TS1^C]^-$  for the  $[1^C]^-$ /ethylene interaction. Level of theory:  $\omega B97XD/def2-TZVPP//SMD(THF)/\omega B97XD/6-31+G^{**}$ ; contour value: 0.04.



ethylene( $\pi$ )  $\rightarrow$  B( $p_z$ )  
43.8 kcal mol $^{-1}$



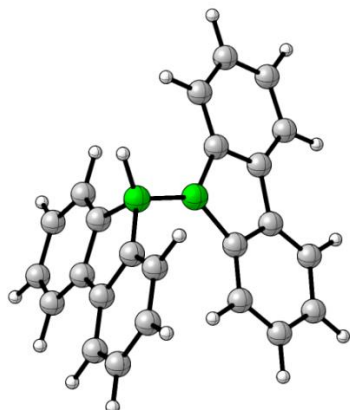
B-Si( $\sigma$ )  $\rightarrow$  ethylene( $\pi^*$ )  
1.9 kcal mol $^{-1}$

**Figure S87.** Dominant NBO orbitals of  $TS2^C$  for the  $2^C$ /ethylene interaction. Level of theory:  $\omega B97XD/def2-TZVPP//SMD(THF)/\omega B97XD/6-31+G^{**}$ ; contour value: 0.04.

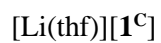
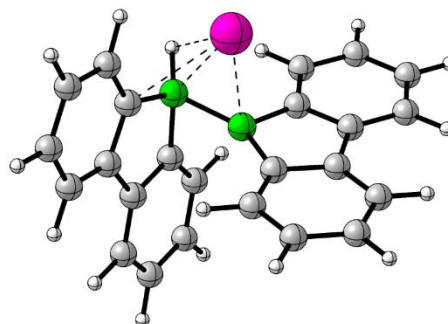
## 4.8 Corrected free energy values of computed compounds



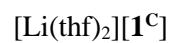
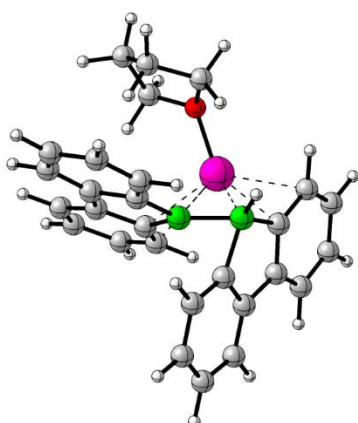
$$G_{298,\text{corr}} = -974.41992306 \text{ Hartree}$$



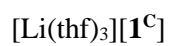
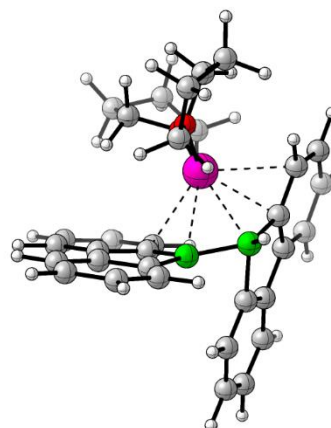
$$G_{298,\text{corr}} = -981.88917597 \text{ Hartree}$$



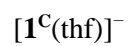
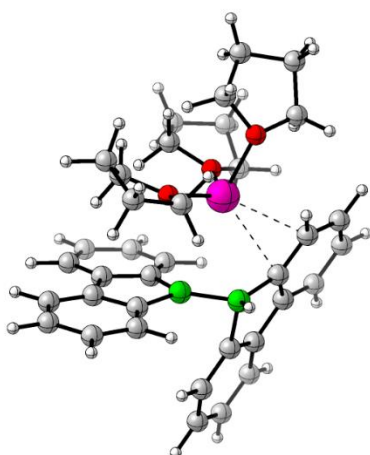
$$G_{298,\text{corr}} = -1214.30526609 \text{ Hartree}$$



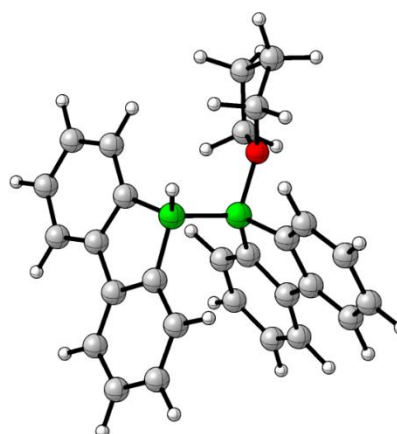
$$G_{298,\text{corr}} = -1446.70800073 \text{ Hartree}$$



$$G_{298,\text{corr}} = -1679.09937265 \text{ Hartree}$$

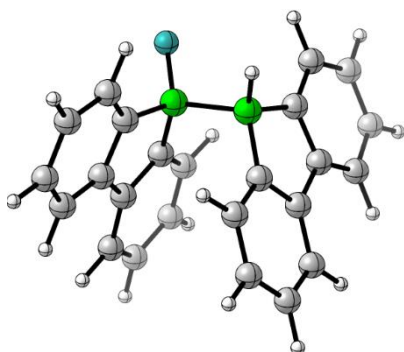


$$G_{298,\text{corr}} = -1206.81004094 \text{ Hartree}$$



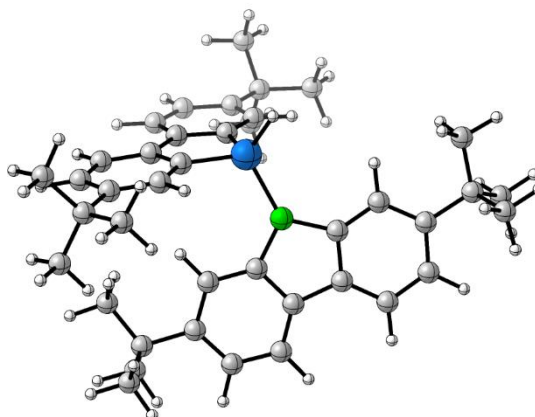
$[1^c(F)]^{2-}$

$G_{298,corr} = -1074.43652700$  Hartree



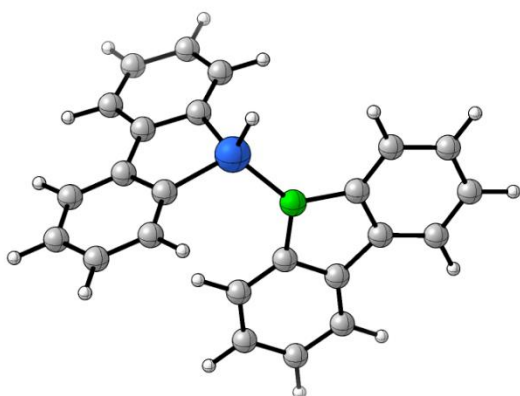
2

$G_{298,corr} = -1867.67334946$  Hartree



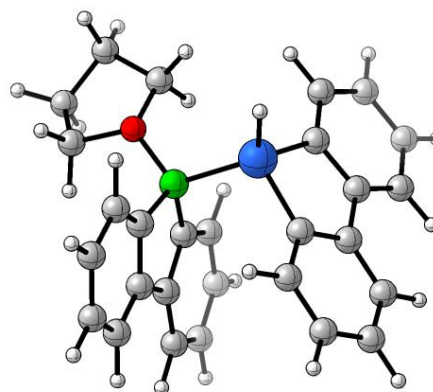
$2^c$

$G_{298,corr} = -1238.96733556$  Hartree



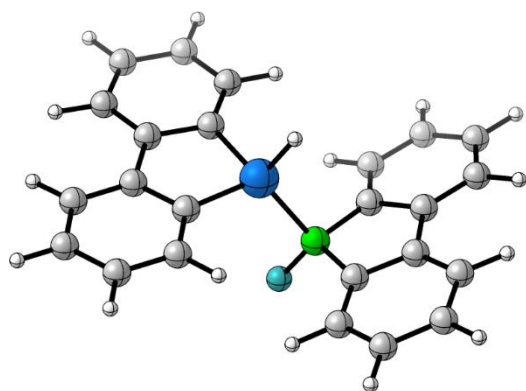
$2^c(thf)$

$G_{298,corr} = -1471.37937722$  Hartree



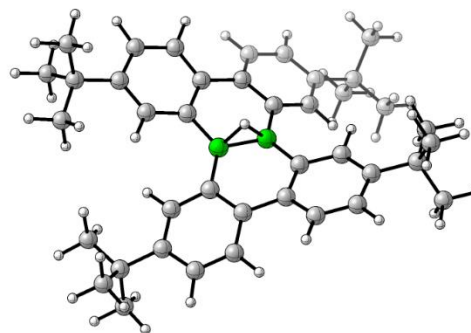
$[2^c(F)]^-$

$G_{298,corr} = -1339.02542044$  Hartree



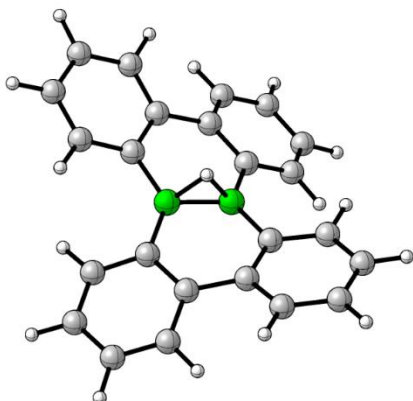
$[3]^-$

$G_{298,corr} = -1603.12237153$  Hartree

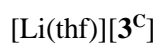
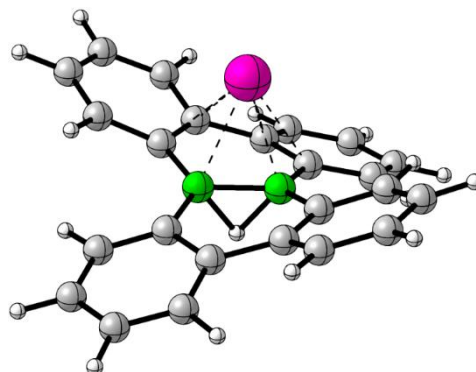




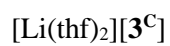
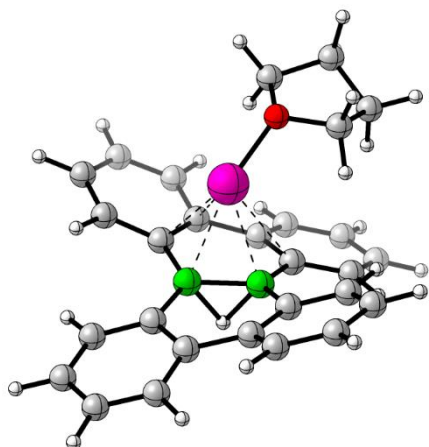
$G_{298,corr} = -974.41730933 \text{ Hartree}$



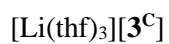
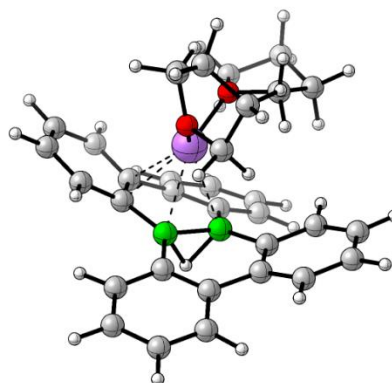
$G_{298,corr} = -981.88895120 \text{ Hartree}$



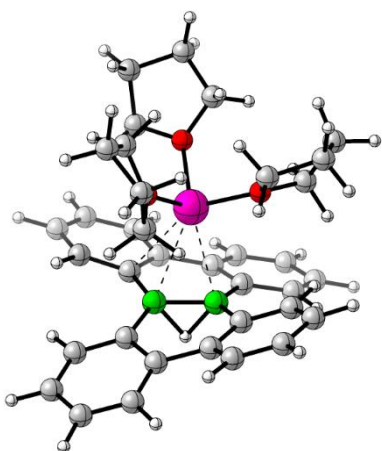
$G_{298,corr} = -1214.30165524 \text{ Hartree}$



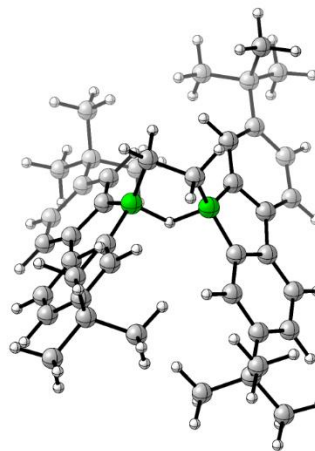
$G_{298,corr} = -1446.71120643 \text{ Hartree}$



$G_{298,corr} = -1679.10600276 \text{ Hartree}$

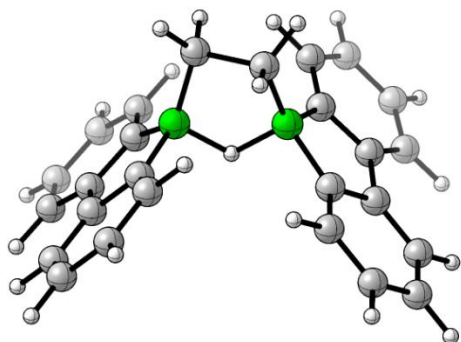


$G_{298,corr} = -1681.72543880 \text{ Hartree}$



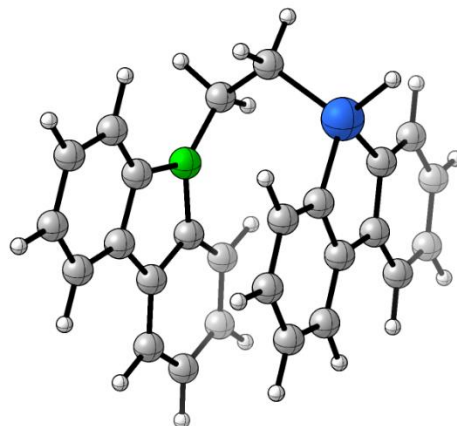
[5<sup>C</sup>]<sup>-</sup>

$G_{298,corr} = -1053.01821663$  Hartree



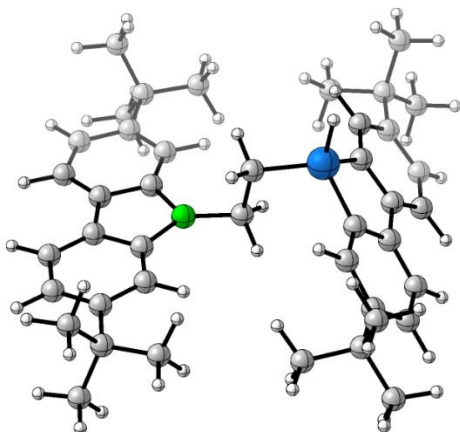
*gauche*-6<sup>C</sup>

$G_{298,corr} = -1317.57882272$  Hartree



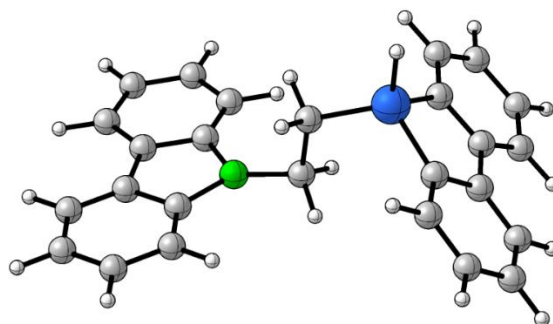
*anti*-6

$G_{298,corr} = -1946.27734734$  Hartree



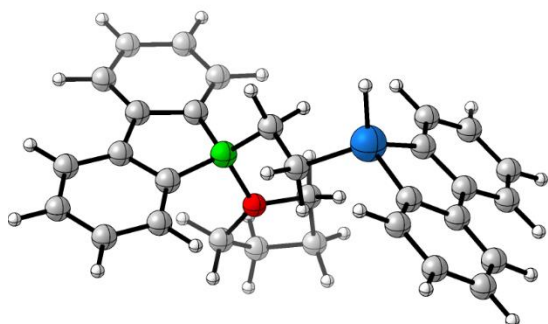
*anti*-6<sup>C</sup>

$G_{298,corr} = -1317.57560275$  Hartree



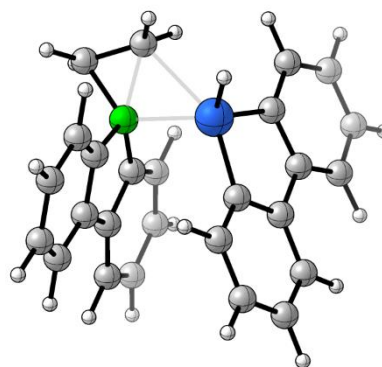
6<sup>C</sup>(thf)

$G_{298,corr} = -1549.97433138$  Hartree



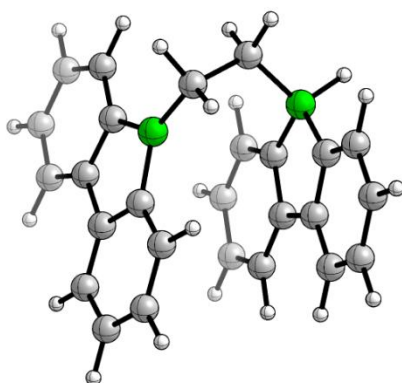
7<sup>C</sup>

$G_{298,corr} = -1317.53930946$  Hartree



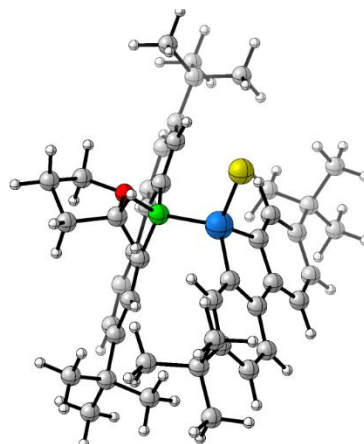
[8<sup>C</sup>]<sup>-</sup>

$G_{298,\text{corr}} = -1053.02176465$  Hartree



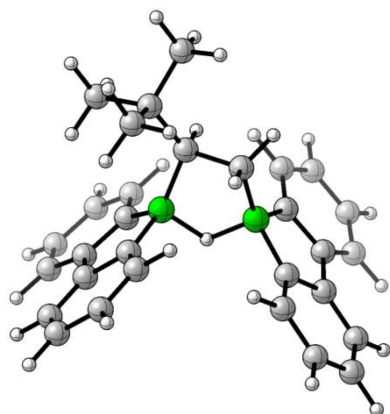
9(thf)

$G_{298,\text{corr}} = -2559.78943963$  Hartree



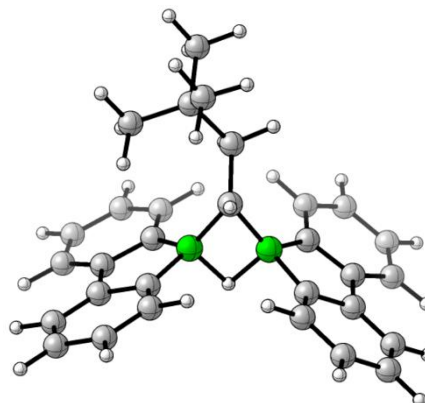
[11<sup>C</sup>]<sup>-</sup>

$G_{298,\text{corr}} = -1210.20036792$  Hartree



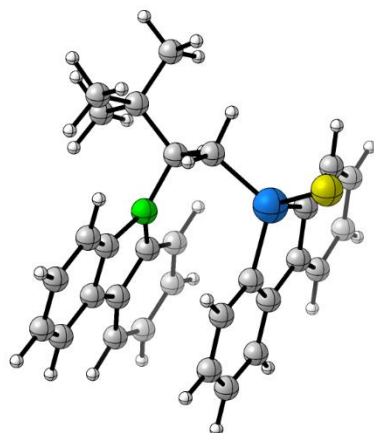
[12<sup>C</sup>]<sup>-</sup>

$G_{298,\text{corr}} = -1210.20987035$  Hartree



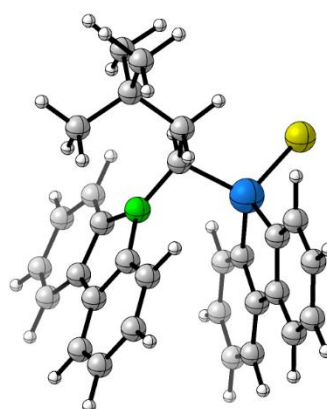
13<sup>C</sup>

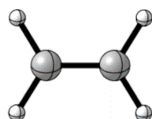
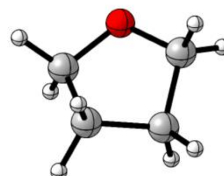
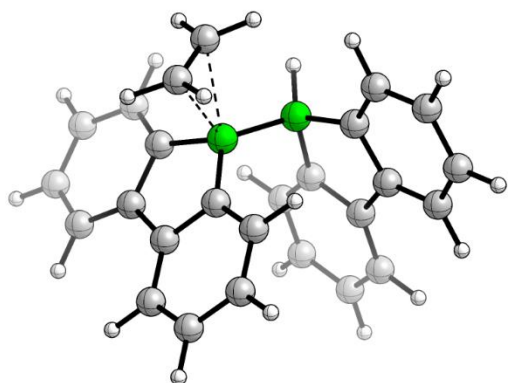
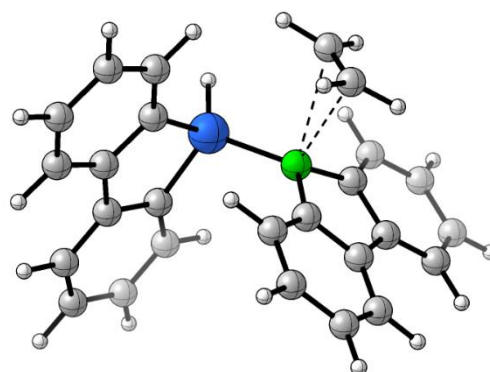
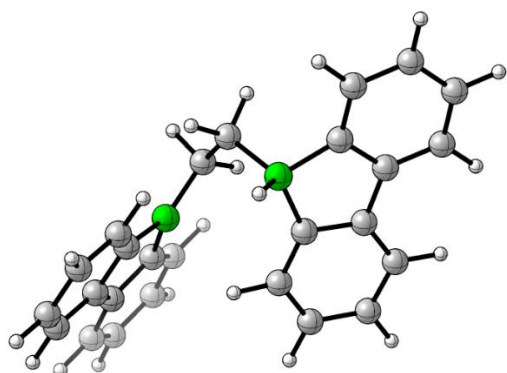
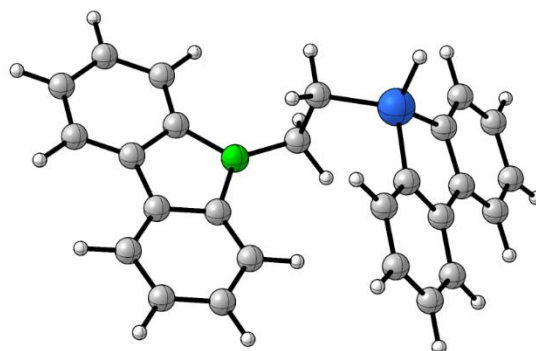
$G_{298,\text{corr}} = -1934.45281692$  Hartree



14<sup>C</sup>

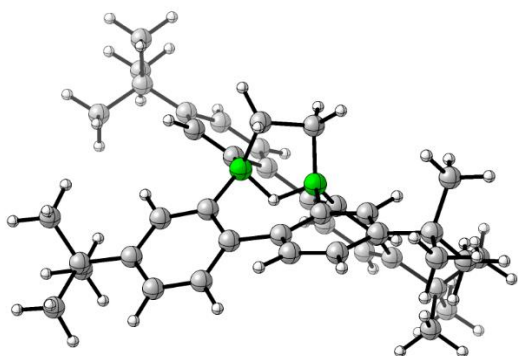
$G_{298,\text{corr}} = -1934.46151876$  Hartree



**Ethylene** $G_{298,\text{corr}} = -78.56327916$  Hartree**THF** $G_{298,\text{corr}} = -232.39533886$  Hartree**[TS1<sup>C</sup>]** $G_{298,\text{corr}} = -1052.96493200$  Hartree**TS2<sup>C</sup>** $G_{298,\text{corr}} = -1317.52078033$  Hartree**[TS3<sup>C</sup>]** $G_{298,\text{corr}} = -1053.00927617$  Hartree**TS4<sup>C</sup>** $G_{298,\text{corr}} = -1317.57055071$  Hartree

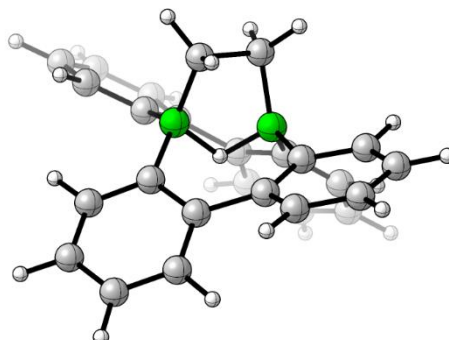
[S4]<sup>-</sup>

$G_{298,corr} = -1681.69839916$  Hartree



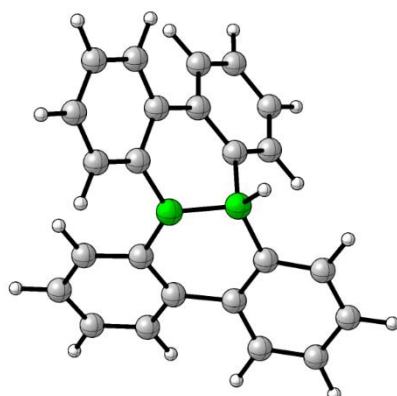
[S4<sup>c</sup>]<sup>-</sup>

$G_{298,corr} = -1052.99103003$  Hartree



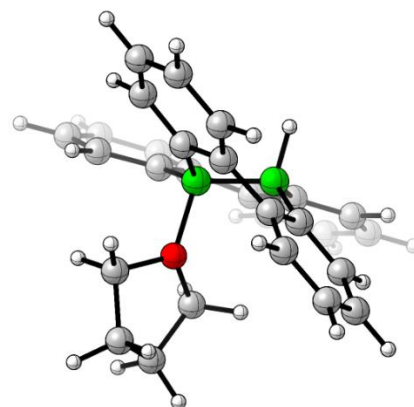
[S5<sup>c</sup>]<sup>-</sup>

$G_{298,corr} = -974.41004058$  Hartree



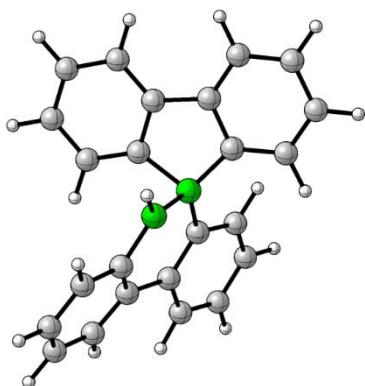
[S5<sup>c</sup>(thf)]<sup>-</sup>

$G_{298,corr} = -$ Hartree



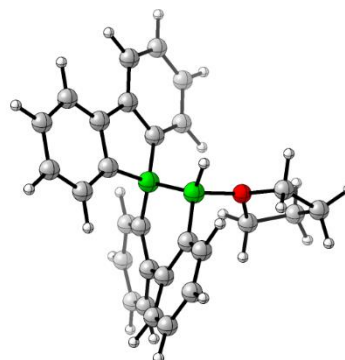
[S6<sup>c</sup>]<sup>-</sup>

$G_{298,corr} = -974.41629781$  Hartree



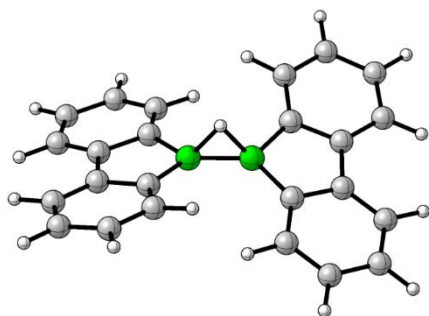
[S6<sup>c</sup>(thf)]<sup>-</sup>

$G_{298,corr} = -$ Hartree



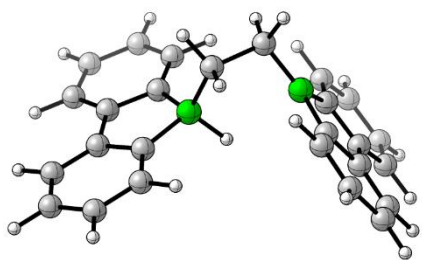
[S7<sup>c</sup>]<sup>-</sup>

$G_{298,\text{corr}} = -974.41692580$  Hartree



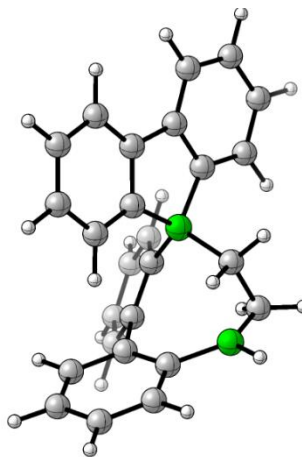
[S8<sup>c</sup>]<sup>-</sup>

$G_{298,\text{corr}} = -1053.01647679$  Hartree



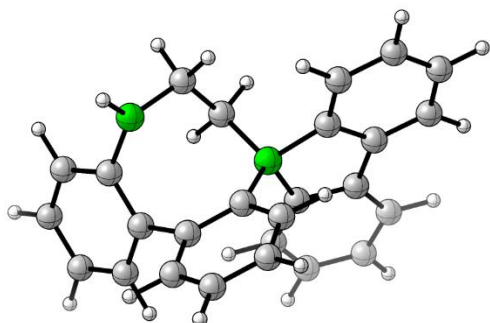
[S9<sup>c</sup>]<sup>-</sup>

$G_{298,\text{corr}} = -1052.99837553$  Hartree



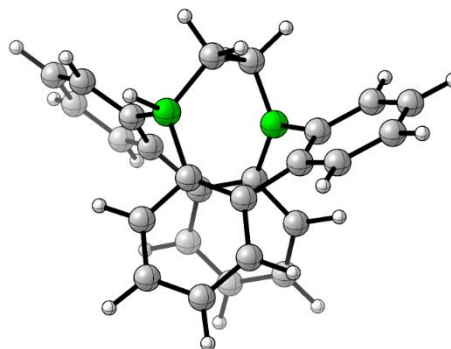
[S10<sup>c</sup>]<sup>-</sup>

$G_{298,\text{corr}} = -1053.00194590$  Hartree



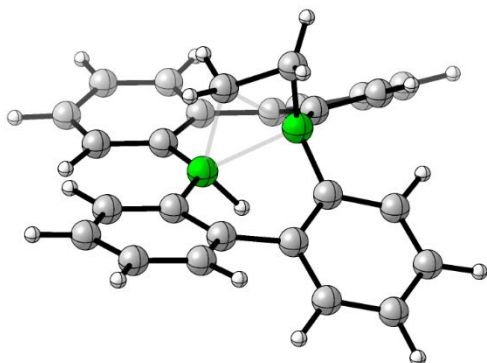
[S11<sup>c</sup>]<sup>-</sup>

$G_{298,\text{corr}} = -1052.99308236$  Hartree



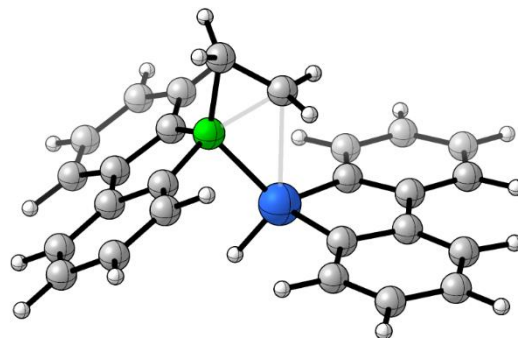
[S12<sup>c</sup>]<sup>-</sup>

$G_{298,\text{corr}} = -1052.95932369$  Hartree



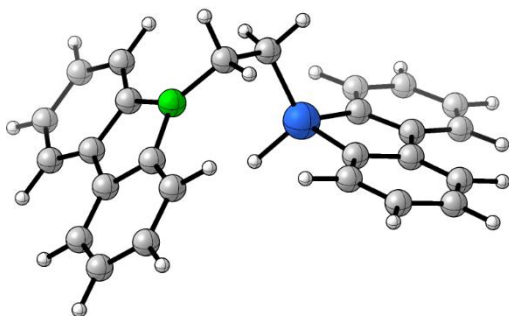
S13<sup>c</sup>

$G_{298,\text{corr}} = -1317.53646143$  Hartree



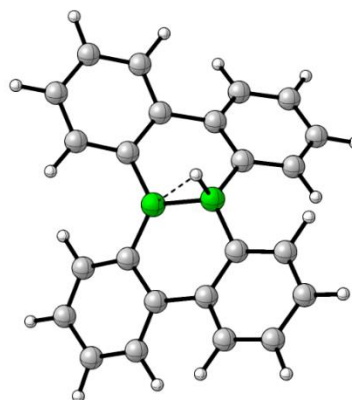
S14<sup>c</sup>

$G_{298,\text{corr}} = -1317.57257008$  Hartree



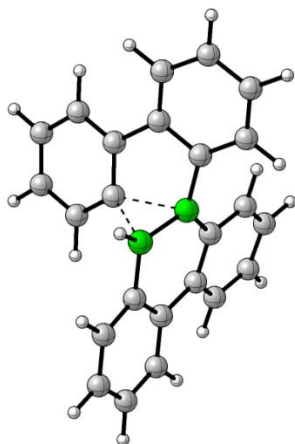
[TSS1<sup>c</sup>]<sup>-</sup>

$G_{298,\text{corr}} = -974.40580839$  Hartree



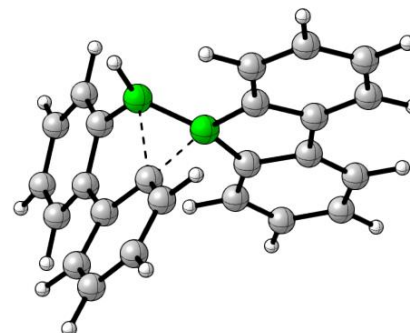
[TSS2<sup>c</sup>]<sup>-</sup>

$G_{298,\text{corr}} = -974.40756813$  Hartree



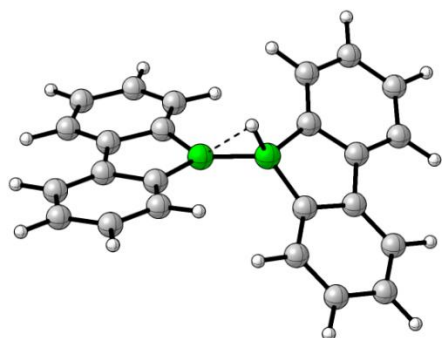
[TSS3<sup>c</sup>]<sup>-</sup>

$G_{298,\text{corr}} = -974.40525264$  Hartree



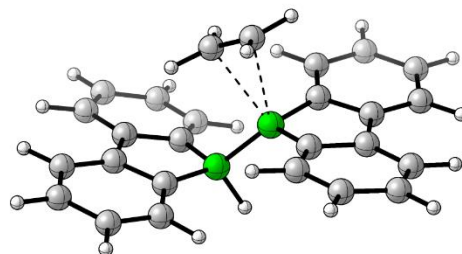
[TSS4<sup>C</sup>]<sup>-</sup>

$G_{298,\text{corr}} = -974.41235729$  Hartree



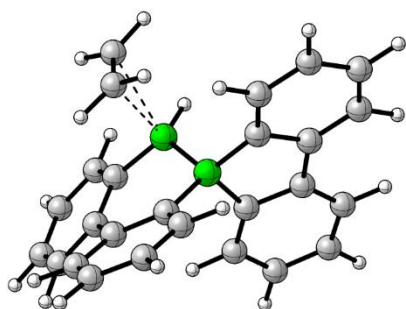
[TSS5<sup>C</sup>]<sup>-</sup>

$G_{298,\text{corr}} = -1052.96100408$  Hartree



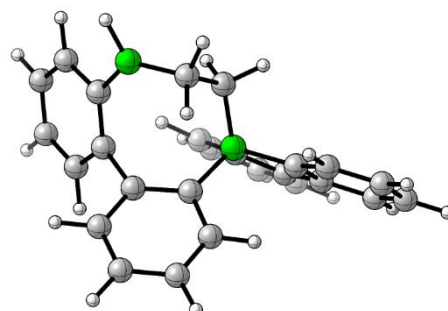
[TSS6<sup>C</sup>]<sup>-</sup>

$G_{298,\text{corr}} = -1052.96291659$  Hartree



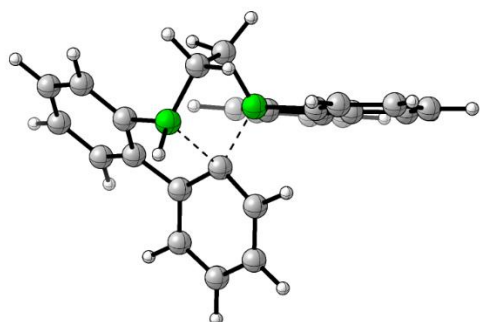
[TSS7<sup>C</sup>]<sup>-</sup>

$G_{298,\text{corr}} = -1052.99462767$  Hartree



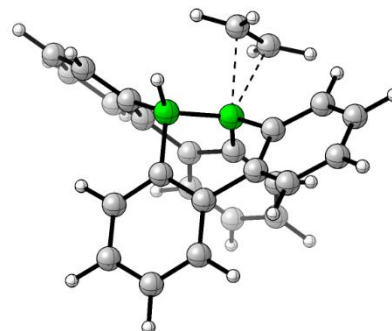
[TSS8<sup>C</sup>]<sup>-</sup>

$G_{298,\text{corr}} = -1052.98755203$  Hartree



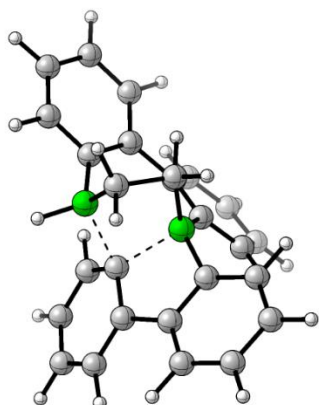
[TSS9<sup>C</sup>]<sup>-</sup>

$G_{298,\text{corr}} = -1052.95443947$  Hartree



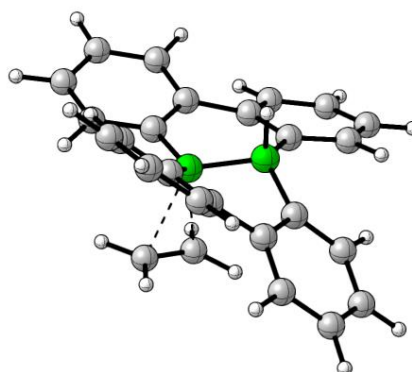
[TSS10<sup>C</sup>]<sup>-</sup>

$G_{298,\text{corr}} = -1052.96414276$  Hartree



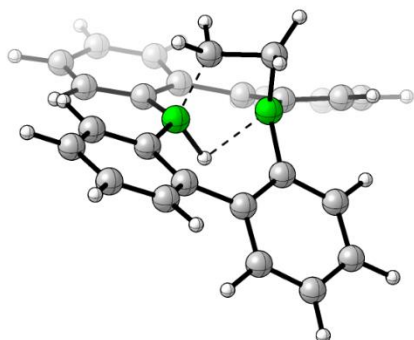
[TSS11<sup>C</sup>]<sup>-</sup>

$G_{298,\text{corr}} = -1052.94258142$  Hartree



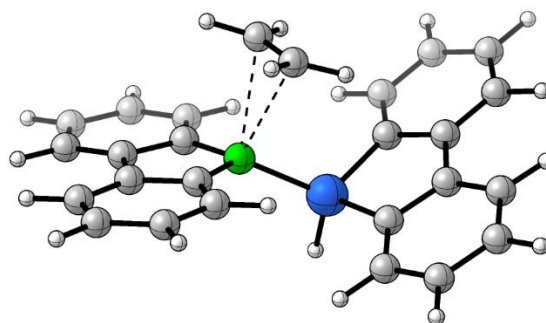
[TSS12<sup>C</sup>]<sup>-</sup>

$G_{298,\text{corr}} = -1052.95695337$  Hartree



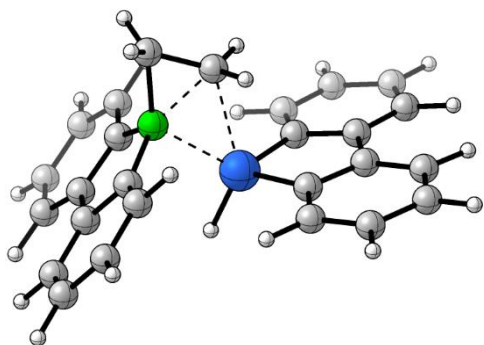
TSS13<sup>C</sup>

$G_{298,\text{corr}} = -1317.51860052$  Hartree



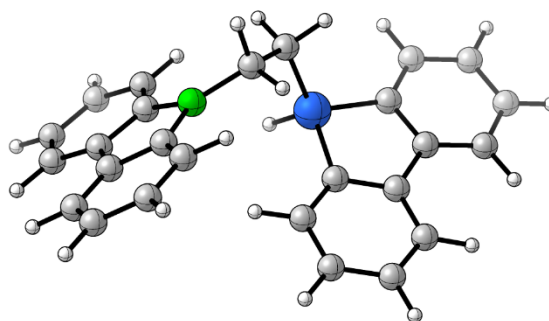
TSS14<sup>C</sup>

$G_{298,\text{corr}} = -1317.53571981$  Hartree



TSS15<sup>C</sup>

$G_{298,\text{corr}} = -1317.56930394$  Hartree



## 5. References

- S1 T. Kaese, H. Budy, M. Bolte, H.-W. Lerner and M. Wagner, *Angew. Chem. Int. Ed.*, 2017, **56**, 7546–7550.
- S2 J. Gilmer, M. Bolte, A. Virovets, H.-W. Lerner, F. Fantuzzi and M. Wagner, *Chem. Eur. J.*, 2023, **29**, e202203119.
- S3 T. Kaese, T. Trageser, H. Budy, M. Bolte, H.-W. Lerner and M. Wagner, *Chem. Sci.*, 2018, **9**, 3881–3891.
- S4 A. Hübner, M. Diefenbach, M. Bolte, H.-W. Lerner, M. C. Holthausen and M. Wagner, *Angew. Chem. Int. Ed.*, 2012, **51**, 12514–12518.
- S5 G. R. Fulmer, A. J. M. Miller, N. H. Sherden, H. E. Gottlieb, A. Nudelman, B. M. Stoltz, J. E. Bercaw and K. I. Goldberg, *Organometallics*, 2010, **29**, 2176–2179.
- S6 (a) G. M. Sheldrick, *SHELXS-97 and SHELXL-97, Program for Crystal Structure Solution and Refinement*, 1997; (b) G. M. Sheldrick, *Acta Crystallogr. Sect. A Found. Adv.*, 2015, **71**, 3–8.
- S7 M. J. Frisch, G. W. Trucks, H. B. Schlegel, G. E. Scuseria, M. A. Robb, J. R. Cheeseman, G. Scalmani, V. Barone, G. A. Peterson, H. Nakatsuji, X. Li, M. Caricato, A. V. Marenich, J. Bloino, B. G. Janesko, R. Gomperts, B. Mennucci, H. P. Hratchian, J. V. Ortiz, A. F. Izmaylov, J. L. Sonnenberg, D. Williams-Young, F. Ding, F. Lipparini, F. Egidi, J. Goings, B. Peng, A. Petrone, T. Henderson, D. Ranasinghe, V. G. Zakrzewski, J. Gao, N. Rega, G. Zheng, W. Liang, M. Hada, M. Ehara, K. Toyota, R. Fukuda, J. Hasegawa, M. Ishida, T. Nakajima, Y. Honda, O. Kitao, H. Nakai, T. Vreven, K. Throssell, J. A. Montgomery Jr., J. E. Peralta, F. Ogliaro, M. J. Bearpark, J. J. Heyd, E. N. Brothers, K. N. Kudin, V. N. Staroverov, T. A. Keith, R. Kobayashi, J. Normand, K. Raghavachari, A. P. Rendell, J. C. Burant, S. S. Iyengar, J. Tomasi, M. Cossi, J. M. Millam, M. Klene, C. Adamo, R. Cammi, J. W. Ochterski, R. L. Martin, K. Morokuma, O. Farkas, J. B. Foresman and D. J. Fox, *Gaussian 16, Revision B.01*, 2016.
- S8 (a) F. Neese, *WIREs Comput. Mol. Sci.*, 2012, **2**, 73–78; (b) F. Neese, *WIREs Comput. Mol. Sci.*, 2022, **12**, e1606.
- S9 G. Knizia, *J. Chem. Theory Comput.*, 2013, **9**, 4834–4843.
- S10 E. D. Glendening, C. R. Landis and F. J. Weinhold, *J. Comput. Chem.*, 2019, **40**, 2234–2241.
- S11 C. Y. Legault, *CYLview*, 1.0b, 2009.
- S12 S. Grimme, J. Antony, S. Ehrlich and H. Krieg, *J. Chem. Phys.*, 2010, **132**, 154104.
- S13 S. Grimme, S. Ehrlich and L. Goerigk, *J. Comput. Chem.*, 2011, **32**, 1456–1465.
- S14 (a) J. P. Perdew, *Phys. Rev. B*, 1986, **33**, 8822–8824; (b) A. D. Becke, *Phys. Rev. A*, 1988, **38**, 3098–3100.
- S15 Y. Zhao and D. G. Truhlar, *Theor. Chem. Acc.*, 2008, **120**, 215–241.
- S16 (a) M. Ernzerhof and G. E. Scuseria, *J. Chem. Phys.*, 1999, **110**, 5029–5036; (b) C. Adamo and V. Barone, *J. Chem. Phys.*, 1999, **110**, 6158–6170.
- S17 J. Chai and M. Head-Gordon, 2008, **10**, 6615–6620.
- S18 R. Krishnan, J. S. Binkley, R. Seeger and J. A. Pople, *J. Chem. Phys.*, 1980, **72**, 650–654.
- S19 T. Kaese, A. Hübner, M. Bolte, H.-W. Lerner and M. Wagner, *J. Am. Chem. Soc.*, 2016, **138**, 6224–6233.
- S20 A. V. Marenich, C. J. Cramer and D. G. Truhlar, *J. Phys. Chem. B*, 2009, **113**, 6378–6396.

- S21 (a) A. Schaefer, H. Horn and R. Ahlrichs, *J. Chem. Phys.*, 1992, **97**, 2571–2577; (b) A. Schaefer, C. Huber, R. Ahlrichs, *J. Chem. Phys.*, 1994, **100**, 5829–5835; (c) K. Eichkorn, F. Weigend, O. Treutler and R. Ahlrichs, *Theor. Chem. Acc.*, 1997, **97**, 119–124; (d) F. Weigend, F. Furche and R. Ahlrichs, *J. Chem. Phys.*, 2003, **119**, 12753–12762.
- S22 (a) C. Riplinger, F. Neese, *J. Chem. Phys.*, 2013, **138**, 034106; (b) C. Riplinger, B. Sandhoefer, A. Hansen, F. Neese, *J. Chem. Phys.*, 2013, **139**, 134101; (c) C. Riplinger, P. Pinski, U. Becker, E. F. Valeev, F. Neese, *J. Chem. Phys.*, 2016, **144**, 024109; (d) M. Saitow, U. Becker, C. Riplinger, E. F. Valeev, F. Neese, *J. Chem. Phys.*, 2017, **146**, 164105; (e) Y. Guo, C. Riplinger, U. Becker, D. G. Liakos, Y. Minenkov, L. Cavallo, F. Neese, *J. Chem. Phys.*, 2018, **148**, 011101.
- S23 (a) C. P. Kelly, C. J. Cramer and D. G. Truhlar, *J. Chem. Theory Comput.*, 2005, **1**, 1133–1152; (b) M. Sparta, C. Riplinger and F. Neese, *J. Chem. Theory Comput.*, 2014, **10**, 1099–1108.
- S24 (a) T. A. Keith and R. F. W. Bader, *Chem. Phys. Lett.*, 1992, **194**, 1–8; (b) T. A. Keith and R. F. W. Bader, *Chem. Phys. Lett.*, 1993, **210**, 223–231; (c) J. R. Cheeseman, G. W. Trucks, T. A. Keith and M. J. Frisch, *J. Chem. Phys.*, 1996, **104**, 5497–5509.
- S25 J. Tao, J. P. Perdew, V. N. Staroverov and G. E. Scuseria, *Phys. Rev. Lett.*, 2003, **91**, 3–6.
- S26 E. Papajak, H. R. Leverentz, J. Zheng and D. G. Truhlar, *J. Chem. Theory Comput.*, 2009, **5**, 1197–1202.
- S27 M. A. Iron, *J. Chem. Theory Comput.*, 2017, **13**, 5798–5819.
- S28 S. E. Prey, C. Herok, F. Fantuzzi, M. Bolte, H.-W. Lerner, B. Engels and M. Wagner, *Chem. Sci.*, 2023, **14**, 849–860.